NATIONAL AERONAUTICS AND SPACE ADMINISTRATION

Technical Report No. 32-1033

Experimental Investigations of Wedge Base Pressure and Lip Shock

Francis R. Hama

JET PROPULSION LABORATORY

CALIFORNIA INSTITUTE OF TECHNOLOGY

PASADENA, CALIFORNIA

December 1, 1966

NATIONAL AERONAUTICS AND SPACE ADMINISTRATION

Technical Report No. 32-1033

Experimental Investigations of Wedge Base Pressure and Lip Shock

Francis R. Hama

Approved by:

Alan L. Kistler

Alan L. Kistler, *Manager*
Fluid Physics Section

JET PROPULSION LABORATORY
CALIFORNIA INSTITUTE OF TECHNOLOGY
PASADENA, CALIFORNIA

December 1, 1966

Prepared Under Contract No. NAS 7-100
National Aeronautics & Space Administration

Contents (contd)

Figures (contd)

Contents

Figures

Contents (contd)

Figures (contd)

Contents (contd)

Figures (contd)

Acknowledgment

I am greatly indebted to Prof. Anatol Roshko, who initially introduced me to the base-pressure problem, for his continued interest and many valuable suggestions. Repeated discussions with Prof. Lester Lees and Prof. Toshi Kubota have also contributed heavily to the progress of this research and to my understanding of the problems involved. Enthusiastic cooperation and tireless assistance provided by many personnel of the Aerodynamic Facilities Section at JPL, particularly Messrs. R. F. Gruber, D. G. Hanks, R. J. King, R. B. Morrow, and H. Velasquez, are gratefully acknowledged.

Abstract

Base-pressure and surface-pressure measurements together with schlieren and shadowgraph observations were conducted on 6-deg half-angle wedges of various separation-edge shapes. The lip shock, which emanates from even a sharp separation edge, was found to be of substantial strength, contrary to the prevailing belief. In most cases investigated here, predominant cause of the lip shock appears to be the viscous separation effect similar to that of the separation shock emanating from a circular cylinder, rather than the inviscid rotational effect.

Experimental Investigations of Wedge Base Pressure and Lip Shock

I. Introduction

The base-pressure problem, which was once thought to be more or less a completely solved problem, is having a revived interest because of increasing practical applications and because of further clarification of the inadequate assumptions involved in existing theories. For example, it was clearly demonstrated by Roshko and Thomke (Ref. 1) that the theoretical reattachment pressure condition assumed by Chapman et al, (Ref. 2) and Korst (Ref. 3) is in fact untrue. Whereas their theories (Refs. 2, 3) assume that the pressure is fully recovered at the reattachment, Roshko's experimental results (Ref. 1) show that the pressure is only half recovered. Such inadequate assumptions in the theories are bound to result in disagreements with experimental base pressures. The disagreements brought in controversies as well as the empirical approach, such as proposed by Nash (Ref. 4) to remedy the inadequacy. Such an approach may find a lucky agreement with experimental data under particular conditions investigated but will not solve the problem at all.

It was our initial goal to experimentally investigate the base-pressure problem of a wedge under a completely laminar condition, in which case only a rigorous theoretical pursuit might be made. In spite of a preliminary estimate based upon Chapman's correlation data (Ref. 2), however, our experimental flow field turned out to be in a transitional range. Although the flow was barely in an entirely laminar condition at the lowest Reynolds number investigated, the free-shear layer became turbulent almost immediately after separation at the base edge at the highest Reynolds number. We were therefore in a somewhat embarrassing situation: we were unable to completely investigate either the laminar or turbulent case. An excuse may be that, after all, most of the existing experimental results are in a similar incomplete state. Perhaps because the test condition was in the transitional range, however, we were indeed fortunate to come across a variety of near-wake shock patterns and other abundant wealth of information which stirred our curiosity.

At the very early stage of the investigation, the so-called lip shock, which emanates from the sharp separation edge, was not only clearly identified but also observed to interact with the wake (recompression or neck) shock so as to form a distinct slip stream. A typical shadowgraph is shown in Fig. 1. It seems to have been conventional to assume that the lip shock is weak and the static-pressure

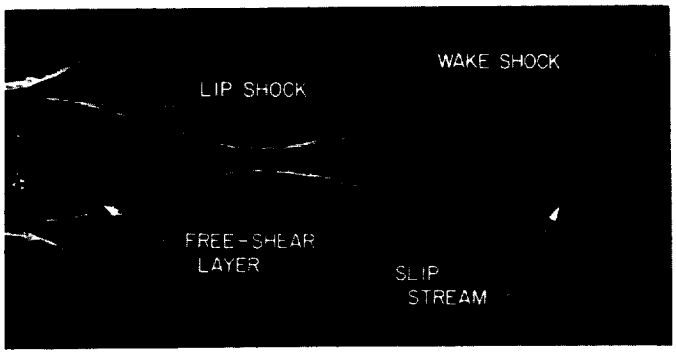

Fig. 1. Shadowgraph of flow field behind wedge ($M_1 = 2.61$, $Re_2 = 1.01 \times 10^6$)

ratio across the lip shock is a matter of a few percentage points increase. If the assumption is correct, however, the slip stream should not be observed so distinctly. A preliminary rough estimate from schlieren pictures indicated that the pressure jump could in fact be several hundred percent. Since, by the presence of the lip shock of substantial strength, the expansion at the separation edge is further complicated, the flow actually overexpands and is then recompressed by the lip shock. Undoubtedly, the initial free-shear layer must have a quite distorted profile. Therefore, even when the reattachment phenomenon of a shear layer becomes completely understood, the base-pressure problem cannot be solved until the distorted initial velocity profile is determined. Moreover, the lip shock could directly influence the pressure-recovery process and the near-wake velocity profile behind the reattachment point through its interaction with the wake shock.

In spite of vast literature existing on the base-pressure and separated-flow problems, the lip shock and its potentially important effects had almost completely escaped theorists' as well as experimentalists' attention. Under these circumstances, our interest was more strongly drawn into the lip shock rather than the base pressure, despite the original intention. Nevertheless, the base pressure was always measured and its data are included in this Report for completeness. Investigations into the lip shock were limited at this time to its strength, cause, and overall effects, but this much information is believed to be sufficient to warrant its publication before more thorough and elaborate, detailed measurements are made.

II. General Description of Experiments

The experiments were conducted entirely in the Jet Propulsion Laboratory 20-in. supersonic wind tunnel, the test section of which was 18 in. wide and 20 in. high. Basic arrangements and dimensions of the test models are shown in Fig. 2. All of the test models were two-dimensional and mounted horizontally, spanning the entire width of the test section. The wedge-plate configuration, Fig. 2 (a), was first tested at the free-stream Mach number, $M_1 = 2.01$, 2.61, 3.02, 3.51, 4.00, and 4.54, and was actually a combination of a solid wedge followed by a plate with its top surface aligned with the centerline of the wedge. The plate had 24 static-pressure holes of 0.031 in. diameter drilled through the plate, the pressure hole nearest the wedge base being 0.031 in. away from the base. The pressure reading of this hole was considered to be the base pressure in this configuration. The purpose of the investigation with this wedge-plate configuration was to obtain data for the solid-wall reattachment and to compare them with those in the wedge-alone case in which the flow underwent fluid–fluid, or free, reattachment.

Several wedge models of essentially the same dimension were used for the wedge-alone case. The solid model was used for optical observations, and a pressure model with altogether thirty pressure taps of 0.031 in. diameter each was fabricated, with particular interest in the detailed pressure distribution near the separation edge and in the spanwise base-pressure distribution.

In addition to these sharp regular wedges, eight modified-edge models were also tested for the specific purpose of investigating the cause of lip shock rather than obtaining engineering data for various geometrical shapes,

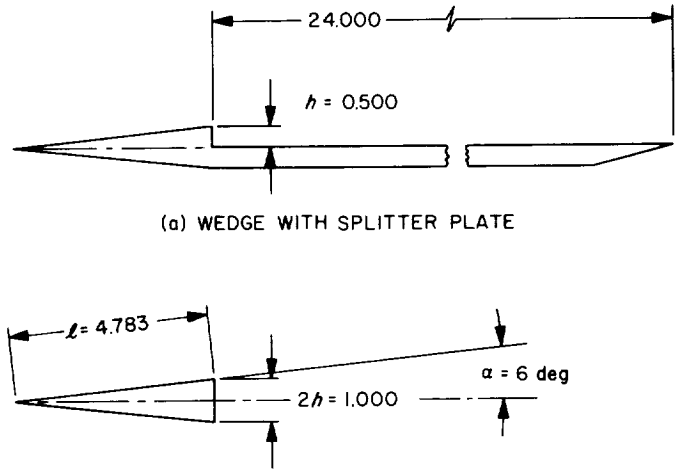

Fig. 2. Basic test model arrangements (dimensions in inches)

although the base pressure was always measured. The modified-edge models consisted of a 3¾-in.-long fixed front part and 1-in.-long interchangeable rear parts. The modified shapes were (Fig. 3): four rounded edges of radii 0.05, 0.10, 0.25 in., and a fully rounded 0.45 in.; a knife edge of 0.02 in. blade thickness and 5 deg undercut edge with < 0.002 in. claimed sharpness at the tip; and three boat-tail models of boat-tail angles 5, 10, and 17 deg. Final optical observations of the regular wedge were actually made by the use of this two-piece model (Fig. 3, top) because the solid one-piece wedge was in such a poor condition when we reached the stage of acquiring good pictures that the separated layer was visibly more disturbed than in preliminary photographs. The knife-edge model had three pressure taps; the boat-tail models and the two rounded models of radii 0.05 and 0.10 had six, but the other two rounded models of radii 0.25 and 0.45 had fourteen and thirteen, respectively.

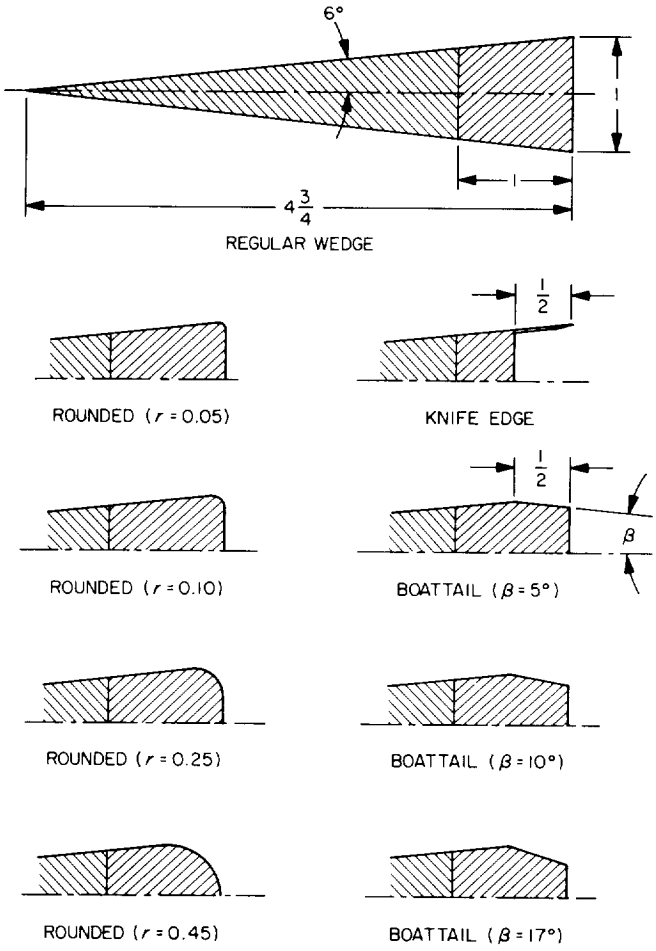

Fig. 3. Test models with modified edge shapes (dimensions in inches)

All of the wedge-alone configurations, regular as well as modified, were tested at $M_1 = 2.61$, 3.51, and 4.54. Nearly full capability of the wind tunnel was utilized at each Mach number, so that the model Reynolds number Re_2 based upon the wedge-surface condition and wedge length ranged from 0.2×10^6 to 2.0×10^6. Static-pressure measurements were made mostly by the use of a multiple-pressure-measuring system (MPMS) which scanned all of the pressures including an accurate reference pressure as well as a vacuum by a single transducer. The transducer was a 5-psia Statham gauge chosen from eight in hand and was extremely linear at any reading. The static-pressure distribution along the centerline of the wedge wake was measured by a 1/16-in. diameter tube, which pierced through the base into the wedge, and the same transducer located outside of the tunnel. Since the available longitudinal traverse was limited to 3 in. by the length of the wedge, three probes having a static-pressure hole of 0.031 in. diameter at different locations were prepared so as to be able to traverse the necessary length.

Pitot-pressure surveys were also conducted, but their purpose was limited to examinations of the assumptions made in estimating the lip-shock strength. Two pitot probes inclined at 0 and 20 deg to the free-stream direction were made from a 0.036-in. hypodermic needle, flattened and ground to 0.025 in. overall thickness at the tip with an opening of 0.009 in. The transducer for the pitot pressure was a 15-psia gauge.

Optical observations consisted of long-exposure (1/125 sec) schlieren and short-exposure (approximately 8 μsec) spark shadowgraph pictures. Sample pictures with a grid mounted on the other side of the tunnel window showed very little distortion except in a narrow region very close to the separation edge.

III. Shock Wave Patterns

Shock-wave patterns for the wedge-plate configuration at six Mach numbers and at six representative Reynolds numbers are shown in Figs. 4a–f. In addition, shock patterns with the triangular tripping device (Refs. 5, 6) mounted on the wedge surface 1 in. from the leading edge are also shown in the six bottom pictures of Figs. 4a–f. The tripped boundary layer cases were made at the maximum Reynolds number condition, but the Reynolds number with artificial trippings has little significance, of course.

It becomes clear by comparing these photographs that relative orientations of the lip shock and the wake shock

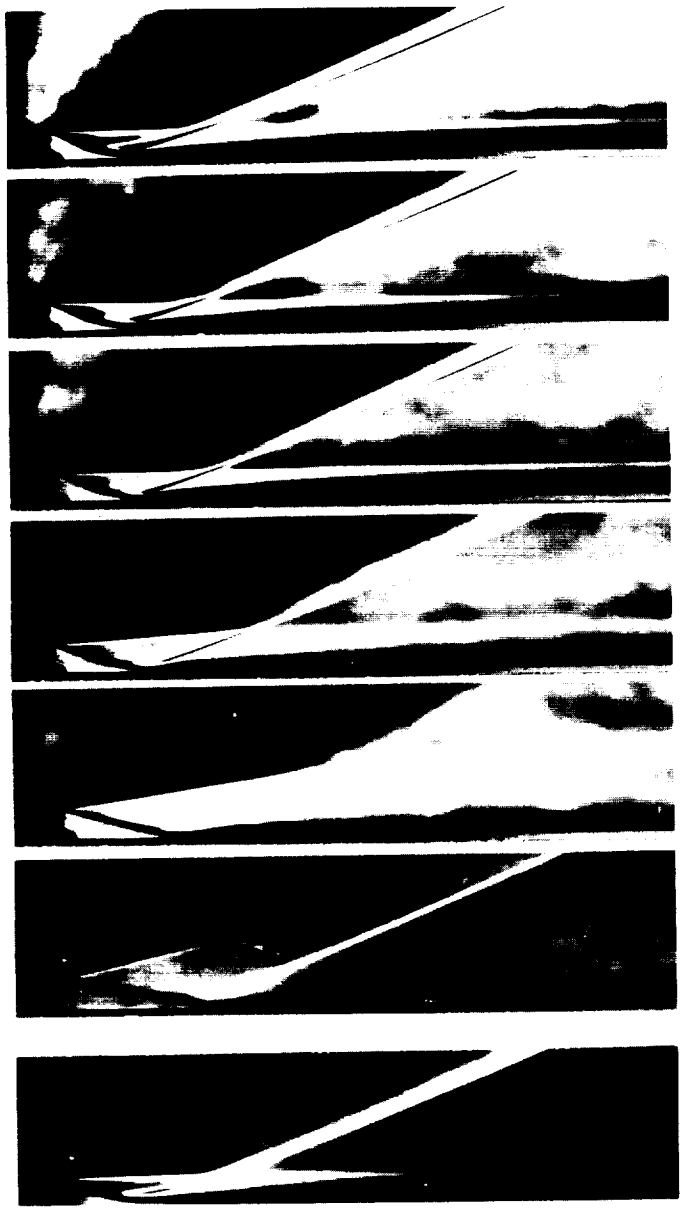

Fig. 4a. Schlieren pictures at $M_1 = 2.01$ (wedge-plate); from top: $Re_2 = 1.78, 1.22, 0.98, 0.64, 0.38$, and 0.19×10^6; at bottom: with boundary-layer trip

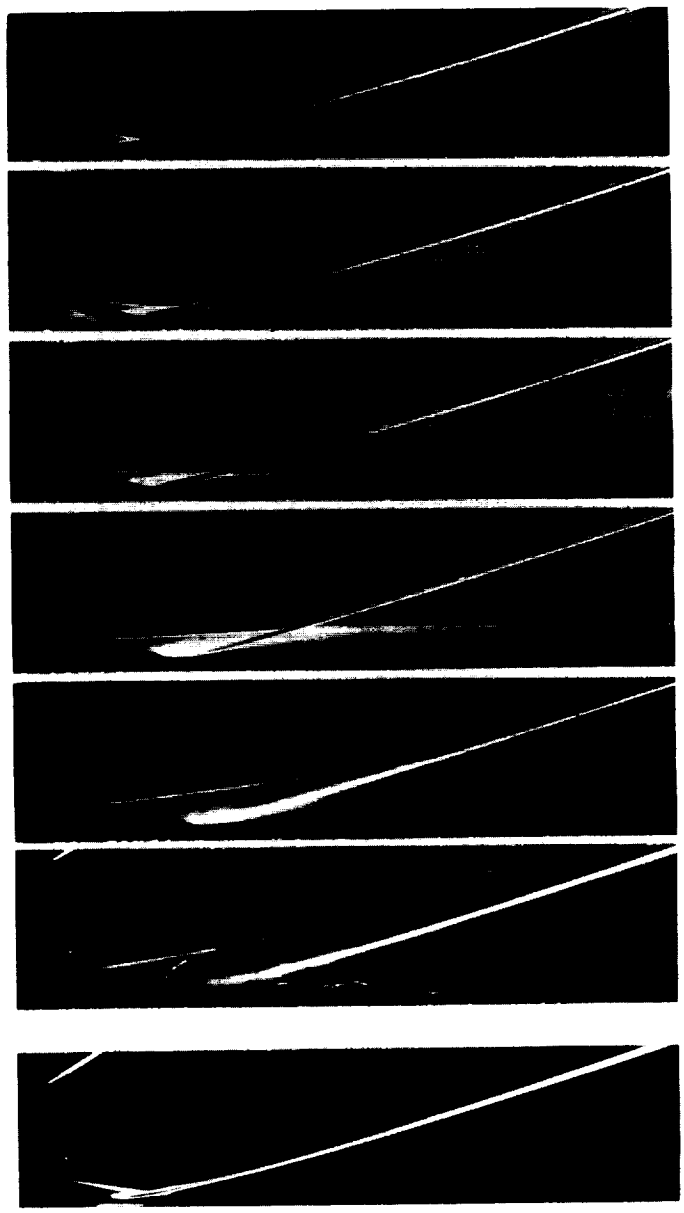

Fig. 4b. Schlieren pictures at $M_1 = 2.61$ (wedge-plate); from top: $Re_2 = 1.83, 1.25, 1.03, 0.66, 0.38$, and 0.19×10^6; at bottom: with boundary-layer trip

are strongly dependent in this Mach number range not only on the Reynolds number but also on the Mach number. The Mach number independence principle does not apply. There is evidence to suspect that the dependence on the Mach number is particularly strong in the Mach number range investigated but perhaps less so beyond this range.

The most pronounced difference is that, whereas the lip shock can be clearly distinguished from the wake shock at lower Mach numbers, the two shocks tend to become inseparable at higher Mach numbers and in fact merge to form one continuous shock at the highest Mach number. This merging of the two shocks is particularly prominent at lower Reynolds numbers, where the flow was entirely laminar as judged from the shadowgraphs simultaneously taken, and was also observed at $M_1 = 6$ (Ref. 7). It is quite unlikely, even at higher Mach numbers, to have the relative orientation of the two shocks reversed; i.e., the lip shock, which must be formed by some mechanism associ-

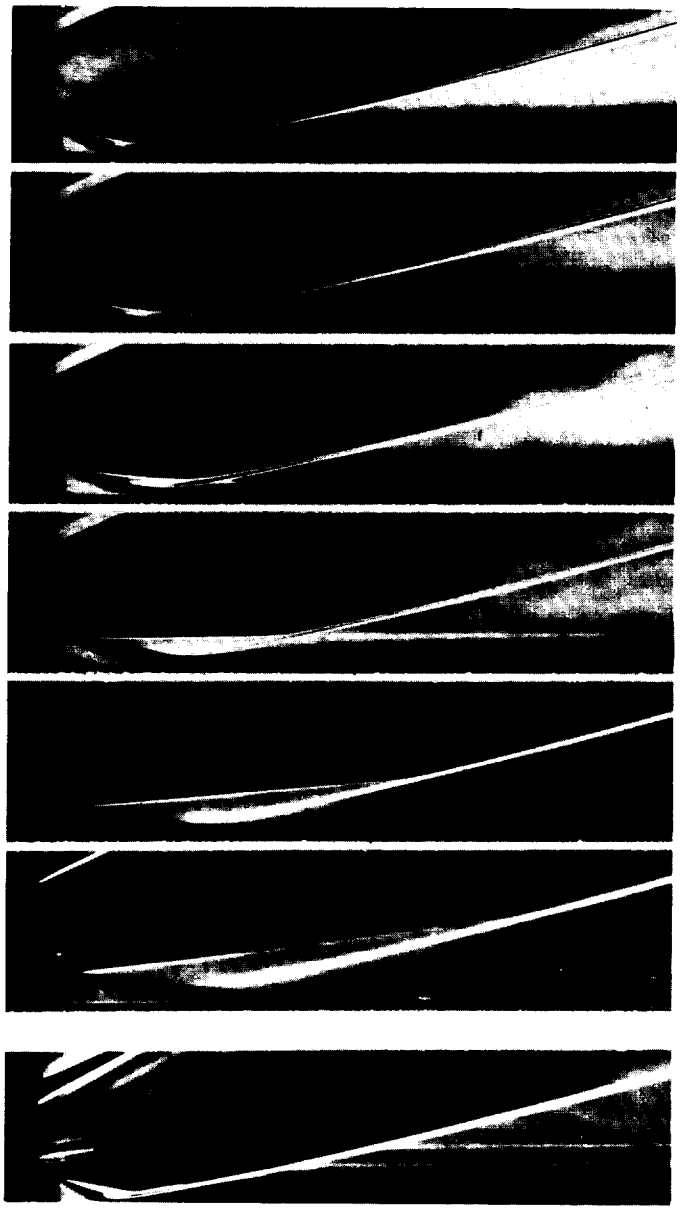

Fig. 4c. Schlieren pictures at $M_1 = 3.02$ (wedge-plate); from top: $Re_2 = 1.93$, 1.32, 1.08, 0.67, 0.42, and 0.21×10^6; at bottom: with boundary-layer trip

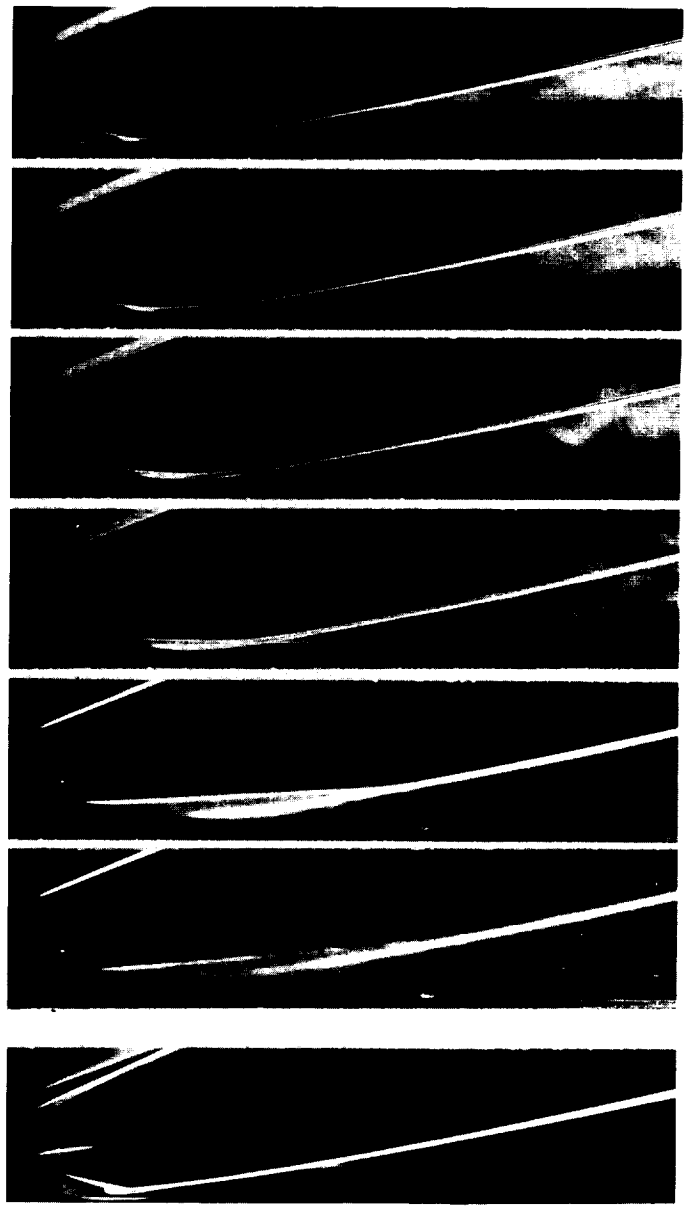

Fig. 4d. Schlieren pictures at $M_1 = 3.51$ (wedge-plate); from top: $Re_2 = 1.95$, 1.33, 1.08, 0.82, 0.42, and 0.21×10^6; at bottom: with boundary-layer trip

ated with the expansion of the viscous layer at the separation edge, is unlikely to be located clearly below the wake shock, which is formed by the turning of the free-shear layer near the reattachment.

Many factors contribute to the variations of the shock pattern. First, for a given base-pressure ratio p_b/p_1, where p_b is the base pressure and p_1 the free-stream static pressure, the direction of the separated free-shear layer, ϵ, is less steep relative to the free-stream direction for larger Mach numbers, as shown in Fig. 5. (This direction was computed from the base pressure by the isentropic inviscid formula and was found to agree well with the observed flow direction.) Therefore, the flow deflection at the reattachment is smaller for larger Mach numbers. Second, since the smaller inclination means a longer length of the free-shear layer, the free-shear layer is thicker at the attachment. Because of the factor $1/\sin \epsilon$ multiplying the thickness and because of the larger boundary-layer thickness before separation, the reattachment process is slower

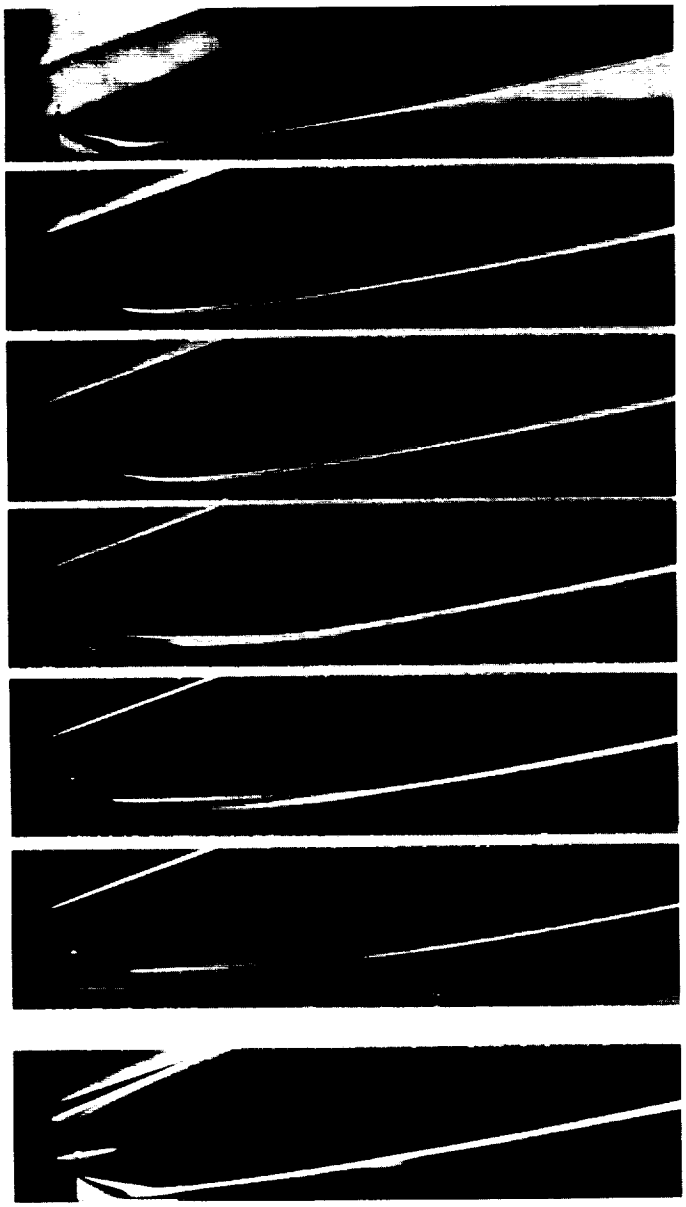

Fig. 4e. Schlieren pictures at $M_1 = 4.00$ (wedge-plate); from top: $Re_2 = 2.06, 1.40, 1.14, 0.72, 0.44$, and 0.22×10^6; at bottom: with boundary-layer trip

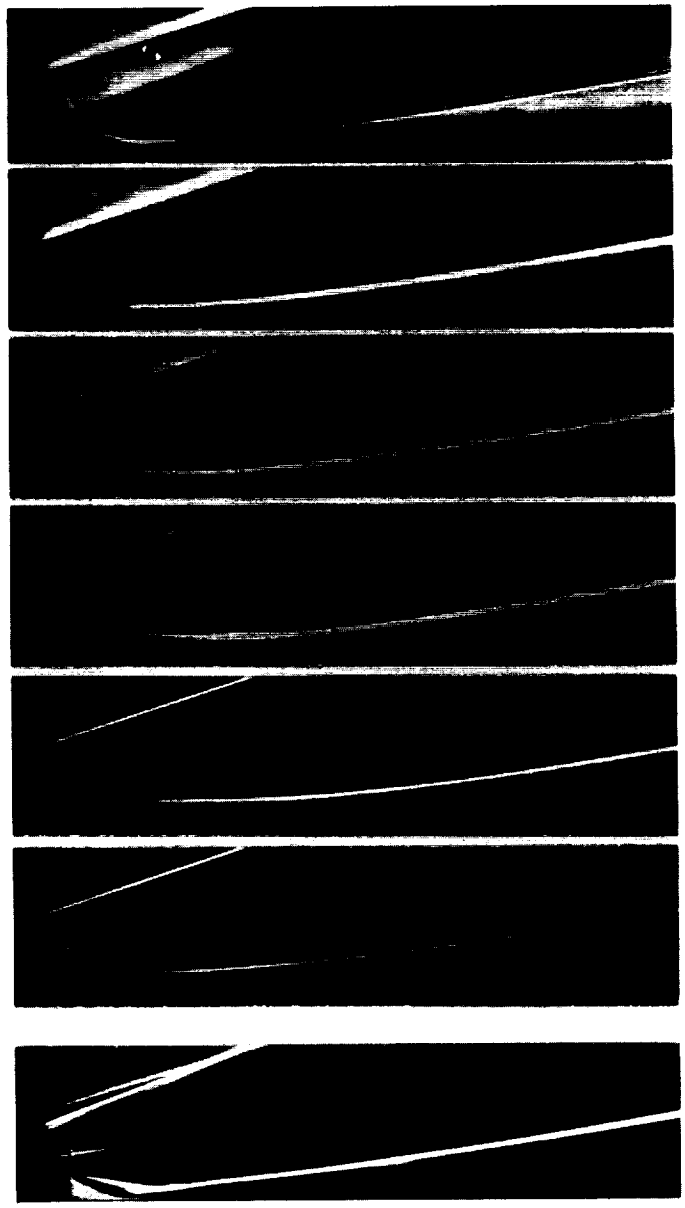

Fig. 4f. Schlieren pictures at $M_1 = 4.54$ (wedge-plate); from top: $Re_2 = 1.93, 1.38, 1.13, 0.72, 0.45$, and 0.22×10^6; at bottom: with boundary-layer trip

for larger Mach numbers (cf. pressure-recovery distribution). Furthermore, the relation between the Mach angle μ and the Prandtl–Meyer angle ν gives

$$\frac{d\mu}{d\nu} = \frac{1 + \frac{\gamma - 1}{2} M^2}{1 \quad M^2}$$

which indicates that, for a given turning angle, coalescence of wavelets takes place more slowly at higher Mach numbers. All told, the higher the Mach numbers, the farther away from the reattachment point the wake shock tends to be formed.

On the other hand, the Mach angle μ relative to the free-shear layer may be taken as an approximate angle of the lip shock if the lip shock is not very strong. Mach-line orientation angles, $\epsilon - \mu$, relative to the free-stream direction, are demonstrated in Fig. 6, in which the negative value of $\epsilon - \mu$ means that the lip shock is inclined

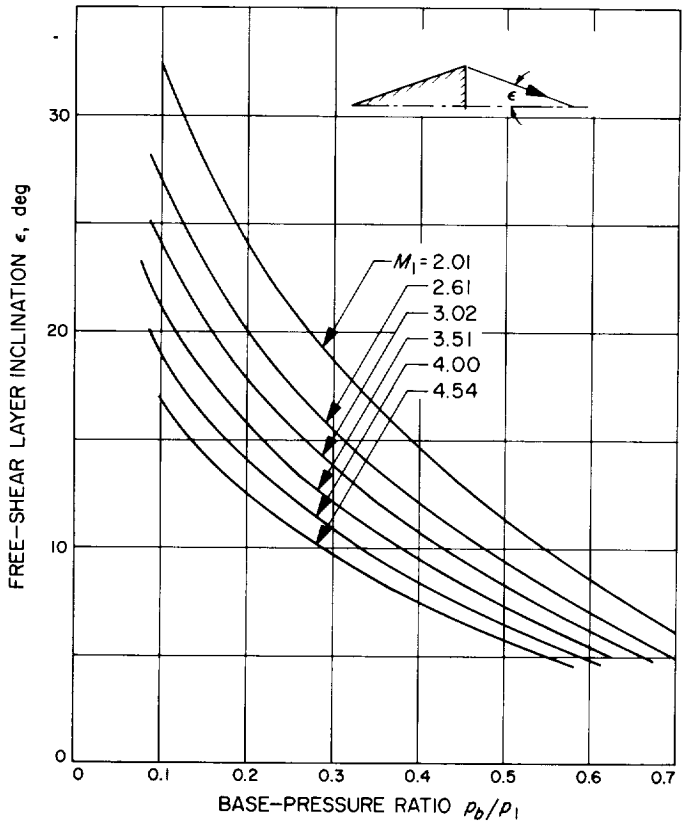

Fig. 5. Isentropic flow direction vs base-pressure ratio

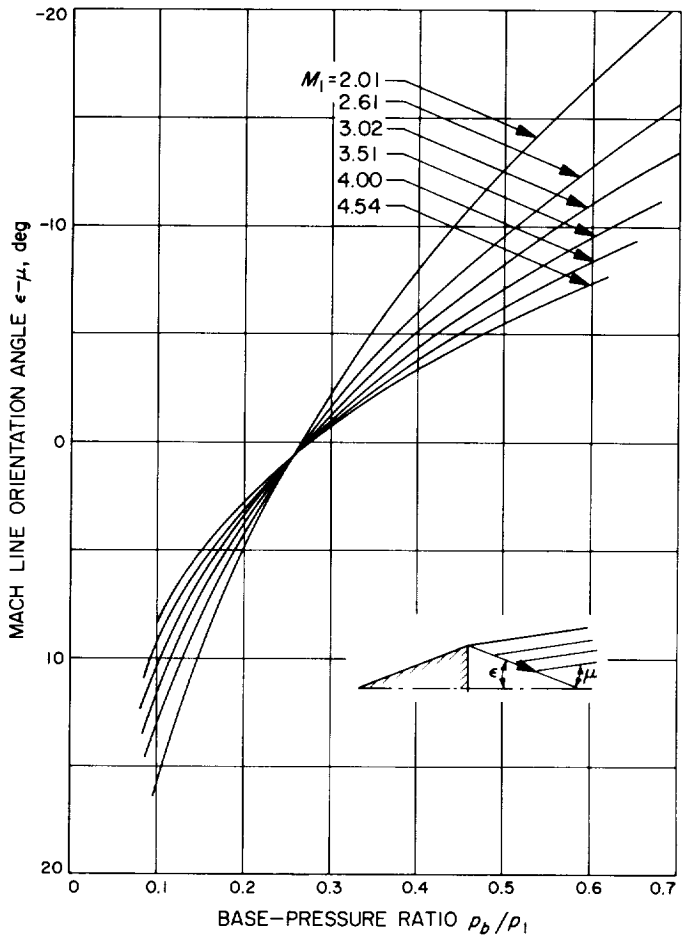

Fig. 6. Mach line orientation angle (isentropic)

upward and *vice versa*. In the range of base-pressure ratio $p_b/p_1 > 0.25$, i.e., in the low Reynolds number range, the Mach line is oriented with a larger negative value at lower Mach numbers. Since the wake shock is formed close to the reattachment region, as described in the preceding paragraph the lip shock and the wake shock are well separated at lower Mach numbers, whereas the two shocks become more and more inseparable as the Mach number increases and eventually merge into one continuous shock. Graphs of the relation between $\epsilon - \mu$ and p_b/p_1 for different Mach numbers cross at about $p_b/p_1 = 0.25$. Accordingly, the shock patterns for different Mach numbers become somewhat similar to each other at large Reynolds numbers.

When the two shocks are clearly distinguishable from each other and the lip shock is not oriented too far upward, i.e., when the Mach number is relatively small and the Reynolds number is sufficiently large, a slip stream parallel to the free-stream direction is seen to emerge as a white line from the point where the two shocks meet each other.

Additional observation worth reporting is the orientation of the lip shock relative to the free-shear layer. The lip shock comes out of the free-shear layer rather quickly at lower Mach numbers, but the lip shock is completely imbedded in the free-shear layer at higher Mach numbers, particularly when the Reynolds number is also large. This is due in part to the smaller Mach angles of the free-shear layer at higher Mach numbers for a given base-pressure coefficient (Fig. 7). The difference in the inclination angle of the lip shock, with which we are concerned, is actually more pronounced because of the observed fact, as shown later, that the larger the Mach number, the stronger the lip shock, i.e., the overexpansion before the lip shock is more enhanced, and hence the lip shock is more tilted toward the free-shear layer direction. Plotted points in Fig. 7 are the lip-shock angle relative to the free-shear layer. Moreover, not only the inviscid approximation dictates a larger area expansion (Fig. 8), but also the initial boundary-layer thickness before separation is already thicker for higher Mach numbers, resulting in even more pronounced difference in the free-shear-layer thickness, as a very rough estimate (Fig. 9) indicates. Both the more

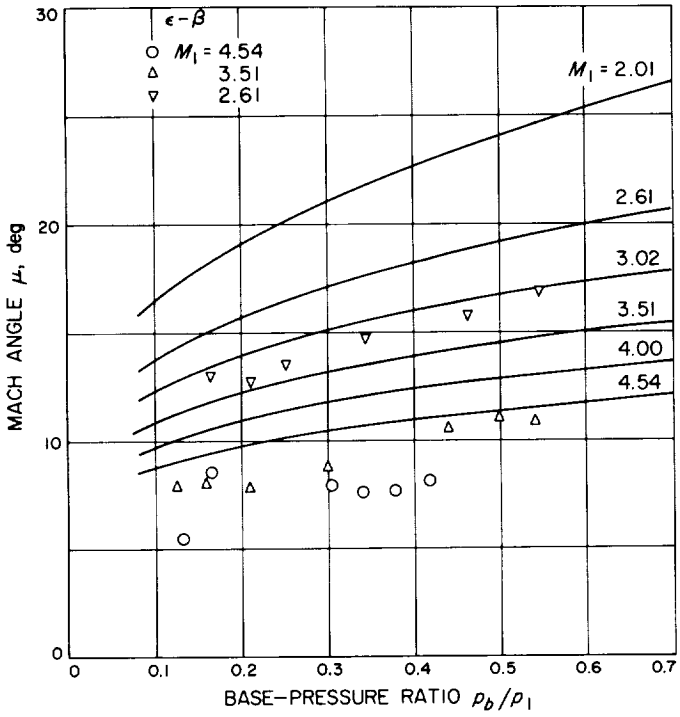

Fig. 7. Mach angle and lip-shock angle relative to free-shear layer

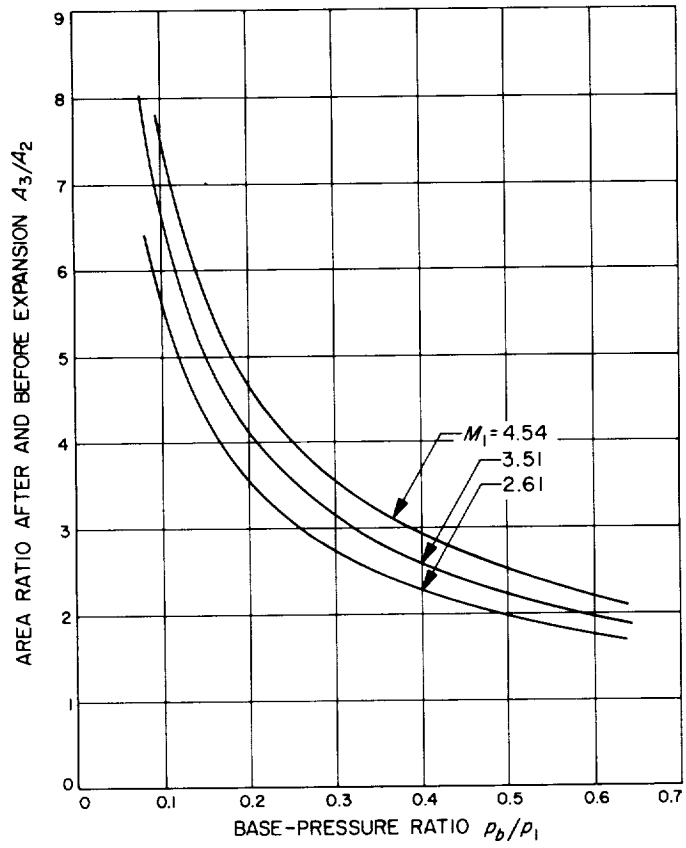

Fig. 8. Area expansion ratio

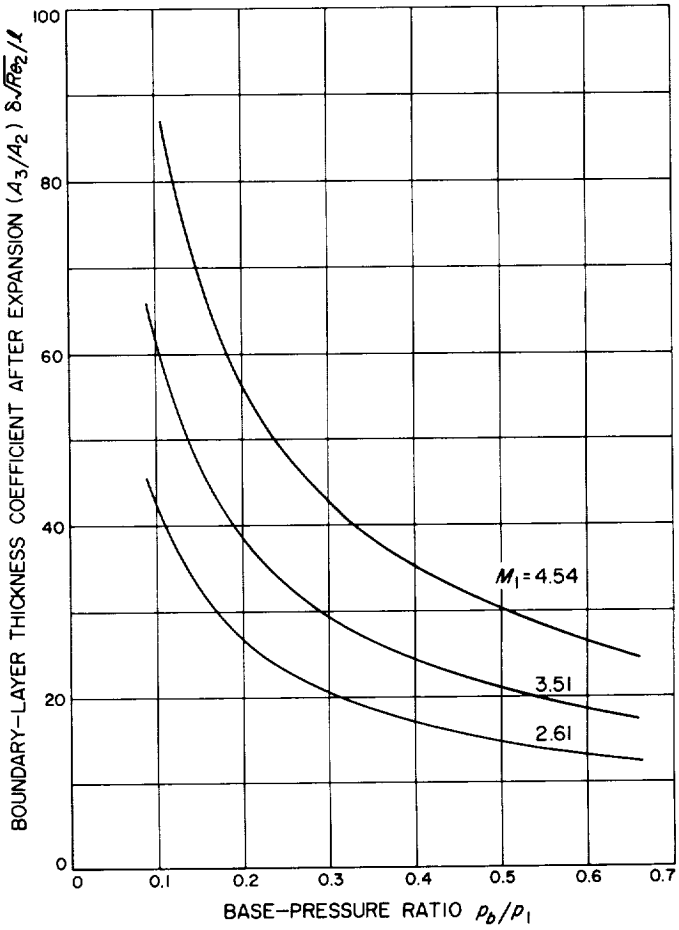

Fig. 9. Boundary-layer thickness coefficient after expansion

nearly parallel lip-shock angle and the thicker free-shear layer contribute to the above phenomenon.

The orientation of the lip shock relative to the wake shock and to the free-shear layer is schematically summarized in Fig. 10, which will be referred to again in connection with the behavior of the static-pressure recovery distribution and with the results of pitot-pressure surveys.

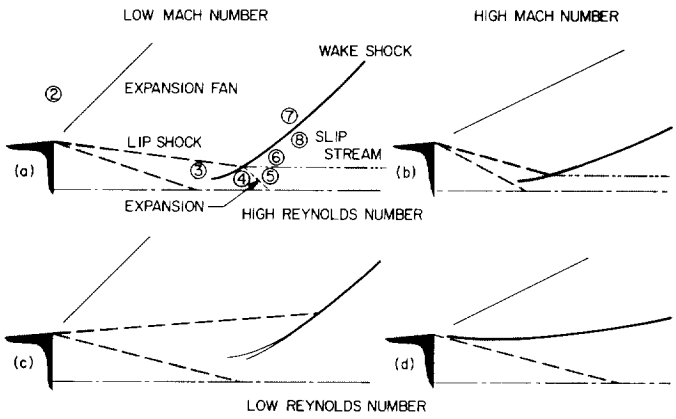

Fig. 10. Dependence of shock pattern on Mach number and Reynolds number (schematic summary)

These observations concerning the shock pattern are described for the wedge-plate configuration, Fig. 2(a). However, as typical comparative shadowgraphs in Fig. 11 indicate, the shock patterns behind the wedge without the splitter plate are quite similar to those with the splitter plate, and the above observations concerning the shock pattern for the wedge-plate configuration equally apply to the shock patterns behind the wedge alone.

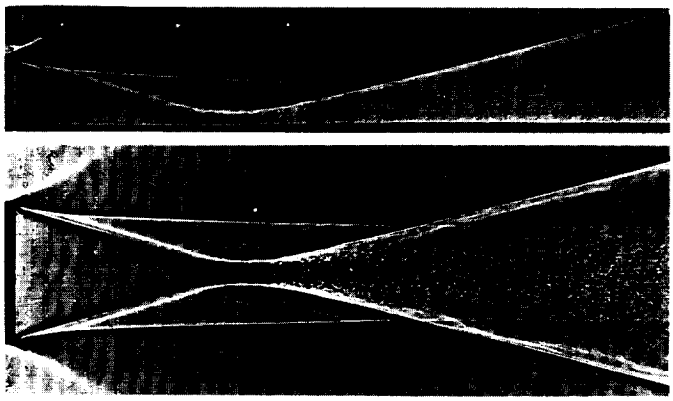

Fig. 11. Shadowgraphs for wedge-plate (top) and for wedge (bottom); $M_1 = 2.61$ and $Re_2 = 1.0 \times 10^6$

IV. Base Pressure

Presented first in Fig. 12 is a comparison between the base pressure for the wedge-plate configuration and that for the wedge alone. There has been only a speculation as to the effect of different reattachment conditions on the base pressure. This figure demonstrates that the base pressures for the two cases are quite close to each other, particularly at lower Mach numbers. Nevertheless, the base pressure for the wedge alone is generally lower than that for the case of solid-wall reattachment. In other words, the free reattachment condition is capable of sustaining a larger pressure recovery, as one might expect, due to lesser energy losses than along a solid boundary.

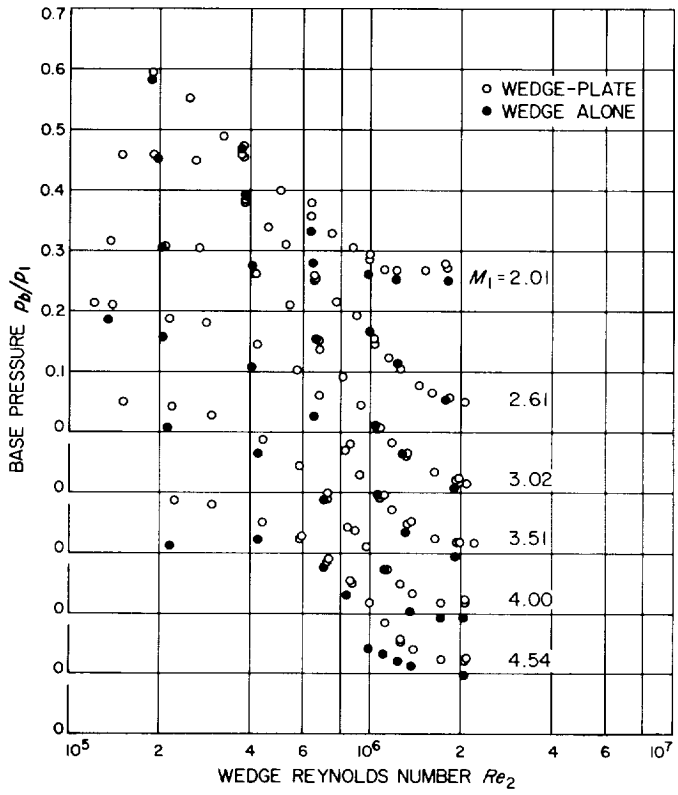

Fig. 12. Base pressures of wedge-plate and wedge alone

These pressure data were obtained with fences of 3 in. length, as depicted in Fig. 13, mounted 2½ in. from the two side walls of the wind tunnel. These fences were originally utilized by Ginoux (Ref. 8) for his base-pressure studies in an attempt to isolate the side-wall boundary-layer effects and to achieve a better two-dimensionality in the central portion. According to Ginoux, the effect of the fence is to increase the base pressure. His test condition

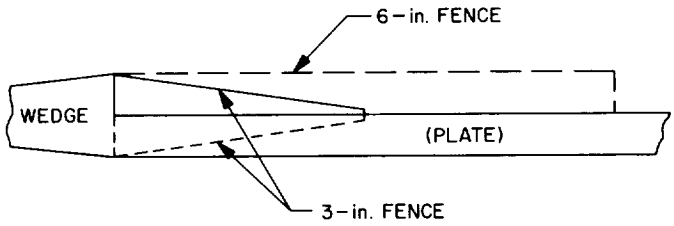

Fig. 13. Fence geometry

roughly corresponds to the second lowest Reynolds number at $M_1 = 2.61$ in the present experiment, and indeed the same effect can be found in Fig. 14 in which the base pressures of the wedge, both with and without the fences, are given. However, this tendency reverses as the Reynolds number increases at the same Mach number. At larger Mach numbers, moreover, the base pressure was consistently lower with the presence of the fence. Figure 15 shows the transverse distributions of the base pressure along the horizontal centerline of the wedge taken at two extreme test conditions ($Z = 0$ is the vertical centerline). Interaction of the side-wall boundary layers, which were always turbulent in the present experiment, with the base flow must be quite complicated; whereas the base pressure in the interacting region is substantially lower than the average base pressure at the lower Mach number and the lower Reynolds number, the situation seems to be somewhat reversed at the opposite test condition. Uniformity of the base-pressure distribution is not appreciably improved with the fences. Nevertheless, with the strength of recent confirmation by Lewis (Ref. 9), we may be justified in assuming that the flow field with the fences is nearly

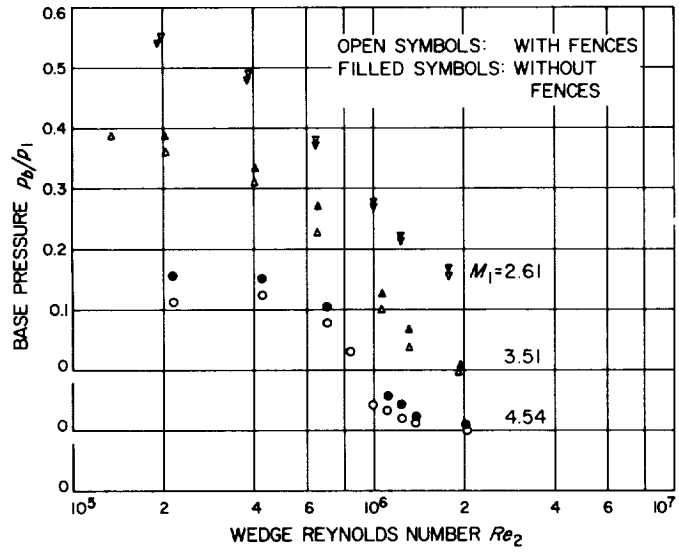

Fig. 14. Effect of fences on wedge base pressure

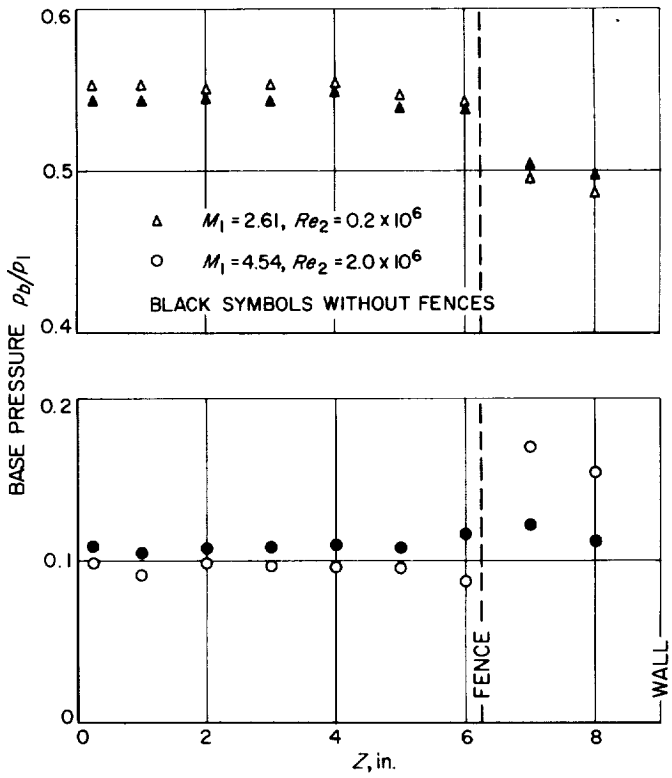

Fig. 15. Spanwise base-pressure distribution of wedge (with and without fences)

two-dimensional. We might add that, although the pressure recovery after the reattachment was seldom completed within the 3-in. distance from the step, the extended fences of 6-in. length did not change the base pressure at all.

The knife-edge model was provided with end plates in its cavity to prevent the seepage of higher pressure on the wedge surface into the low-pressure cavity, and with a partition 2½ in. from each end to reduce the possible cross flow caused by the side-wall boundary-layer interaction (Fig. 16). The end plates and the partitions were 1/16-in.-thick Lucite. By the insertion of the partitions, the flow

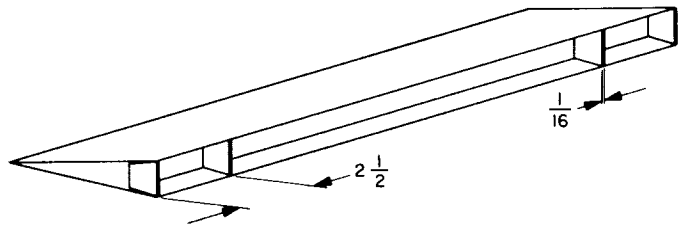

Fig. 16. Partitions mounted in cavity of knife-edge model (dimensions in inches)

field was assumed to have been made effectively two-dimensional, and the base pressure thereby obtained was compared with that of the regular wedge with the fences in Fig. 17. Although the base pressure of the knife-edge model is somewhat lower than that of the regular wedge at lower Reynolds numbers and at the lowest Mach number investigated, the base pressures for the two models are essentially identical to each other in most conditions, the result of which was rather surprising to us. As will be shown later, the shock patterns and the lip-shock strengths were also virtually identical for the two models.

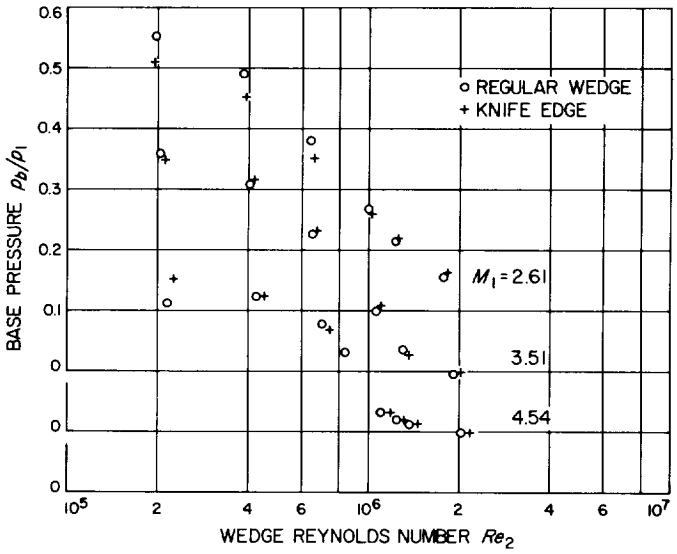

Fig. 17. Base pressures of regular wedge and knife-edge wedge (with fences)

The rounded-edge models were not provided with the fences, and their base-pressure data are presented in Fig. 18 in comparison with those of the regular wedge without the fences. The base pressure of these models was somewhat larger than that of the regular wedge, particularly at larger Reynolds numbers and larger Mach numbers. Increase in the base pressure was enhanced with increasing radius.

Figure 19 demonstrates the effect of boattailing on the base pressure. Since the fences were not mounted on the boattail models, the base pressure of the regular wedge without the fences is again shown for comparison. The boattail models were found to have a substantially larger base pressure than the regular wedge. At the expansion corner preceding the boattail, the boundary layer on the wedge surface is drastically expanded. The boundary layer is therefore much thicker, when it separates either at the separation edge at the rear end of the wedge or from the boattail surface, than that on the regular wedge. The larger

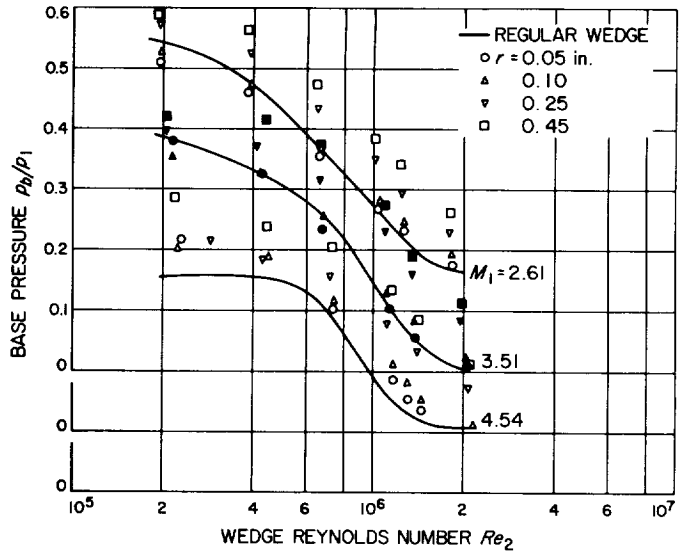

Fig. 18. Base pressures of rounded-edge wedges (without fences)

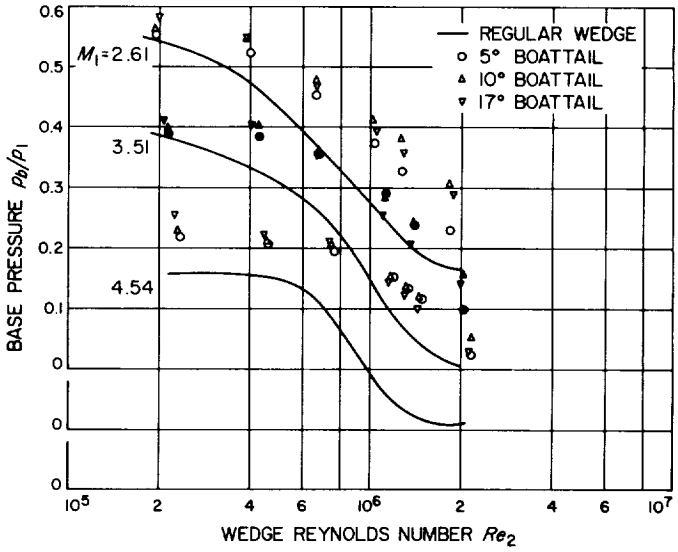

Fig. 19. Base pressures of boattail wedges (without fences)

boundary-layer thickness combined with the shortened base height by boattailing may be considered to reduce the effective Reynolds number of an equivalent regular wedge. Roshko and Lau (Ref. 10) suggest, on the other hand, that the transition distance in the free-shear layer is scaled to approximately sixty times the momentum thickness at separation. The thicker boundary layer at the separation edge of the boattail models would then extend the laminar region, at least, in the free-shear layer and could also delay transition even after reattachment. Such effects

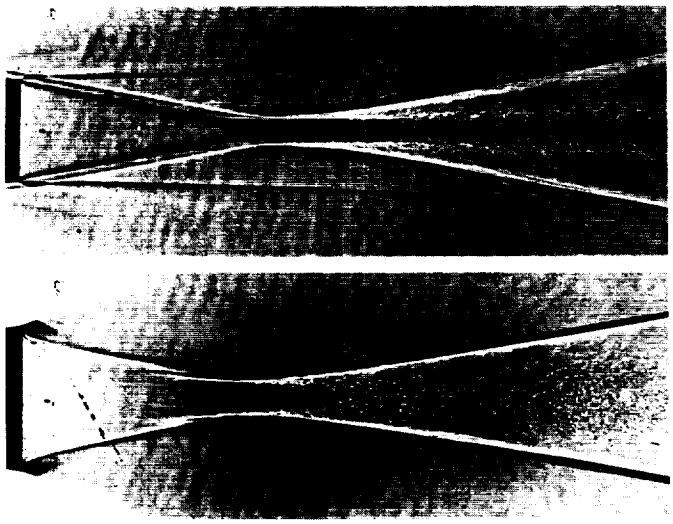

Fig. 20. Flow patterns behind 10-deg boattail wedge (top) and regular wedge (bottom); $M_1 = 3.51$ and $Re_2 = 1.35 \times 10^6$

are clearly seen in the comparative shadowgraphs, Fig. 20. Since our base-pressure data were taken in the transitional range, the effect of delayed transition is such as to shift the base-pressure curve of the regular wedge to higher Reynolds numbers, or as mentioned above, the effective Reynolds numbers of the boattail models are smaller than the actual ones. In any event, the base pressure of the boattail models should be larger than that of the regular wedge in the present test conditions. Nevertheless, there appear to be other significances of the base-pressure data; for example, substantially larger base pressure even under the laminar reattachment condition at $M_1 = 4.54$ cannot be explained by the simple argument as above. More systematic investigations into the effect of boundary-layer thickness relative to the base height are to be made in the near future and may enable us to answer these questions.

Undoubtedly, the Reynolds number in the present experiment was in the transitional range. Since we have not made the hot-wire studies, it is difficult to exactly determine the transition point. However, judged from those shadowgraphs taken at lower Mach numbers (so that the density was large enough to show detailed conditions of the free-shear layer), we are inclined to take the same viewpoint as Holder and Gadd (Ref. 11) (Fig. 21). Roshko (Ref. 12) speculates in a somewhat different manner in identifying the pressure-coefficient variations in terms of the transition location.

Attempts were made to correlate the pressure data for different Mach numbers, to compare the pressure coefficients with the Chapman and Korst theories, and to estimate Nash's partial pressure-recovery numbers. Those data, however, are believed to be of little value, particularly in the transitional range, and are not presented here.

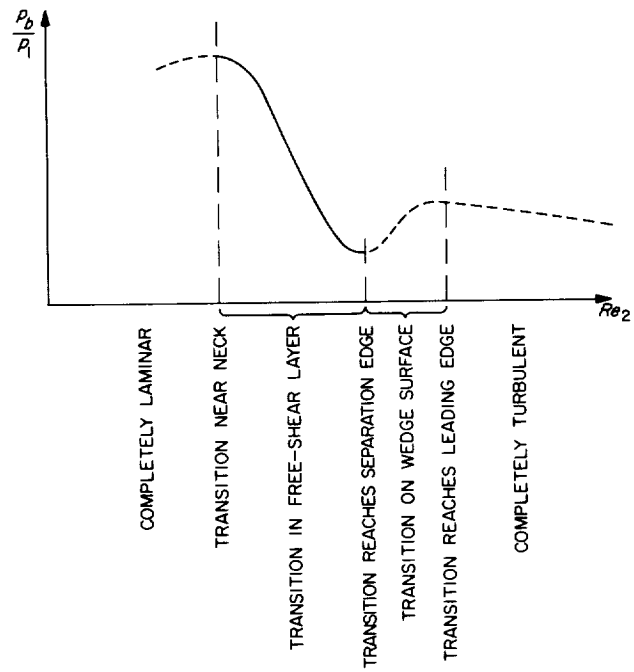

Fig. 21. Variation of base pressure in relation to transition location

V. Pressure-Recovery Distribution

The static-pressure recovery distribution was measured for the wedge-plate configuration by a row of pressure holes of 0.031-in. diameter tapped through the plate. On the other hand, the static pressure distribution along the centerline of the wake of the wedge alone was measured by a 1/16-in. static pressure probe, which pierced through the base of the wedge, thereby avoiding the tip effect (Fig. 22). The measurements were made for three typical Reynolds numbers at each of the three Mach numbers, $M_1 = 2.61, 3.51$, and 4.54. Results are shown in Figs. 23–25; p is the static pressure, p_1 the free-stream static pressure, and X the distance downstream from the base. In addition, Fig. 26 shows the pressure-recovery distribution with a tripping device mounted on the wedge surfaces. The boundary layer on the wedge surfaces was always laminar without the tripping device in the present experiment. The separated shear layer became turbulent almost immediately after the separation at the largest Reynolds number.

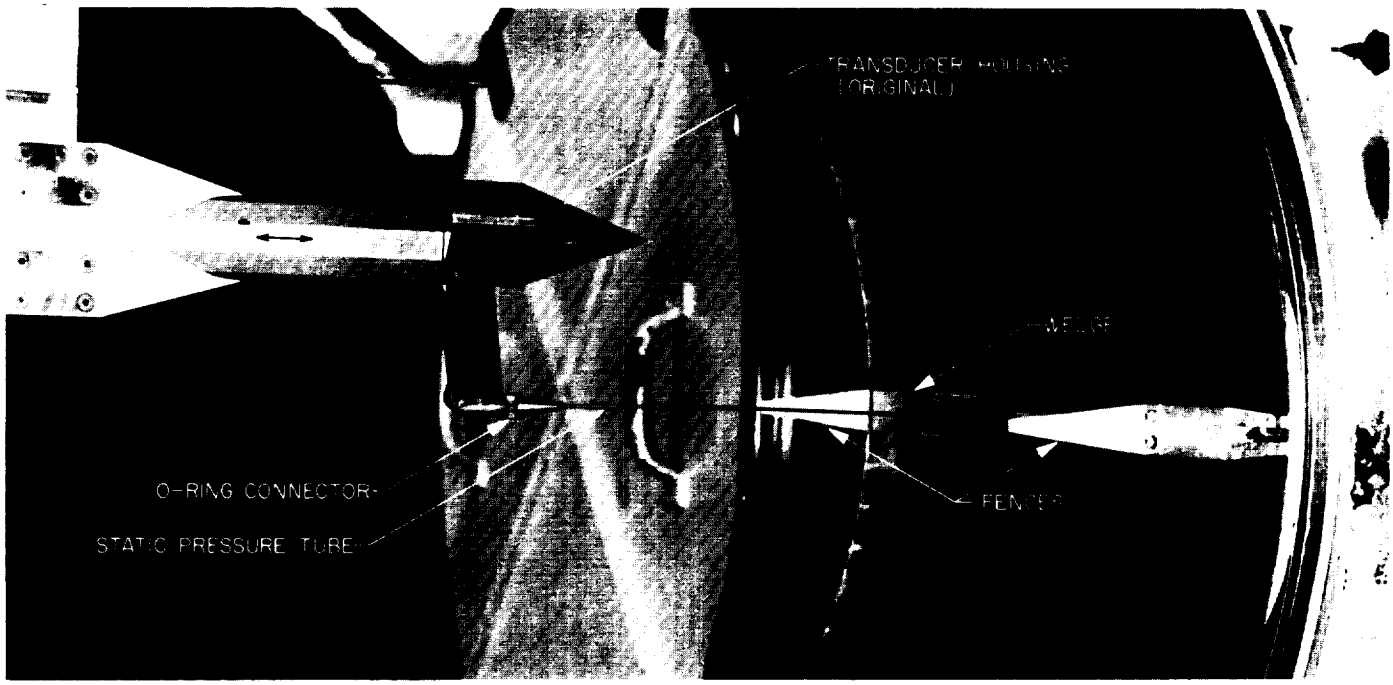

Fig. 22. Static-pressure probe

At the intermediate Reynolds number, the transition took place somewhat downstream but still in the free-shear layer, and the reattachment was therefore turbulent. The flow field was entirely laminar until after the reattachment at the lowest Reynolds number investigated.

Characteristically, the pressure-recovery distributions for the two different reattachment conditions are not appreciably different from each other. This is particularly true for the low Reynolds number cases; the static pressure is monotonically recovered. It seems to be a general tendency that, as the Mach number decreases, the static pressure overshoots the free-stream value. While the reason for it is unknown, the overshoot is generally observed also in the low-speed experiments (Tani, Ref. 13), as long as the boundary layer separates more or less parallel to the main flow (Roshko and Lau, Ref. 10). There are, however, minor differences between the two cases. The pressure is recovered slightly more quickly behind the wedge than with the plate, at least in the case of laminar reattachment. This difference must have resulted in part from the difference in the behavior of the dividing streamline near the reattachment; the dividing streamline should bend toward the plane of symmetry to cross it orthogonally at the reattachment point behind the wedge, (Kubota, Ref. 14), whereas the dividing streamline makes an angle with the plane of a solid boundary (Oswatitsch, Ref. 15). In addition, after the reattachment, the distributed stress in the shear layer might be more quickly released due to the zero-stress condition (instead of the zero-velocity condition) on the centerline in the case of free reattachment behind the wedge, resulting in a quicker readjustment of the pressure. The static pressure also begins to rise somewhat earlier than with the plate. This earlier rise is due not only to the orthogonality condition described above, which brings the reattachment point closer to the base for a given base pressure, but also due to the free-shear layer direction, which is more sharply tilted toward the centerline because of the lower base pressure at a given Reynolds number. It is still desirable to carry out a theoretical investigation as to why the base pressure behind the wedge is lower than that with the splitter plate.

When the reattachment is turbulent at higher Reynolds numbers, the pressure-recovery distribution displays a more complicated behavior. It shows a hump in the midst of pressure-recovery process at higher Mach numbers or a local peak after the pressure is sufficiently recovered at lower Mach numbers. Such anomalies are particularly pronounced when the wedge-surface boundary layer was made turbulent (Fig. 26).

These humps and local peaks can be attributed to the interaction of the lip shock, whose strength was found to be substantial (cf. Sec. VI), with the wake shock. Take, for example, a schematic shock pattern, as in Fig. 10a,

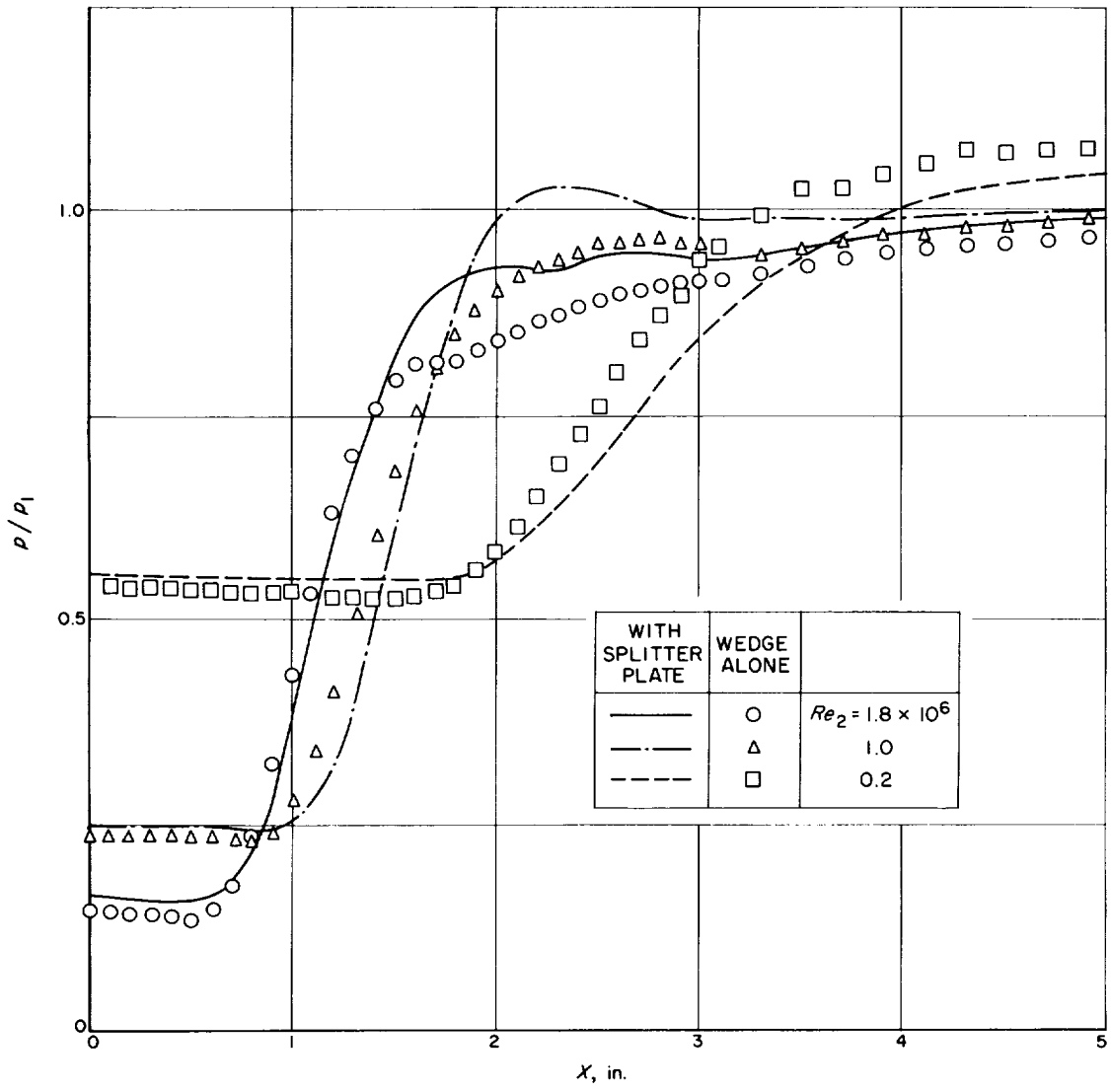

Fig. 23. Pressure-recovery distribution behind a wedge with or without a splitter plate ($M_1 = 2.61$)

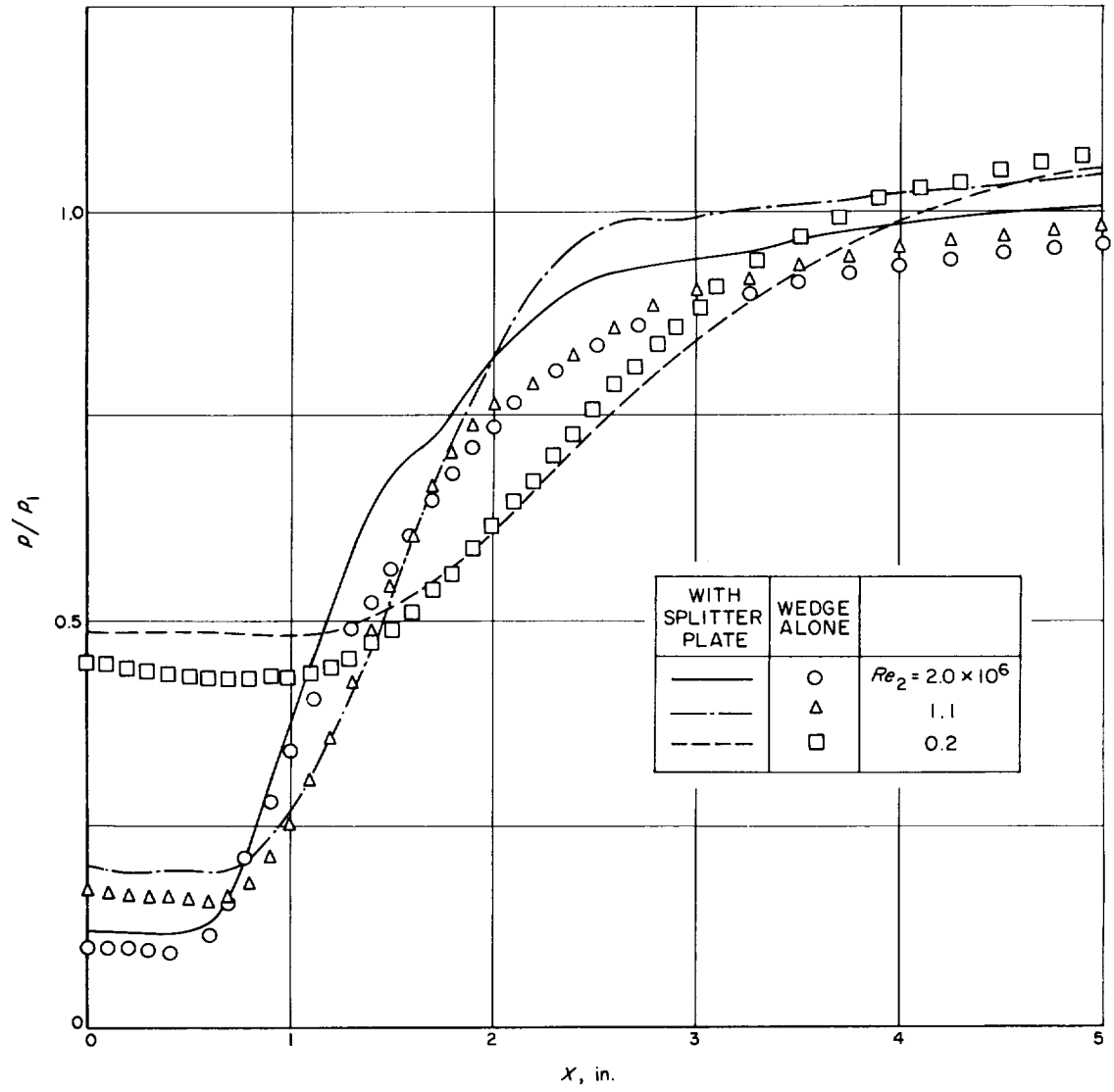

Fig. 24. Pressure-recovery distribution behind a wedge with or without a splitter plate ($M_1 = 3.51$)

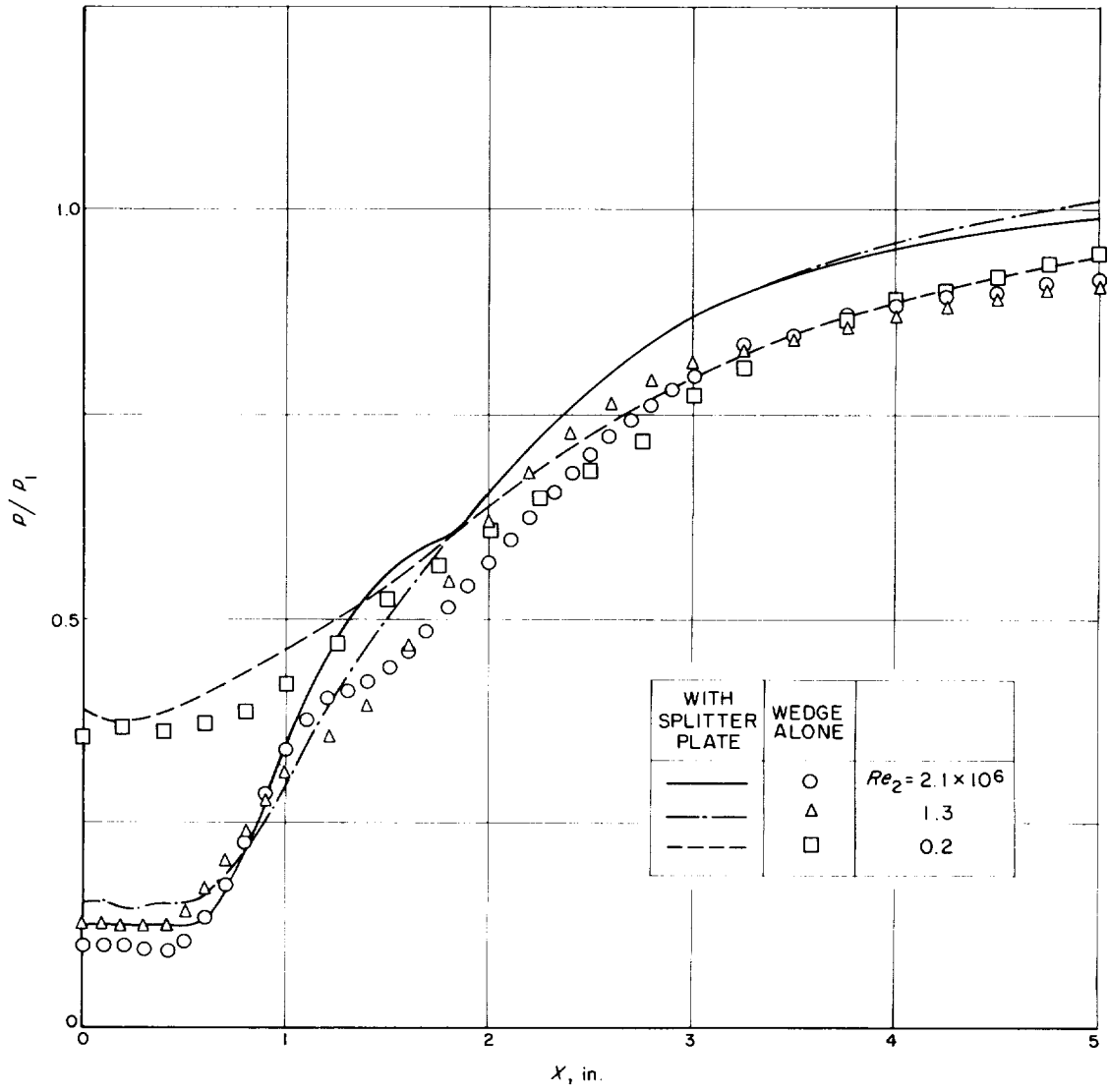

Fig. 25. Pressure-recovery distribution behind a wedge with or without a splitter plate ($M_1 = 4.54$)

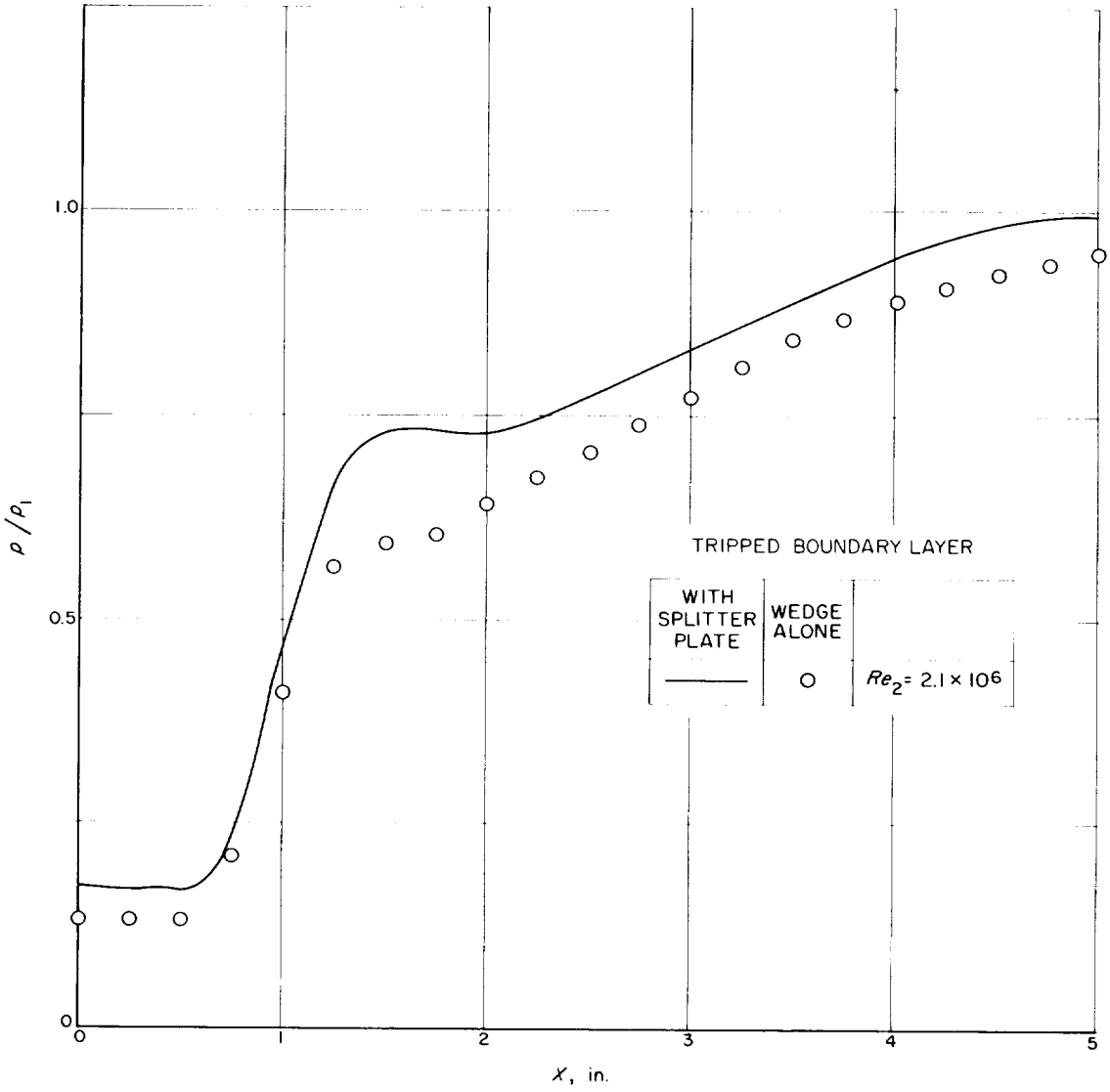

Fig. 26. Pressure-recovery distribution behind a wedge with or without a splitter plate (with boundary-layer trip; $M_1 = 4.54$)

which roughly corresponds to the case, $M_1 = 2.61$, $Re_2 = 1.0 \times 10^6$ in Fig. 23. The flow near the shear layer is expanded first through the expansion fan generated at the separation edge, recompressed by the lip shock to Region 3 where the pressure is approximately equal to the base pressure, and further compressed by the wake shock to reach Region 4. On the other hand, the flow farther away from the shear layer is recompressed only through the wake shock. Therefore, the pressure in Region 4 is higher than that in Region 6, and must be readjusted by a weak expansion wave so that the pressure in Region 5 balances that in Region 6, the two regions being separated by a slip stream. Since the pressure in Region 5 or 6 is normally lower than the free-stream static pressure, the pressure must slowly increase to attain the free-stream value eventually. This situation explains the appearance of the pressure peak and the pressure minimum which follows. Numerical estimates of the peak and minimum values agree rather well with the experimental results in this example. Moreover, the location of the pressure minimum is shown to have a good correlation with the location where the lip shock meets the wake shock (Fig. 27). The location of the pressure peak, on the other hand, does not necessarily correlate with the lip shock–wake shock point, because the wake shock is formed by a coalescence of weak compression waves which are emanated from the slow turning of the flow near the reattachment point. The pressure peak could therefore appear even upstream of the lip shock–wake shock point and nearer the reattachment point. Indeed, as shown in Fig. 28, the pressure-peak location correlates well with the isentropic reattachment point, which was computed from the base pressure by the use of a flow table.

At higher Mach numbers the same process must occur, but the lip shock is now completely imbedded within the free-shear layer, as shown in Fig. 10(b). This is particularly true for the tripped boundary layer, since the shear layer is already quite thick at the separation. In such cases, the pressure variation due to the lip shock–wake shock interaction appears as the hump in the midst of the pressure-recovery process of the shear layer, rather than as the distinct local pressure peak after the static pressure is almost completely recovered.

The dependence on the Mach number of the appearance of the hump or the peak should not be looked upon as universal. If the step or the base height is sufficiently large, the flow pattern as shown in Fig. 10(b) should approach that as shown in Fig. 10(a), even at a fixed Mach number. Consequently, the location of the hump will move toward the end of the pressure-recovery process, and the hump may eventually become the peak. Such a tendency

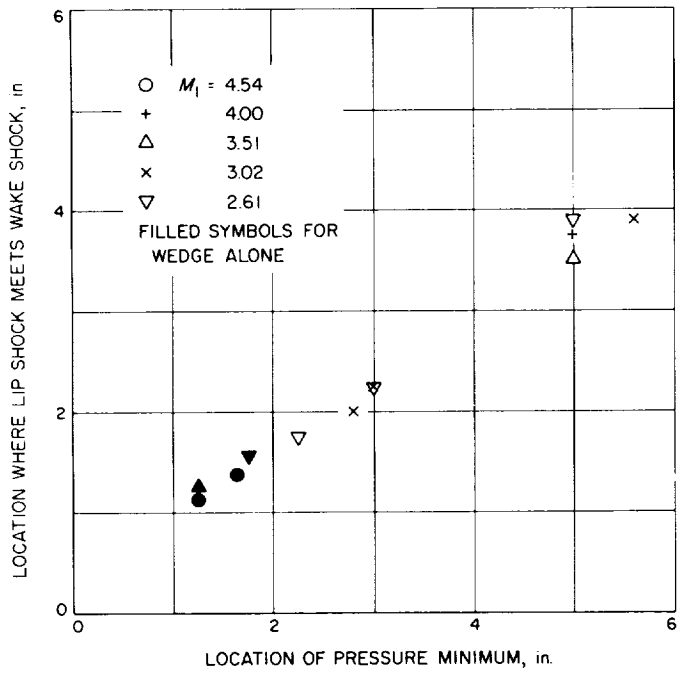

Fig. 27. Correlation between location of pressure minimum and location where lip shock meets wake shock

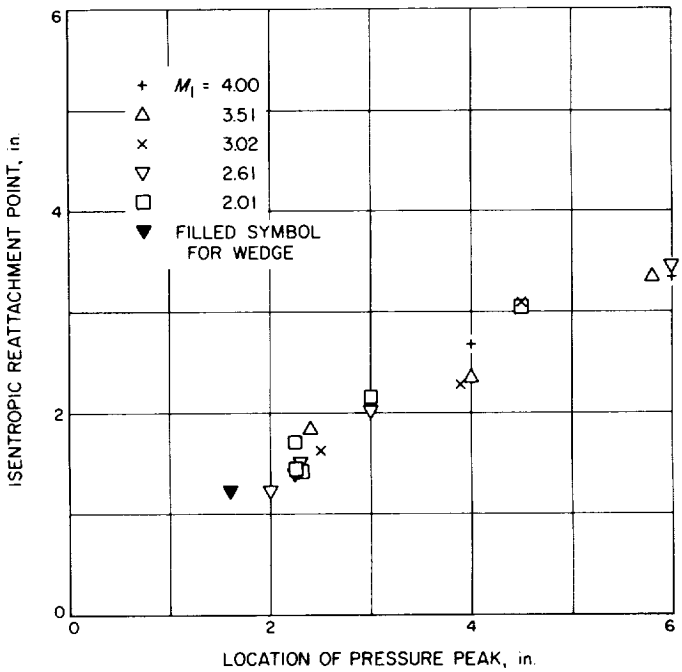

Fig. 28. Correlation between location of pressure peak and isentropic reattachment point

is clearly seen in the pressure distributions measured by Roshko and Thomke (Ref. 1) for three different step heights.

The pressure initially recovered in Region 5 or 6 after a relatively steep increase is substantially lower than the free-stream pressure because the wake shock is quite strong. The higher the Mach number, the lower the initial recovery pressure, reflecting the stronger wake shock. The pressure now continues to increase rather slowly. The slow pressure recovery might be in part attributable to the non-uniform static pressure distribution behind the wake shock. Since the wake shock is covered by the expansion fan, the pressure away from the shear layer (Region 8) is higher than that in the near Region 6. As the shear layer grows after the reattachment, it slowly penetrates into higher and higher pressure regions, resulting in the slow increase in the static pressure along the centerline.

These explanations, which attribute the cause of the humps to the interference of the lip shock, were substantiated, indirectly though, by Roshko in his unpublished experimental results. When the separation edge has been smoothly tapered to give a proper boattail angle so that the flow direction before the separation is guided to be almost parallel to the free-shear layer direction, no expansion should be involved and hence the lip shock is expected either to be eliminated or to reduce its strength. Under such conditions, the hump in the pressure-recovery distribution was indeed observed to disappear. Our experience was that it is very difficult to completely eliminate the lip shock; if the matching of the pressure before the separation edge and that on the base is such that the former is larger than the latter, the regular lip shock is formed; whereas if the former is smaller than the latter, the flow separates on the boattail surface, and the lip shock emerges from the separation point as a separation shock. It will be a subject of, perhaps academic, interest whether the lip shock can be completely eliminated if the matching is perfect. By the reasonable matching, in any event, the lip-shock strength is not only reduced, but also the lip-shock inclination is shifted outward. Both effects account for the disappearance of the hump.

Contrary to the turbulent reattachment, the effect of the lip shock–wake shock interaction is unlikely to appear in the low-Reynolds-number laminar reattachment. At lower Mach numbers, the two shocks are well separated, as shown in Fig. 10(c). The lip shock, however, is weak and oriented away from the recompression region. The interaction is therefore not only weak, but has little influence on the recompression process. On the other hand, the two shocks are merged to become one continuous shock at higher Mach numbers, as shown in Fig. 10(d). Therefore, the interaction as described above simply does not take place. Nevertheless, the merged shock is not of negligible strength, and the recompression process is slower than that at lower Mach numbers.

VI. Lip Shock

A. Estimation of the Strength of Lip Shock

As already discussed, the lip shock interacts with the wake shock to form a slip stream which can be distinctly observed. The lip shock, furthermore, appears to be responsible for a queer behavior of the static-pressure recovery distribution. These two effects of the lip shock point out that the lip shock must be of finite strength. If this expectation is indeed the case, the lip shock not only affects the pressure recovery, but should also contort the initial velocity profile of the free-shear layer so that the basis of most of the base-pressure theories would be endangered. In this section, therefore, an inquiry is made as to the strength of the lip shock based upon shadowgraphs which give a better definition of the lip shock than schlieren pictures.

Some of the earlier investigators assumed that the expansion fan, which spreads out approximately from the separation edge, ended somewhat ahead of the lip shock, as sketched in Fig. 29(a). Such an assumption, which must have been made upon the unfounded and erroneous conviction that the lip shock is negligibly weak, is incompatible with the fact that the lip shock must catch up

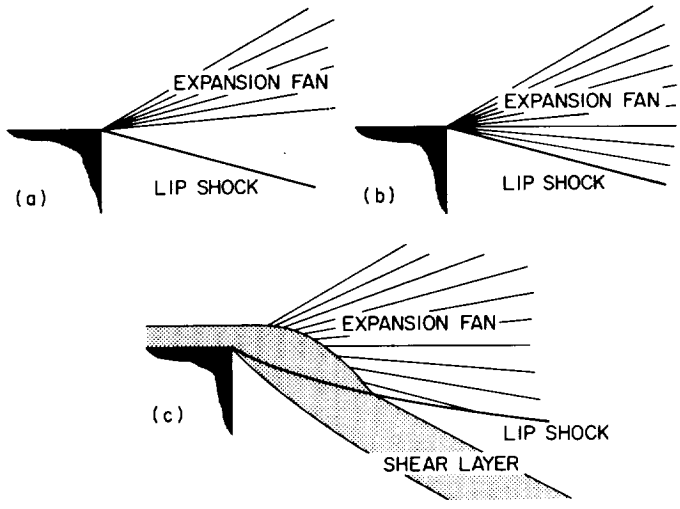

Fig. 29. Lip shock and expansion fan

with the expansion fan inasmuch as the lip shock is a wave of any strength. Indeed, schlieren pictures always indicate that the region between the front edge of the expansion fan and the lip shock is entirely expanding. Therefore, our preliminary assumption was made such that the lip shock was the terminal ray of the expansion fan, Fig. 29(b).

Estimation of the lip-shock strength based upon this assumption was made first by the use of schlieren pictures since our shadowgraphs were not yet taken at the time. It was immediately discovered that the expansion fan extended to result in a substantial overexpansion far below the base pressure, which must predominate behind the lip shock, and hence that the lip shock was of substantial strength. The shock configuration as depicted in Fig. 29(b) is then equally inaccurate because the shock angle should be steeper than the Mach angle and hence the lip shock cannot be one of the rays emerging from the center of the expansion fan. In the meantime, shadowgraphs were taken and provided a better understanding of the lip-shock orientation. The lip shock was found in fact to be slightly curved, and the eccentricity between the center of the expansion fan and the extension of the lip shock toward the separation edge was conveniently negotiated by the presence of the separating shear layer, Fig. 29(c). Although the behavior of the lip shock within the shear layer is most difficult to understand, it is easy to understand why the lip shock must be curved. Since the lip-shock strength is finite, and the shock angle is steeper than the Mach angle, the shock penetrates deeper and deeper into the expansion fan, i.e., into lower Mach-number regions, as it moves from the edge until it is intercepted by the wake shock. The shape of the lip shock under such circumstances is a curve, as is well known.

In order to compute the lip-shock strength, the expansion fan was assumed to be centered at the separation edge, although the center of the expansion fan was actually covered by the shear layer and its location was not precisely known. The estimation proceeded as follows:

Since the shear layer, as well as the lip shock, is clearly seen in most of the shadowgraph pictures, a point P (Fig. 30) was chosen on the lip shock and fairly close to, but outside of, the outer edge of the separated free-shear layer. Upon drawing a line joining the point P and the separation edge S (the chain line in Fig. 30), the angle η is determined. In the following, the condition before the separation will be denoted by a subscript 2 and that immediately in front of the lip shock by 3′. Since the chain line passing through the point P is one of the rays in

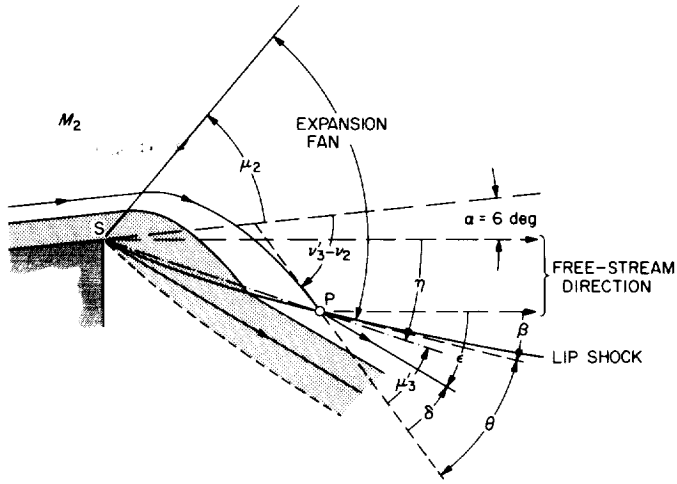

Fig. 30. Flow field and notations pertinent to estimation of lip-shock strength

the expansion fan and is the Mach line corresponding to the condition 3′, there is a relation

$$\nu_3' - \nu_2 = \alpha + \eta + \mu_3'$$

or

$$\nu_3' - \mu_3' = \nu_2 + \alpha + \eta$$

where μ is the Mach angle, ν the Prandtl–Meyer angle, and α the half-angle of the wedge, which is the flow direction before separation relative to the free-stream direction. Angle ν_2 is known for a given free-stream Mach number M_1, and $\nu_3' - \mu_3'$ can be computed, which uniquely gives M_3'. Because the expansion process from 2 to 3′ is isentropic outside of the shear layer, the pressure just before the lip shock, p_3', can be determined.

On the other hand, the static pressure immediately behind the lip shock, p_3, must be approximately equal to the wedge-base pressure p_b, because a) the free-shear layer is usually quite straight in the present experiment except for those conditions depicted in Fig. 10(b) and hence the pressure gradient across the free-shear layer must be quite small, and b) the point P is chosen to be near the outer edge of the free-shear layer. Under this assumption, the lip-shock strength, $\xi = p_3/p_3'$, is taken to be equal to p_b/p_3'.

The lip-shock strength thus computed for the wedge-plate model is plotted in Fig. 31. It is clear that the lip shock is of substantial strength, quite contrary to the common belief that the increase in static pressure across the lip shock must be merely a matter of a few percent. Results of similar analyses applied to the schlieren pictures for both free-wedge and step configurations taken by

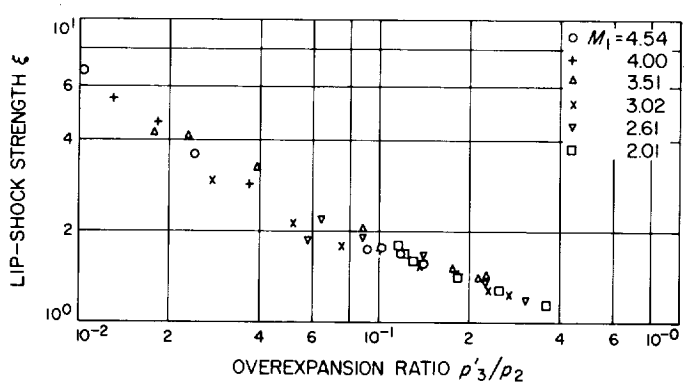

Fig. 31. Lip-shock strength for wedge-plate configuration

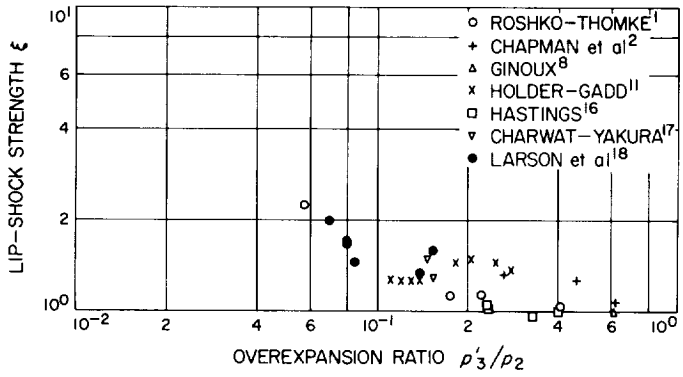

Fig. 32. Lip-shock strength from schlieren pictures taken by other authors

other authors (Refs. 1, 2, 8, 11, 16–18) are given in Fig. 32, which equally shows substantial strength of the lip shock. [Schlieren pictures do not have as much resolution as shadowgraphs. The estimate of the lip-shock strength had to be made by a rougher assumption, depicted in Fig. 29(b), and gave not only inaccurate but also somewhat smaller values of ξ than the more rigorous estimate applied to shadowgraphs.]

It is almost incredible to us why such a simple estimate has never been attempted before and why the unfounded assumption of negligibly weak lip shock has been left uncontested. Only experimental evidence that tends to substantiate the weak-lip-shock assumption is found in an attempt by Hastings (Ref. 16) to measure the static-pressure field. Although his use of a reflection plate is somewhat questionable, the result revealed a negligible strength of the lip shock in his case. However, our estimate from his accompanying schlieren picture also gave a negligible strength. Therefore, our use of his experimental result is only to substantiate our method of estimation, but should not be taken to conclude that the lip shock is always weak.

The estimated lip-shock strength was also obtained for the regular wedge and the knife-edge wedge (Fig. 33), for the rounded-edge models (Fig. 34), and for the boattail models (Fig. 35). For the boattail models, the lip-shock

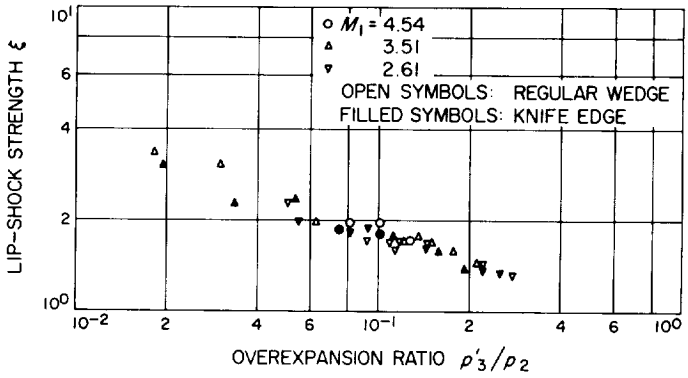

Fig. 33. Lip-shock strength for regular wedge and knife-edge wedge

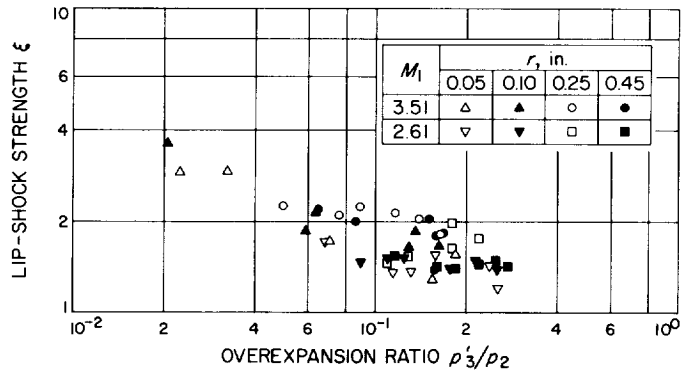

Fig. 34. Lip-shock strength for rounded-edge wedges

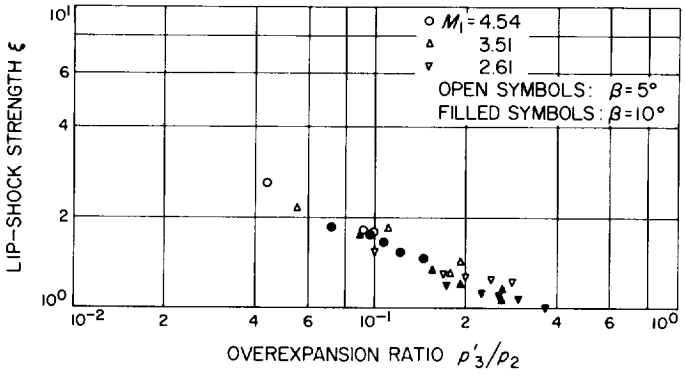

Fig. 35. Lip-shock strength for boattail wedges

strength was estimated only for those lip shocks which emerge from the rear separation edge. As will be discussed later, similar shocks can also emerge from the boattail surface. For the boattail and rounded-edge models, a somewhat different procedure had to be used because the center of the expansion fan was even more ill-defined for these models. The lip-shock orientation angle β was measured as a tangent to the lip shock relative to the free-stream direction. Since (cf. Fig. 30 again)

$$\nu'_3 - (\nu_2 + \alpha) = \beta + \theta$$

we can find the conventional shock angle θ with respect to the flow direction ahead of the lip shock by assuming ν'_3. Since ν'_3 also determines M'_3 and p'_3, we obtain p_b from

$$(M'_3 \sin\theta)^2 = \frac{(\gamma+1)\xi + (\gamma-1)}{2\gamma}$$

and

$$\frac{p_b}{p_2} = \xi \frac{p'_3}{p_2}$$

We could obtain ξ by iteration until p_b agrees with the experimental value.

The lip shock is not only of substantial strength, but the strength is also about the same for all models in terms of the overexpansion ratio p'_3/p_2. We are not certain why the lip-shock strength ξ has a good correlation with p'_3/p_2, independently of the Mach number, at least for a given geometry. We only note here that the correlation between ξ and p'_3/p_2 presented in Figs. 31, 33–35 was actually replotted from an extremely good correlation obtained first between the overexpansion ratio p'_3/p_2 and the base-pressure ratio p_b/p_2, for example, Fig. 36. Several other correlations were also attempted, but in no case was as good a correlation as that in Fig. 36 achieved.

Approximate similarity in the dependence of ξ on p'_3/p_2, regardless of model shape however, does not imply that the lip-shock strength at a given free-stream condition is independent of model shape. Since the base-pressure coefficient p_b/p_1, and hence p_b/p_2, varies for different model shapes, the lip-shock strength varies as well.

In spite of the good correlation above, neither the overexpansion ratio p'_3/p_2 nor the base-pressure ratio p_b/p_2 can be determined *a priori* when a test condition is given; the correlation exists between the overexpansion ratio, which

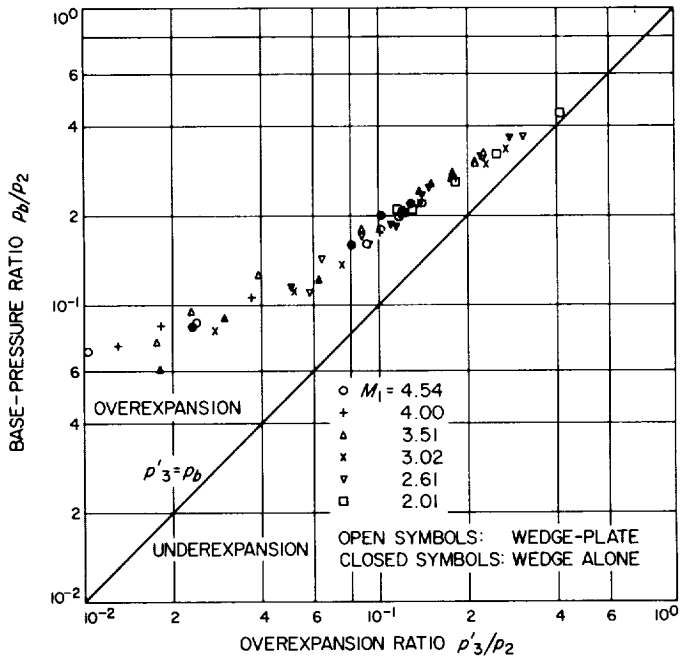

Fig. 36. Correlation between base pressure and pressure in front of lip shock

can be determined from shadowgraphs, and the base pressure measured experimentally. Although, once the base pressure has been measured, the overexpansion ratio, and hence the lip-shock strength, can be determined from Fig. 36, it may still be desirable to have some, even if rough, means to present the lip-shock strength in terms of predeterminable quantities, i.e., Mach number and Reynolds number. It was found that the lip-shock strength could be roughly correlated with a somewhat strange combination, $M_2 Re_2$, as shown in Fig. 37, whereas when lip-shock strength is plotted against Re_2, a strong dependence on the Mach number was noticed. Since the data are limited and

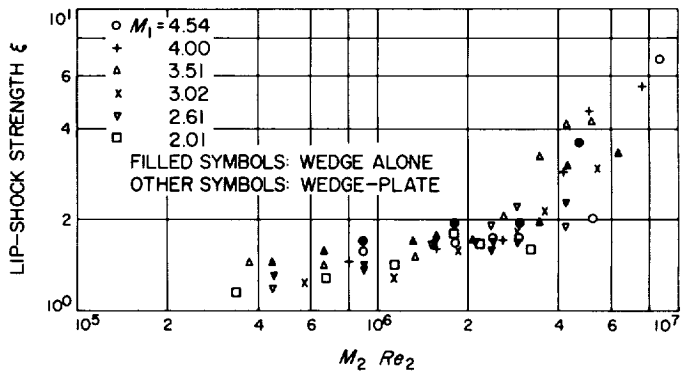

Fig. 37. Reynolds number dependence of lip-shock strength (wedge-plate and wedge alone)

dependence of lip-shock strength on the Mach number is still noticeable, and particularly since the significance of M_2Re_2 is not clear, the correlation in Fig. 37 should not be taken too seriously. Nevertheless, this sort of plotting serves the purpose of demonstrating, for example, that the lip-shock strength for the boattail models (Fig. 38) is appreciably weaker than that for the regular wedge at a given test condition. This fact is hidden in the ξ vs p'_3/p_2 plottings.

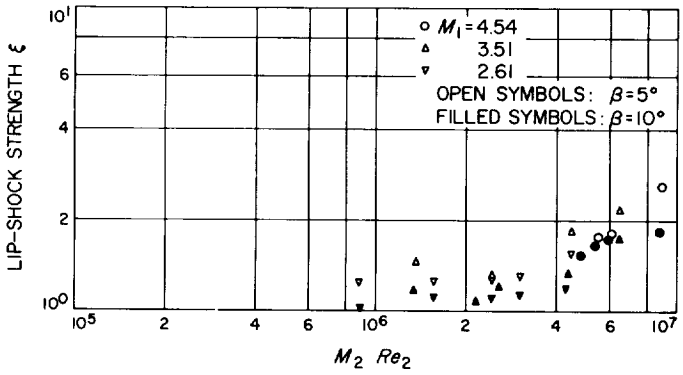

Fig. 38. Reynolds number dependence of lip-shock strength (boattail)

Before leaving this section a remark is in order relative to Fig. 33. The lip-shock strengths for the regular wedge and the knife-edge model are seen to be very well correlated with each other. Since the base pressures for the two models were already found to be virtually identical (Fig. 17), not only the lip-shock strengths but also the shock patterns must be the same for the two models under a given free-stream condition. Although these observations might not be too much of a surprise since the undercut step has been known to give nearly the same flow field as the rectangular step (Ref. 16), they are still contrary to our expectations and will be referred to again near the end of Sec. VI-D.

B. Examinations of the Estimation

Since the discovery of the substantial strength associated with the lip shock is contrary to the prevailing belief, examinations of the adequacy of the estimation are in order.

First, the measured expansion angle η is plotted against the base-pressure coefficient p_b/p_1 in Fig. 39. Plotted also in the same figure are the expansion angles for the trailing end of the expansion fan if there were no overexpansions, i.e., $\xi = 1$. With differences between the two angles amounting to as much as 10° or even more, there is no

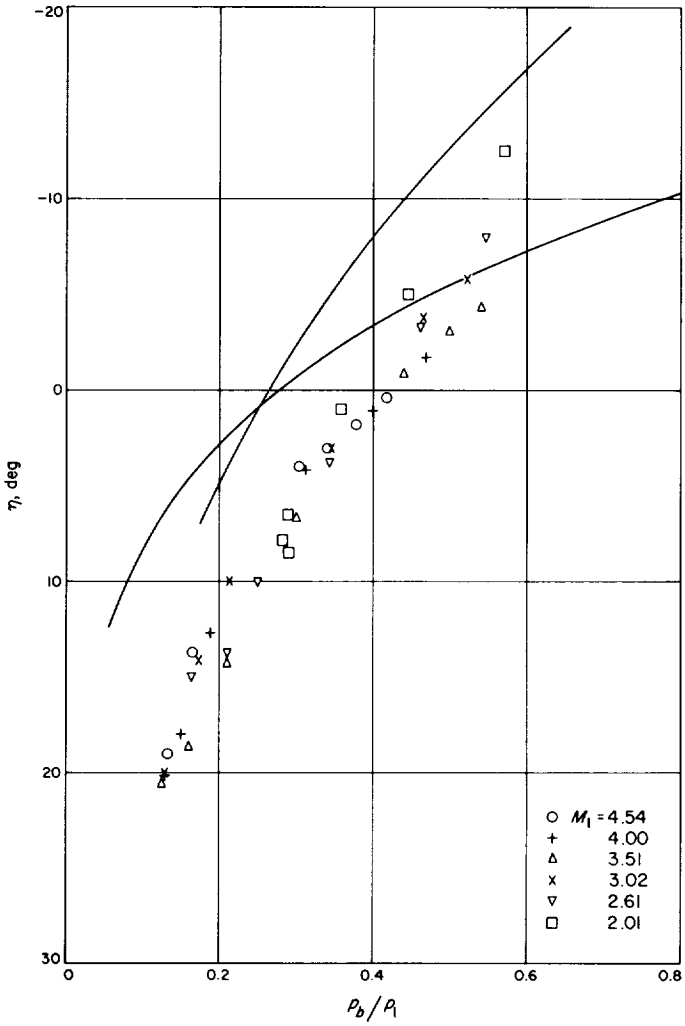

Fig. 39. Overexpansion angle for lip shock (wedge-plate); lines indicate trailing-end angles of expansion fan without overexpansion

doubt that the flow has definitely overexpanded and that the finite strength as estimated is not due to error in measuring expansion angles.

Once the angle η and hence the local Mach number M'_3 as well as the pressure p'_3 were determined, three quantities, ξ, θ, and p_b/p_1, were involved with respect to the lip shock. The following examinations were made:

(1) By knowing p_b/p_1, we immediately found ξ, as in the preceding estimation. From ξ and M'_3, the shock angle θ or its orientation angle β could be computed. The computed β shows good agreement with β measured in the shadowgraph pictures in Fig. 40. In other words, the shock angle is compatible with the estimated lip-shock strength.

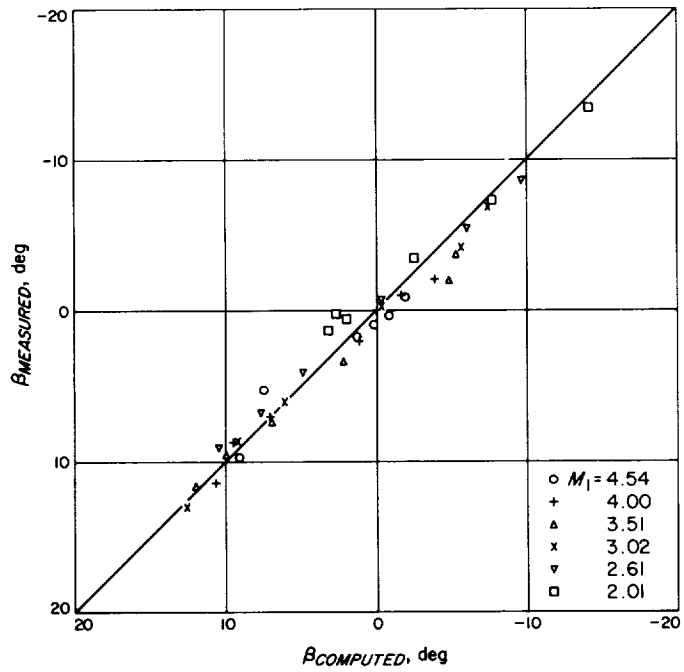

Fig. 40. Comparison of measured and computed lip-shock inclination angles

(2) M_3' determined the flow direction ahead of the lip shock. Therefore, the measured β gave the shock angle θ. From θ and M_3', the lip-shock strength ξ could be computed without knowing p_b/p_1. The lip-shock strength ξ thus computed shows good agreement with ξ previously determined as p_b/p_3' in Fig. 41, i.e., the measured shock angles give appropriate shock strengths.

(3) Finally, although redundant, the base-pressure coefficient p_b/p_1 was computed from ξ obtained above and p_3', and compared in Fig. 42 with the p_b/p_1 experimentally obtained. Agreement in this comparison is somewhat less satisfactory than the previous two agreements. This deficiency, however, has resulted mainly from the inaccuracy in determining the angle β of a tangent to the lip shock. In fact, once we obtained the comparison in Fig. 42, we could readjust β readings within plausible error limits so as to obtain an almost perfect correlation. Such iterations were not made, however, in order to demonstrate largest possible errors involved in our estimation procedure. Nevertheless, it is confirmed that the measured expansion angle η and the measured shock angle β provide appropriate base pressures.

We are quite convinced after these examinations that our estimate of the lip-shock strength was reasonable and the strength could indeed be substantial.

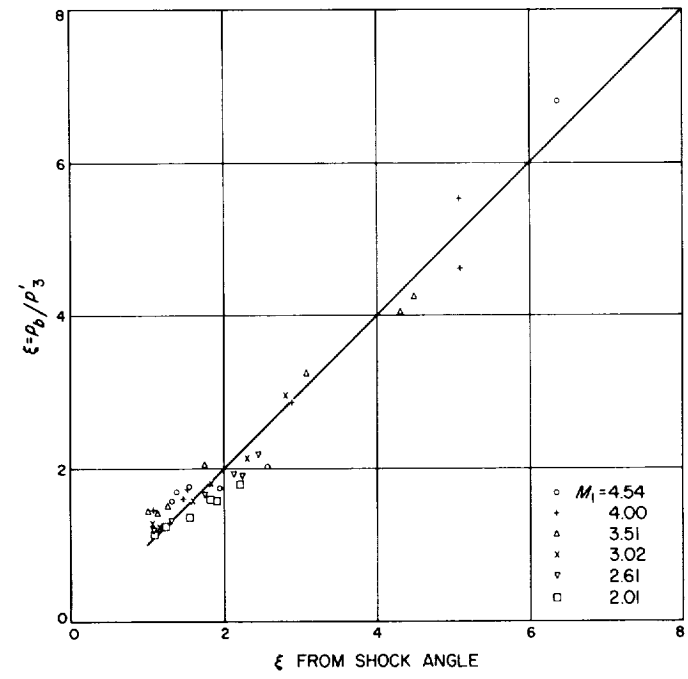

Fig. 41. Comparison of lip-shock strengths; estimated from base pressure vs the strength computed from shock angle

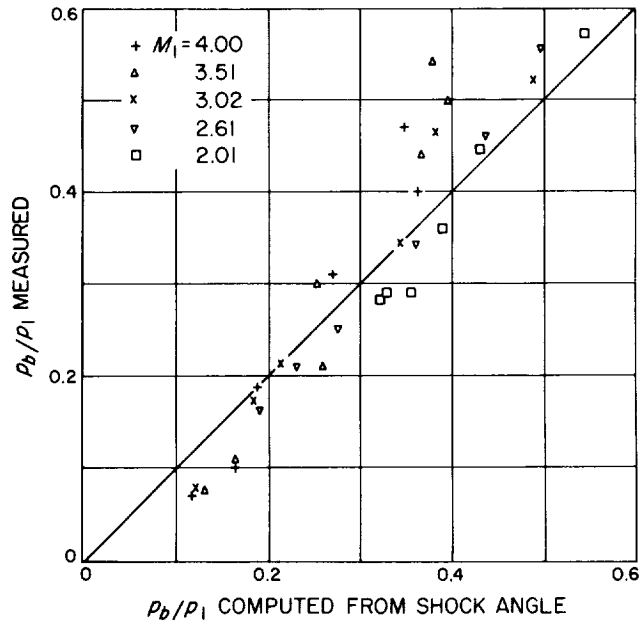

Fig. 42. Comparison of measured base pressure and pressure estimated from shock angle

During these computations we noticed that, for a given Mach number, the shock angle θ was constant for a wide range of Reynolds number and could be given by a simple interpolation formula

$$\sin\theta = 0.7\, M_2^{-5/6}$$

from which the lip-shock strength could be computed and is shown in Fig. 43 in good overall agreement with the experimental results. Included in this figure also is a line for $M_1 = 6.00$ by extrapolating the above formula obtained in the present experimental range. If this extrapolation holds, no significant change in the lip-shock strength is anticipated, even at this higher Mach number, in this manner of correlation. Physical significance of the approximately constant shock angle is unknown.

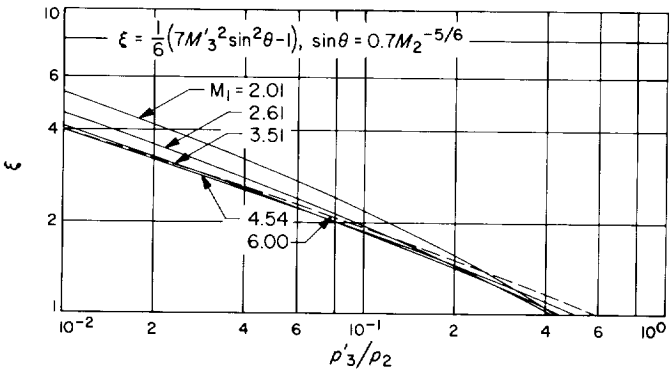

Fig. 43. Computed lip-shock strength with constant shock angle

By knowing M'_3 and ξ, we could find the refraction angle δ. Since we already know the flow direction corresponding to M'_3, we could also find the flow direction behind the lip shock. On the other hand, we can compute the flow direction corresponding to the base pressure under the assumption of isentropic expansion, i.e., without the lip shock. Sample comparisons of the two angles thus computed actually showed good agreement with each other within a fraction of a degree. Therefore, the flow direction could be determined with a good approximation by the latter simple isentropic computation. In fact, the flow direction determined from the free-shear layer direction in shadowgraphs agreed quite well with such an estimation (Fig. 44). Needless to say, this correspondence is only an approximation in the case of finite shock strength.

C. Experimental Determination of the Lip-Shock Strength

Although the lip-shock strength estimated from shadowgraphs was believed to be reasonably accurate, it was

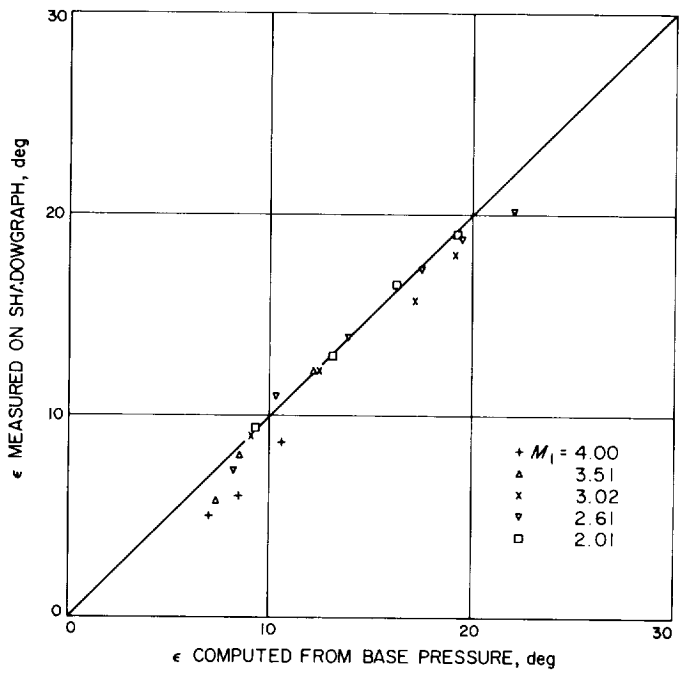

Fig. 44. Separated flow direction; measured on shadowgraphs vs isentropic computation

felt desirable to experimentally substantiate the assumptions involved in the estimation procedure and verify the finite strength. Since static pressure is rather difficult to measure, particularly in such a field where the flow direction is rapidly changing as in the present case, pitot surveys were made under a condition equivalent to the case shown in Fig. 1, i.e., $M_1 = 2.61$, $Re_2 = 1.0 \times 10^6$. In this example, the separated free-shear layer appears to be laminar until it approaches the reattachment point, and is well isolated from the lip shock except in the region very near the separation edge. Losses in the total pressure across the bow shock and the lip shock were estimated to be 0.4% and less than 0.3%, respectively, and the total pressure other than in the shear layer can therefore be assumed to be constant and equal to the tunnel supply pressure (62 cm Hg) for all practical purposes. Thus, the pitot-pressure distribution, except in the shear layer, could be subjected to numerical estimate. The raw data of the pitot surveys are plotted in Figs. 45 and 46.

Interpretations of the flow field are well substantiated by these measurements. The expansion fan extends all the way to the lip shock. Jumps in the pitot pressure correspond accurately to the lip-shock locations. Following the joint between the lip shock and the wake shock, a small discontinuity in the total pressure indicates the enthalpy discontinuity across the slip stream.

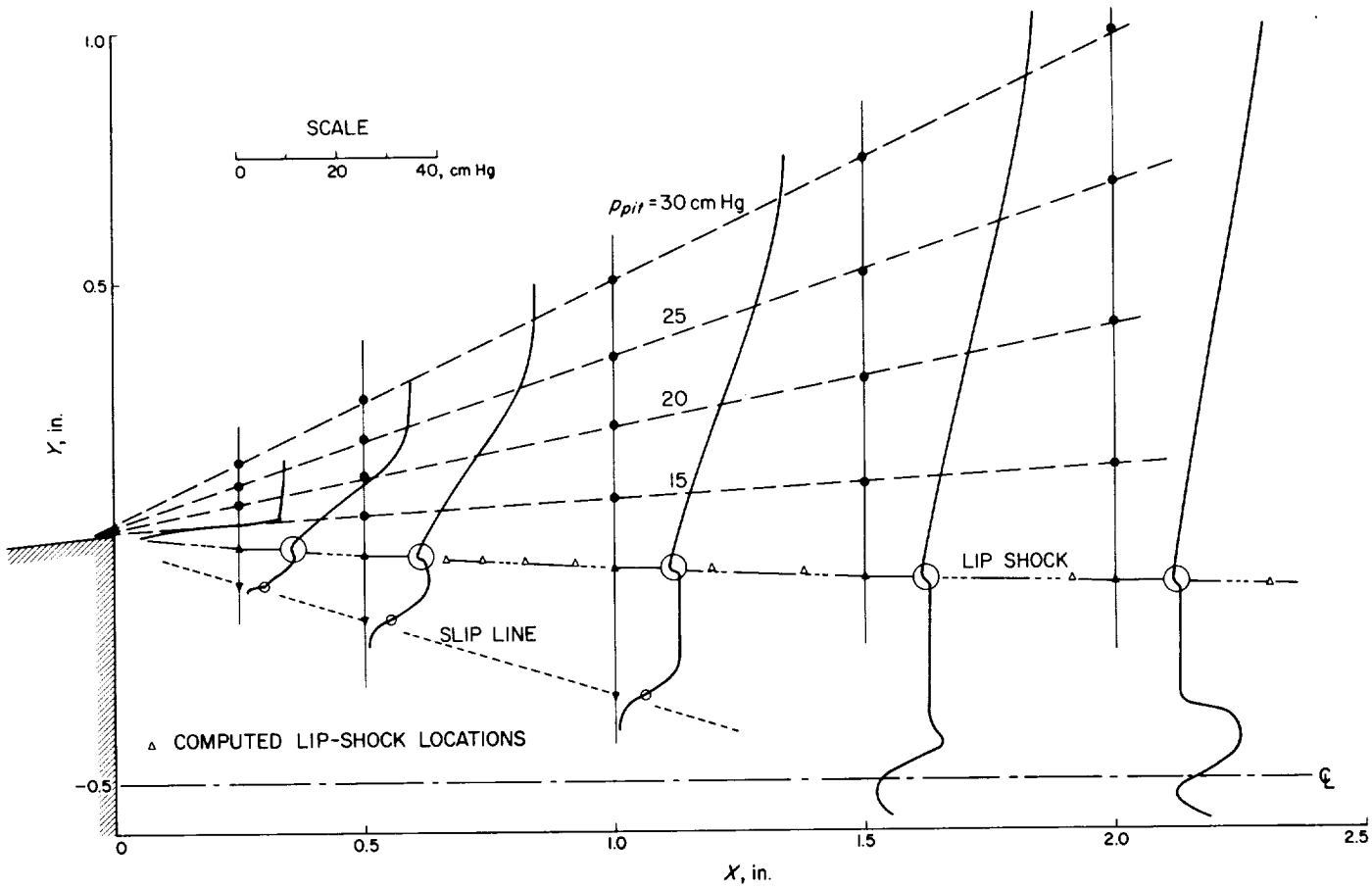

Fig. 45. Pitot-pressure profiles at $M_1 = 2.61$ and $Re_2 = 1.0 \times 10^6$

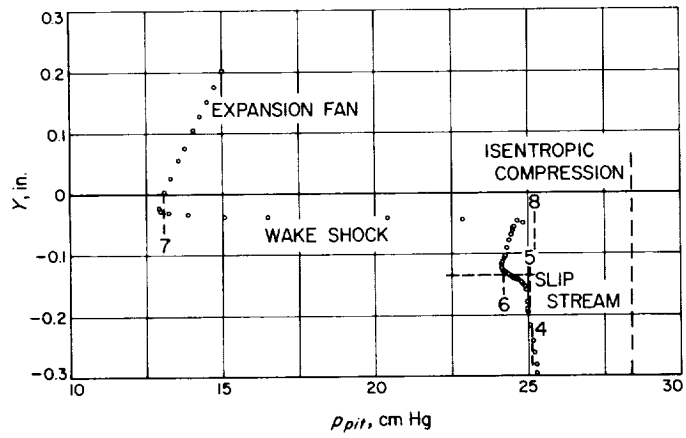

Fig. 46. Pitot-pressure profile at X = 3.5 in. ($M_1 = 2.61$ and $Re_2 = 1.0 \times 10^6$). Numbers refer to regions indicated in Fig. 10

In addition to these general observations, minute discontinuities were also detected in the pitot-pressure profile across the free-shear layer. These discontinuities must be the same slip line as that reported by Charwat and Yakura (Ref. 17). In many of the shadowgraphs taken at lower Mach numbers and at moderate to low Reynolds numbers, two nearly parallel white lines were seen (cf. Fig. 1). While the outer white line can be recognized as the outer edge of the free-shear layer due to a large second derivative of the density profile, the inner edge should have been seen only as a dark line if there were no anomalies. The inner white line is now recognized as the slip line since the locations of the two coincided perfectly. The slip line appears to be closely related to the separation point and hence to the dividing streamline, but its cause is not exactly known. What is believed to be the case, however, may be explained by the use of Fig. 47. The boundary layer (A) becomes fatter (B) as it approaches the expansion corner. As the flow goes through the expansion fan, the shear-layer profile is further fattened and even the layer very near the surface must be strongly accelerated, except for the fluid which directly attaches the surface (C) Now, the flow separates from the surface, and the inner shear layer begins to develop (D). This situation may be clearly seen in the pitot-pressure profile at $X = 0.25$ in.

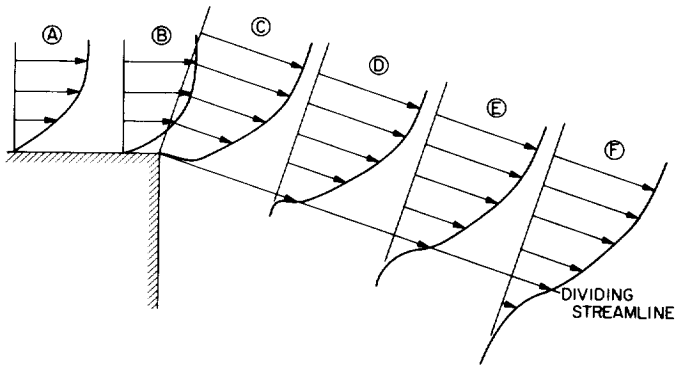

Fig. 47. Suspected development of free-shear layer

In this situation, the density distribution will be such that there are two positive maxima of its second derivative corresponding to the outer edge of the inner shear layer as well as to the outer edge of the entire free-shear layer, and one negative maximum corresponding to the inner edge of the inner shear layer, thus resulting in two white lines and one dark shade inside of the inner white line in the shadowgraphs. As the inner shear layer develops, its sharp outer edge gradually dissolves into the whole free-shear layer, (E) and (F), and the inner white line fades away. Under this interpretation, the "slip" line seems to be somewhat of a misnomer since there is no slip in the sense of slip stream or otherwise. The overshoot in the pitot pressure distribution experimentally observed by Charwat and Yakura at the slip line must have given them an impression of the presence of some kind of slip, but should rather be looked upon as no more than the well-known behavior of pitot tube readings near the outer edge of high-shear layers such as thin laminar boundary layers.

This suspected behavior of the free-shear layer is, of course, closely related to or derived from the idea of two-layer analysis currently being considered in connection with the base-pressure prediction. There is some reason to speculate that the velocity along the dividing streamline might overshoot an asymptotic value and then approach it from above under such circumstances as considered here, rather than approaching it monotonically from below.

Further noted is that the initial recompression process as the flow approaches the reattachment point appears to be confined within the shear layer. Finally, the centerline of the reattached viscous wake was observed to be shifted downward by about 0.025 in. from the geometrical centerline. The shift, which could also be detectable from the neck shock locations in the shadowgraph, is probably due to the imperfect matching of the front and rear parts of the model rather than possible error in the pitching angle of the model.

The first of more quantitative examinations of the pitot-survey data was made in order to determine the center of the expansion fan. By extrapolation, the center was found to be located slightly upstream of the separation edge; when the center was taken to be at $X_0 = -0.04$ in. and $Y_0 = 0$ in. in the coordinate system shown in Fig. 45, the pitot-pressure data not only correlated well with each other, but also agreed with the Prandtl–Meyer relation, Fig. 48. The good agreement should be emphasized for $Y - Y_0 < 0$ as well as for $Y - Y_0 \geqq 0$. The upstream shift was approximately equal to the computed boundary-layer thickness, 0.035 in., and its smallness substantiates the assumption that the expansion fan is centered at the separation edge, at least in this test case. Consequently, the static pressure p'_3 estimated previously from shadowgraphs can now be trusted.

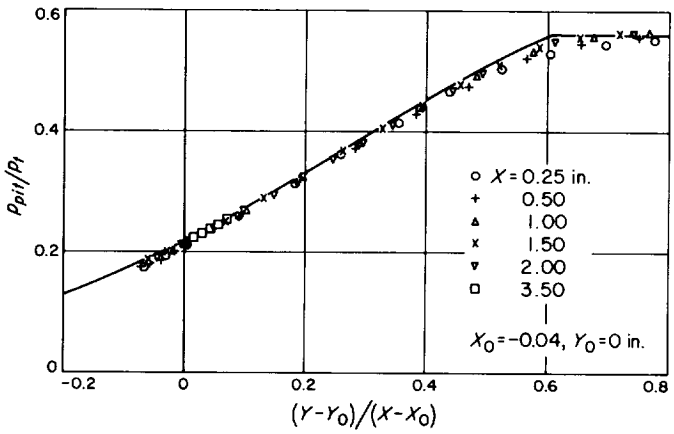

Fig. 48. Pitot-pressure distribution in expansion fan; curve is computed with center at $X_0 = -0.04$ and $Y_0 = 0$

Since the total pressure was virtually constant across the lip shock as well as the bow shock, the static pressure p_3 behind the lip shock could be computed from the pitot pressure and was found to be constant in the region between the lip shock and the free-shear layer but approximately 10% smaller than the measured base pressure. A small streamline curvature is enough to account for this much pressure difference, but there was no indication of pressure gradient across the flow to verify the streamline curvature. Probable cause of the pressure difference is still unknown.

Insertion of the pressure probe of a finite size could cause a local flow distortion and result in erroneous readings. In this case, however, we are inclined to believe in this lower static pressure because of the following indirect evidence. If one denotes by (X, Y) the location of the lip shock relative to the separation edge,

$$-Y/X = \tan\eta \qquad \text{and} \qquad -\frac{dY}{dX} = \tan\beta$$

by definition (cf. Fig. 30). The general formulae for the lip-shock coordinates are

$$\frac{X}{X_1} = \exp\left\{\int_{\eta_1}^{\eta} \frac{d\eta}{\cos^2\eta\,(\tan\beta - \tan\eta)}\right\}$$

and

$$-\frac{Y}{X_1} = \frac{X}{X_1}\tan\eta$$

in which (X_1, Y_1) are the coordinates of a reference point on the lip shock. At each given value of η, the Prandtl–Meyer relation gives the conditions in front of the lip shock, M'_3, p'_3, and Mach angle μ'_3. Now, if one assumes the static pressure behind the lip shock to be the base pressure p_b or takes the measured value p_3, the lip shock strength will be either $\xi_b = p_b/p'_3$ or $\xi_3 = p_3/p'_3$. The shock angle θ is then computed from M'_3 and either ξ_b or ξ_3 by the oblique-shock relation. β will then be related to η by $\beta = \eta + \mu'_3 - \theta$, and the integrand in the above formula can be evaluated at each η. Therefore, by knowing the location (X_1, Y_1) of one point on the lip shock, the entire shape of the lip shock outside of the shear layer can be computed. In the present sample case, (X_1, Y_1) were chosen to be (0.50, − 0.045). Two shock shapes were obtained for ξ_b and ξ_3 (Fig. 49). The shape obtained from ξ_3 was found to coincide with the lip shock observed in the shadowgraph as well as with that determined by the pitot surveys (Fig. 45) almost perfectly, whereas the one from ξ_b did not, obviously because the shock angle was too large due to too large values of ξ. Although admittedly circumstantial, this piece of evidence appears to verify that the pressure behind the lip shock is truly lower than the base pressure.

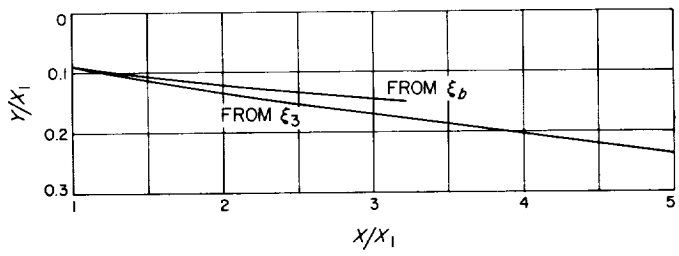

Fig. 49. Computed lip-shock shapes; lower curve is replotted in Fig. 45

The above computation relates η to X. The pitot and static pressures in front of the lip shock and hence the lip-shock strength also were initially computed as functions of η, but they are now related to X. The computed distributions of these quantities along the lip shock are compared in Figs. 50, 51, and 52 with the experimental values. Thus, the basic assumptions made in estimating the lip-shock strength have been completely substantiated, except for the unexpected and as yet unexplainable lower pressure behind the lip shock. As shown in Fig. 52, the lip-shock strength reduces as X increases in this test case.

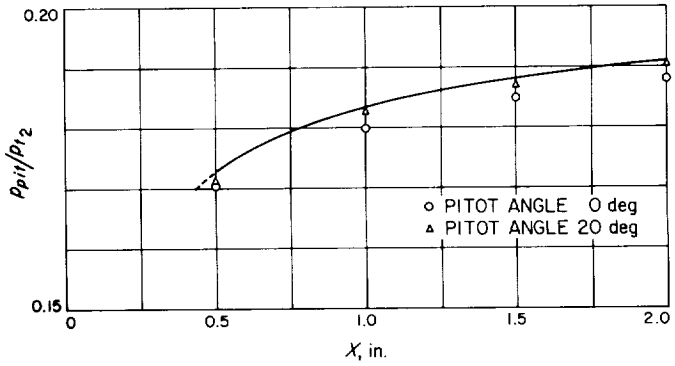

Fig. 50. Pitot pressure immediately ahead of lip shock in comparison with computed curve

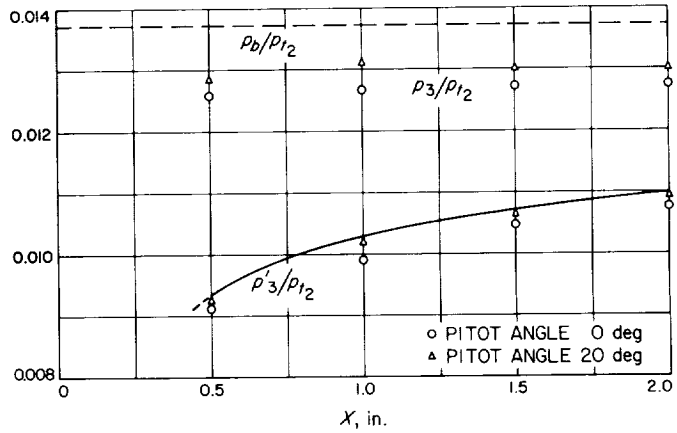

Fig. 51. Static pressures immediately ahead of and behind lip shock computed from pitot pressures, in comparison with computed curve and measured base pressure

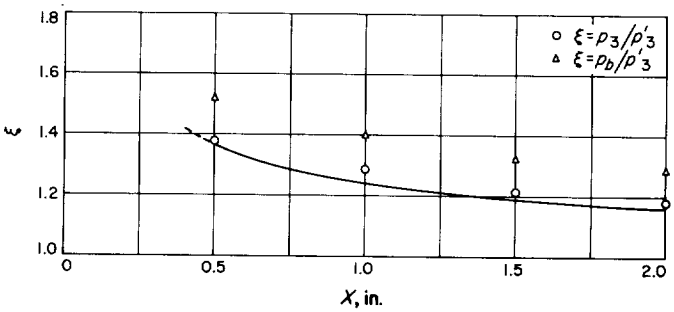

Fig. 52. Lip-shock strength distribution in comparison with computed curve

It should be noted that, when the lip shock smoothly merges to the wake shock at higher Mach numbers but lower Reynolds numbers, the strength of the merged shock would continuously increase.

Since the computation procedure has now been confirmed, we may extend our computation to find the pitot pressures in the Regions 3 through 8 in Fig. 10(a). As marked by short vertical lines with numbers identifying the regions in Fig. 46, those computed pitot pressures are compared with the pitot-pressure distribution at $X = 3.5$ in., which is approximately ½-in. behind the location where the lip shock meets the wake shock. Agreements are seen to be extremely good. Therefore, the pitot surveys have not only demonstrated the essential adequacy of the lip-shock-strength estimation procedure but have also proven that the interpretation of the entire flow field as judged from the optical observations is correct.

Indicated also in Fig. 46 is the value of pitot pressure if the flow outside the free-shear layer were to undergo an isentropic compression by changing its direction around the reattachment. The experimental pitot pressure is seen to fall far short of the isentropic value. Therefore, the wake shock originates so close to the reattachment point in this test case that nowhere in the flow field does an isentropic compression take place in the recompression process. This is not to rule out, however, the possibility of isentropic compression at lower Reynolds numbers or of pseudoisentropic streamtubewise compression within the shear layer.

While the test case was mainly aimed at quantitatively verifying the lip-shock strength, further pitot surveys were conducted with a boundary-layer trip attached on both surfaces of the wedge. Although the lip shock was clearly seen with the tripped boundary layers (Figs. 4a–f and 53) and the humps in the pressure-recovery distribution, which are specifically attributable to the lip shock, are

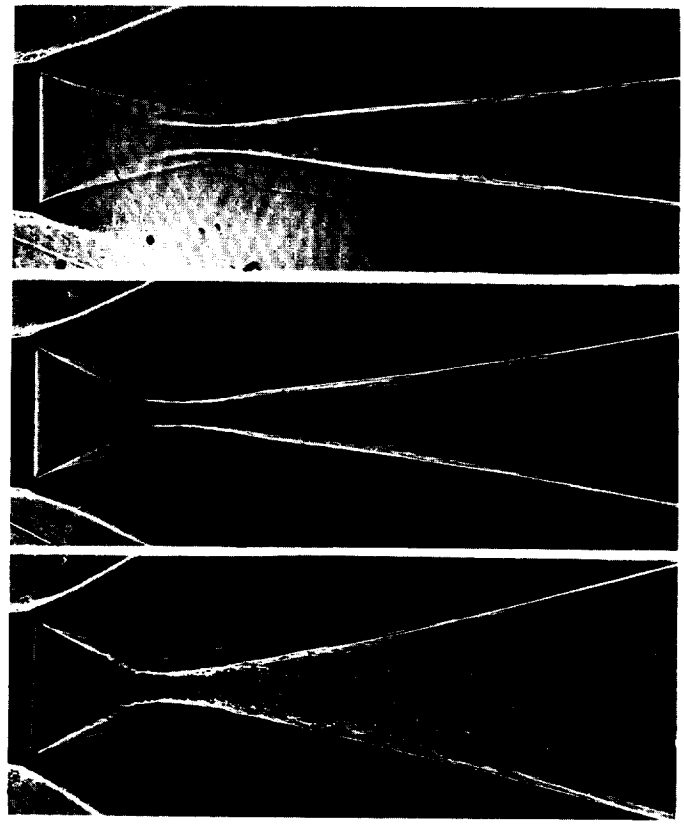

Fig. 53. Shadowgraphs behind a wedge with boundary-layer trip; from top: $M_1 = 4.54$, 3.51, and 2.61

present even with the naturally provoked transition (Ref. 1), there has been some speculation that the lip shock might not exist if the boundary layer was turbulent. It was therefore felt desirable to experimentally confirm the presence of the lip shock even in the turbulent condition. The tripped turbulent boundary layers were inherently much thicker than the untripped ones, and the flow patterns were like Fig. 10(b) at any Mach number with the lip shock completely imbedded in the free shear layer. The pitot surveys alone were not capable of determining the shock strength in such cases, and only the raw data for $M_1 = 4.54$ are shown in Fig. 54, to unequivocally verify the presence of the lip shock.

Figure 55 shows the pitot pressure distribution at an X location which was after the reattachment and behind the location where the lip shock met the wake shock. A discontinuity of the pitot-pressure profile in the viscous wake can be identified as the slip stream caused by the interaction between the two shocks, although the slip stream, which was also imbedded within the reattached viscous wake, could not be seen in the shadowgraph

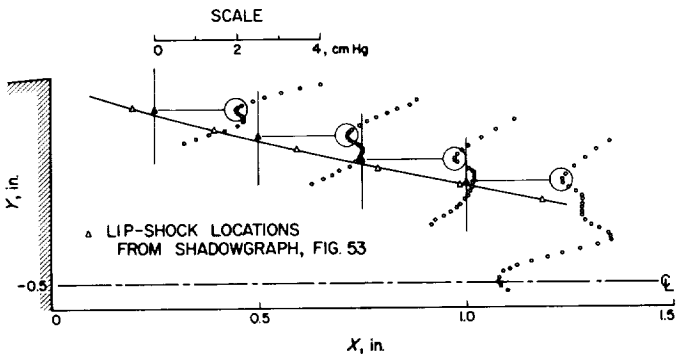

Fig. 54. Pitot-pressure profiles behind a wedge with boundary-layer trip ($M_1 = 4.54$, $p_t = 300$ cm Hg)

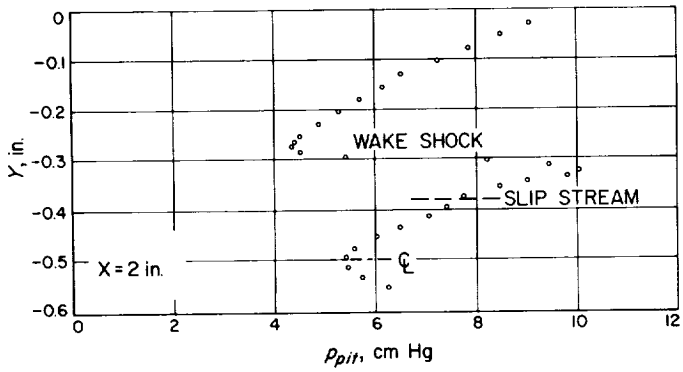

Fig. 55. Pitot-pressure profile at X = 2 in. behind a wedge with boundary-layer trip ($M_1 = 4.54$, $p_t = 300$ cm Hg)

because of a highly turbulent condition in this case. This distorted pitot-pressure profile is another manifestation of the strong effects of the lip shock and implies additional complications in dealing with the base-pressure problem theoretically.

As discussed already in reference to Fig. 29 and as computed in Fig. 49, the shape of the lip shock in the isentropic field of the expansion fan is concave upward. It might look somewhat strange that the lip shock is still concave even when it is completely imbedded in the shear layer, as particularly seen in the case of tripped boundary layers. In such cases of substantial lip-shock strengths, the concave shape may have resulted from a) a strongly diverging flow field and/or b) a shock wave intensifying toward the outer edge of the shear layer. In contrast, a weak lip shock is seen to be convex behind the 17-deg boattail model, in which case the flow was not diverging either (cf. Sec. VI-B).

D. Inquiry into the Cause of Lip Shock

It has now been confirmed that the flow associated with the so-called Prandtl–Meyer expansion is not a simple expansion, contrary to the assumption usually made, but actually overexpands first and is then recompressed by the lip shock of a finite strength. Further experiments were conducted in an attempt to inquire what really caused the lip shock.

A prevailing thought on the cause of lip shock, which seems to have been originally proposed by Charwat and Yakura (Ref. 17) and has recently been worked out by Weinbaum and Weiss (Refs. 19, 20), is the coalescence of the reflected second family of characteristics that originate from the interaction between the oncoming boundary layer and the expansion fan (Fig. 56). In this theory the shear layer is treated as an inviscid rotational field and the reflection of the characteristics is assumed to take place at (or near) the sonic line. This theory will be hereafter referred to as the inviscid rotational theory. The computed result is claimed to have good agreement with the Minnesota experiment by Larson *et al.* (Ref. 18), although it is not quite certain whether the computation has been really carried out.

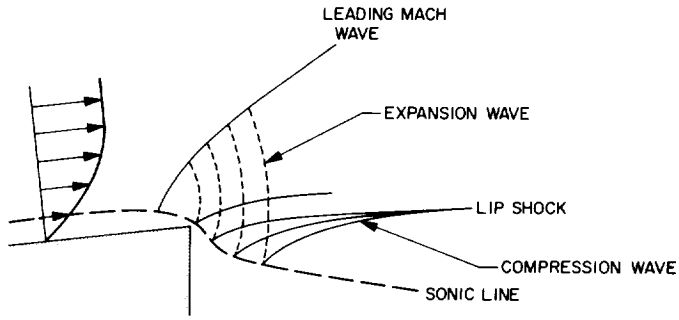

Fig. 56. Lip-shock formation according to purely inviscid rotational field theory (after Weiss and Weinbaum)

The lip shock, however, is observed to be formed immediately at the body surface in almost all of the present test conditions except at the highest Mach number and the lowest Reynolds number. Such prompt shock formations already led us to suspect that the inviscid rotational theory might not be the essential explanation of the lip shock formation, since the theory is to result in a relatively slow coalescence of the reflected wavelets away from the surface.

On the other hand, the flow over a circular cylinder experiences an overexpansion, and the boundary layer is

bound to separate in the region of adverse pressure gradient (Ref. 21). Since the streamline in a viscous layer makes a finite deflection at the separation point given by

$$\tan \delta = -3 \frac{d\tau_0}{dx} \Big/ \frac{dp}{dx}$$

where τ_0 is the shearing stress at the surface ($y = 0$) (Ref. 15), and since the sonic line must be located close to the surface after the overexpansion, the so-called separation shock could be formed very near the surface. At first sight, it might not be easy to visualize that the same mechanism could take place also at the sharp separation edge, but this viscous separation effect was suspected to be the real culprit for the lip-shock formation because of the apparent resemblance between the separation shock and the lip shock.

Surface-pressure distribution, particularly near the separation edge, was measured first in order to obtain an insight into the overexpansion phenomenon and the cause of lip shock. It is well known that the surface pressure before the separation should gradually decrease toward the separation edge because the effect of the expansion fan propagates upstream through the subsonic portion of the approaching boundary layer. The surface-pressure distribution on the base, on the other hand, has been conceded to be uniform except in the case of low density and low Reynolds number (Ref. 22).

Our measurements were made to the point as close as 0.031 in. from the separation edge, and the results are plotted in Fig. 57a–d. The upstream effect is seen to extend to the distance of approximately the boundary-layer thickness as expected and in accord with the location of the center of the expansion fan determined previously. What was not expected was a sharp overexpansion in the surface pressure on the base face immediately behind the edge which was consistently observed for free-stream Mach numbers greater than 3.51. A similar overexpansion might exist at smaller Mach numbers in a narrower region and in a lesser amount.

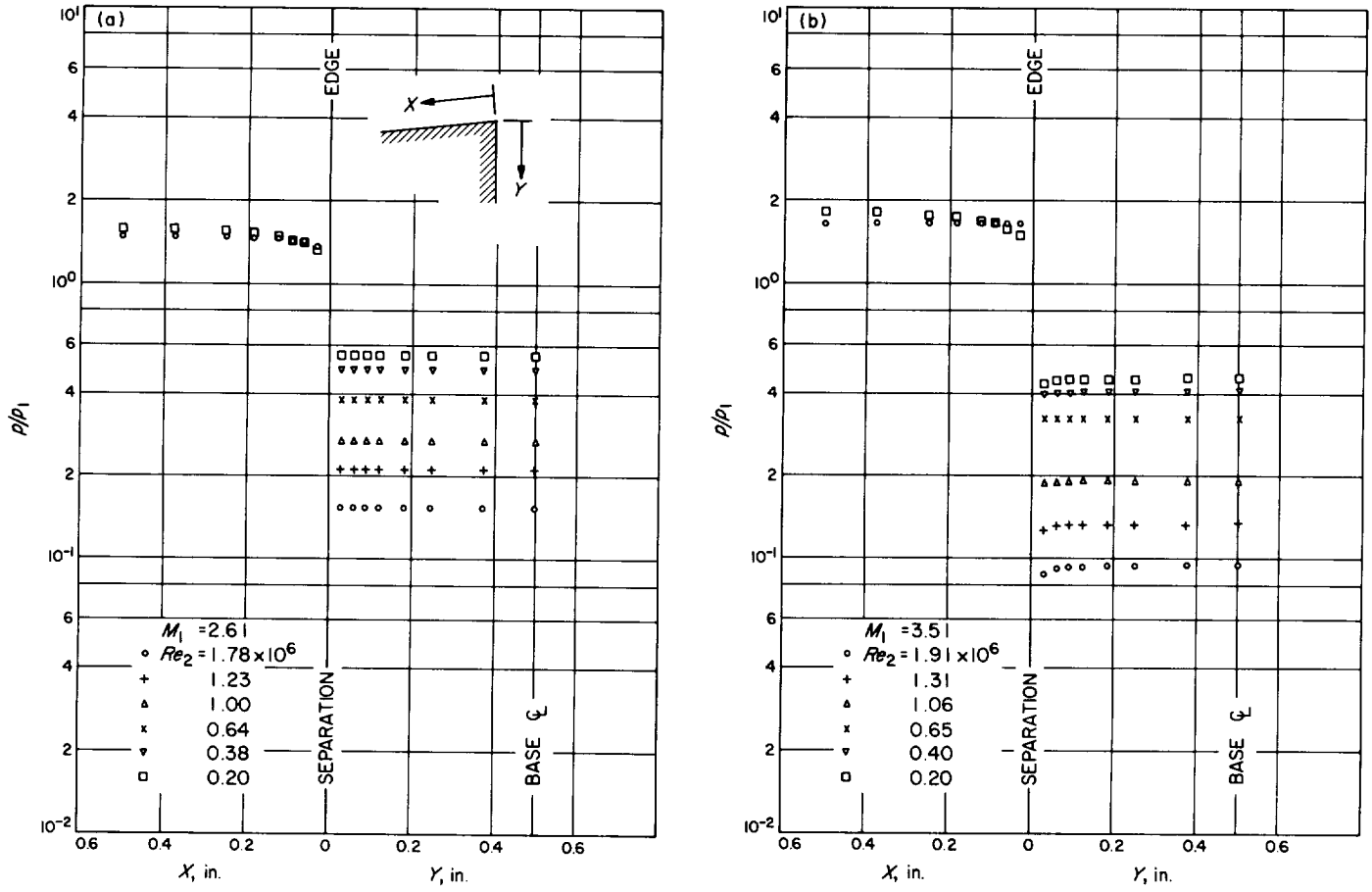

Fig. 57. Surface-pressure distribution near separation edge (regular wedge)

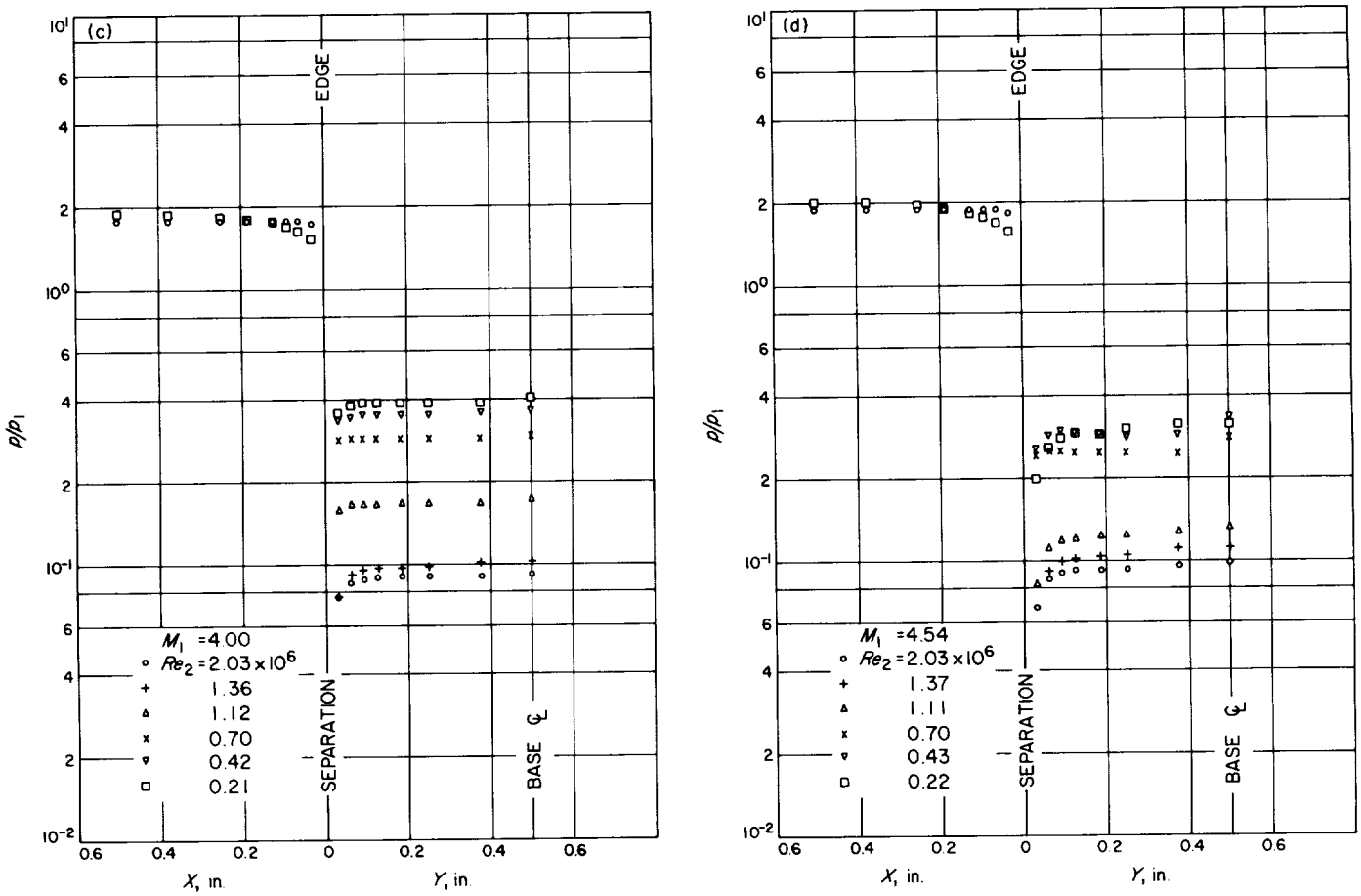

Fig. 57 (contd)

Such a pressure distribution reminded us of a subsonic flow around a sharp corner, as can be found in the incompressible potential flow or in the experimental pressure distribution around a flap hinge of an aerofoil, and led us to believe, tentatively, that the flow adjacent to the wedge surface must have turned sharply around the separation edge and then separated from the base face in the region of rapidly rising pressure. This suspected flow behavior and the lip-shock formation that would result are schematically depicted in Fig. 58(a).[1]

Inspired by such new experimental information and the conjecture derived thereof (Ref. 23), Weinbaum (Ref. 24) made a theoretical study on the behavior of a viscous fluid near the 90-deg separation edge. He found that the separation point was indeed on the base face if the upstream effect of the expansion around the edge was taken into account. The streamline pattern obtained by him is reproduced in Fig. 59, and is quite similar to what was speculated by the present author in Fig. 58(a). Although the theory is restricted to the slow motion of an incompressible viscous fluid, the flow behavior near the surface may be quite similar in the supersonic flow also. Weinbaum is now inclined to believe that the concave streamline pattern above the dividing streamline and near the separation point is directly responsible for the lip-shock formation, rather than the slower and weaker purely inviscid rotational effect which he also computed previously. The pressure distribution on the base face as computed from his formula is also quite similar to our experimental results (Fig. 60).

The overexpansion as seen in the surface-pressure distribution is more pronounced at higher Mach numbers and at larger Reynolds numbers, and is consistent with the

[1]One may tend to draw the same conclusion from shadowgraphs, e.g., Fig. 1, in which the separation point and the root of the lip shock appear to be visibly below the separation edge. Optical distortion inherent to the shadowgraph technique, however, increases the image of the base height appreciably larger than the true 1-in. height. Even if the separation truly occurs below the edge, its location must be actually very close to the edge as judged from the shadowgraphs.

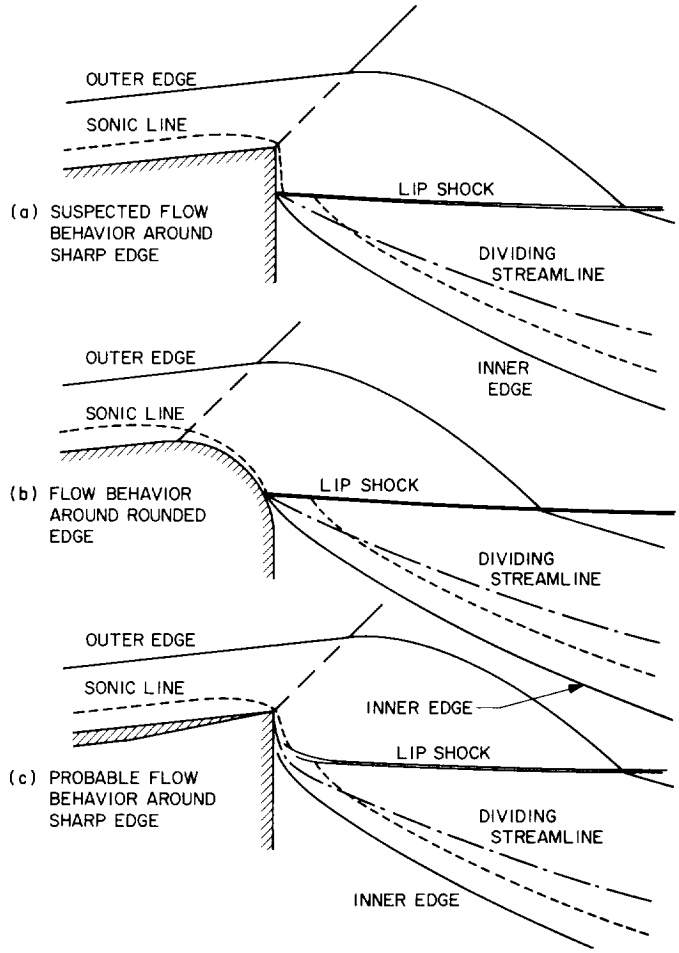

Fig. 58. Flow behavior near separation and formation of lip shock

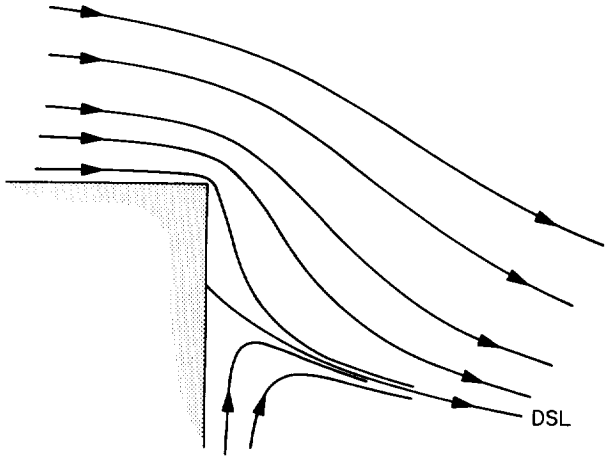

Fig. 59. Behavior of viscous flow around separation edge with upstream effect (after Weinbaum)

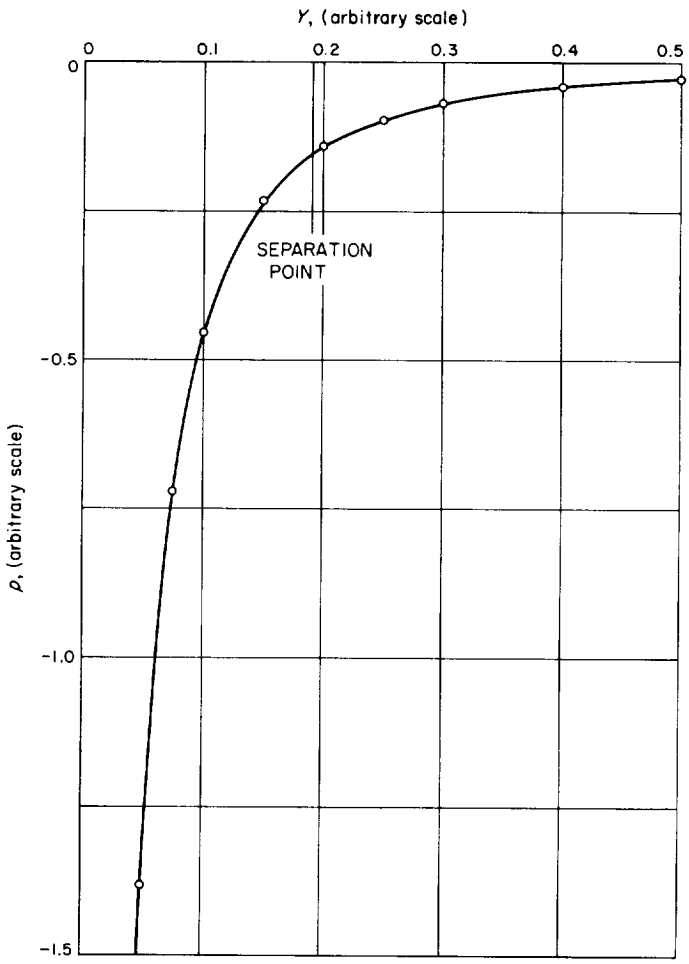

Fig. 60. Base-pressure distribution relative to Fig. 59 (from Weinbaum's formula)

lip-shock strengths. Examination of the dependence on the Reynolds number of the pressure distribution over the base face indicates that the overexpansion is pronounced at high and low Reynolds numbers but not so much at intermediate Reynolds numbers, as perhaps best seen among the pressure distributions for $M_1 = 4.00$. This double dependence on the Reynolds number suggests that there might be two different mechanisms for the overexpansion. Furthermore, at the maximum Mach number investigated ($M_1 = 4.54$) and at the intermediate Reynolds numbers 0.70×10^6 and 0.43×10^6, local peaks of the pressure distribution exists at $Y = 0.06$ and 0.1 in., respectively, immediately following the overexpansion. No additional investigations have been made on these details.

Although a speculation as to the possible flow behavior around the separation edge could be put forward based upon the surface-pressure distribution, all the phenomena, expansion, overexpansion, separation, recompression, and

lip shock, are crammed into a very small region and are difficult to identify. In an attempt to disclose what phenomena are really taking place, the rounded-edge models were tested.

Figure 61a is a set of shadowgraphs behind the rounded wedges of various radii, taken at an identical free-stream condition. It is first noted that the variation of the shock pattern with the edge roundings is that of a gradual change from the shock pattern behind the sharp-edged regular wedge. Therefore, the separation and the shock-formation phenomena must be essentially the same for all the models.

On all the rounded-edge models, on the other hand, it can be clearly seen that the flow separates from the curved portion of the body with a certain deflection angle and that the lip shock emanates at or near the separation point. This situation is schematically depicted in Fig. 58(b) and endorses the view that the lip shock is formed in exactly the same manner as the so-called separation shock, which, most prominently, emerges from a circular cylinder. Because of the observation in the preceding paragraph that the limiting case of the regular wedge is not significantly different from the rounded ones, it is reasonable to conclude that the essential cause of the lip shock is the viscous separation effect even in the case of sharp regular wedge.

Before proceeding to the results of surface-pressure measurements on the rounded models, attention is drawn

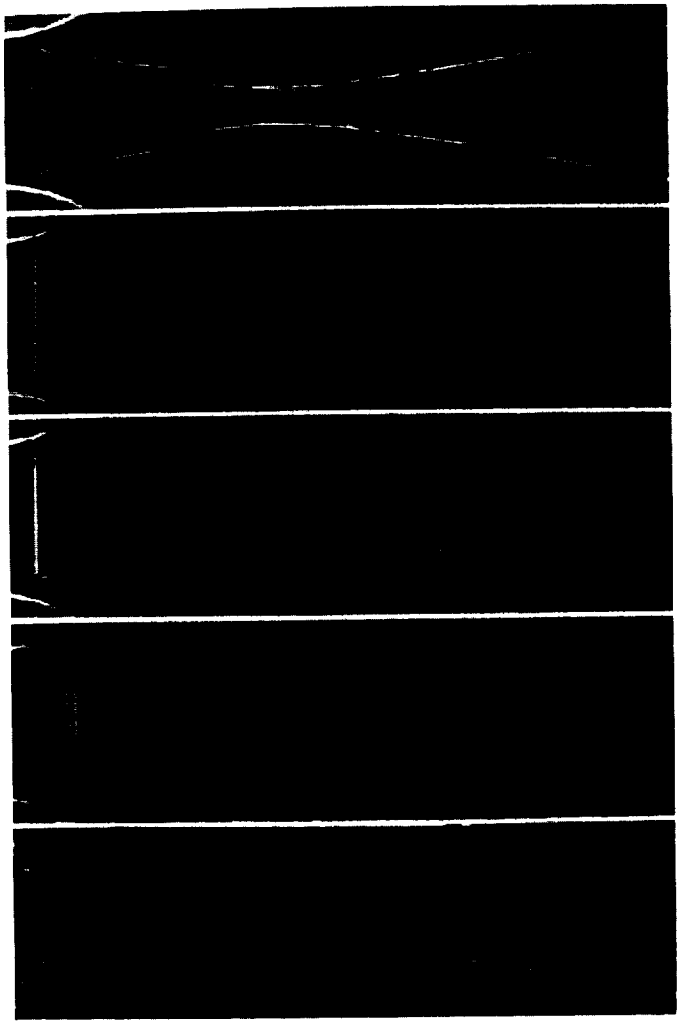

Fig. 61a. Shadowgraphs at $M_1 = 3.51$ and $Re_2 = 1.1 \times 10^6$. From top: regular wedge; rounded wedges $r = 0.05$, 0.10, 0.25, and 0.45 in.

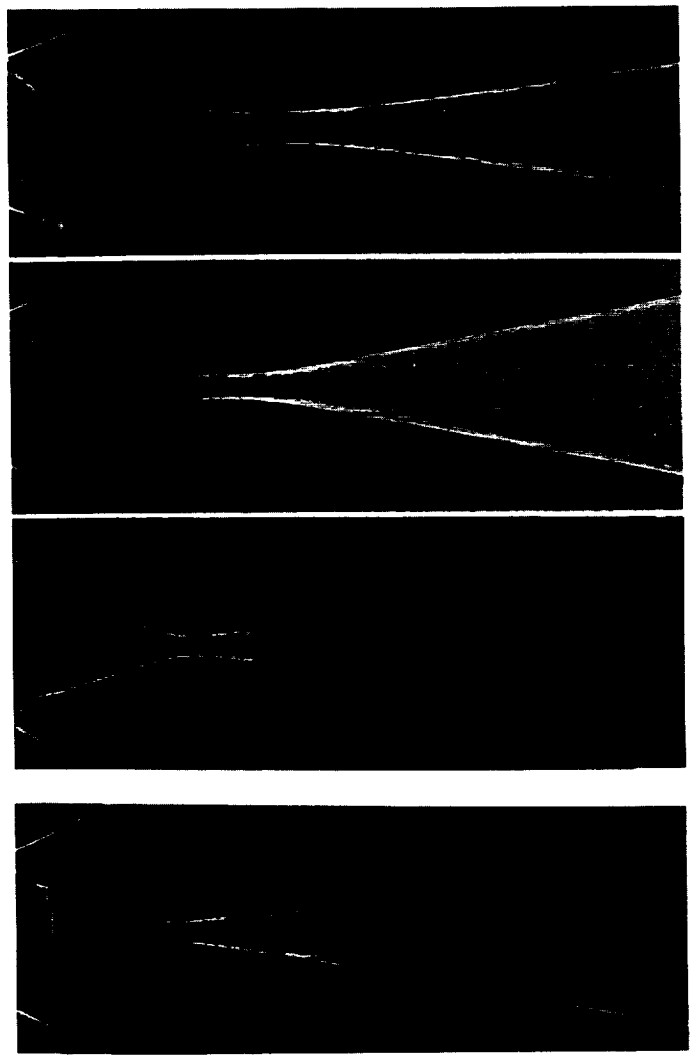

Fig. 61b. Shadowgraphs behind fully-rounded wedge; from top: $M_1 = 4.54$, 3.51, and 2.61; at bottom: $M_1 = 3.51$ with boundary-layer trip; Reynolds number based on diameter and free-stream condition: 3×10^5

to the shock patterns behind the fully-rounded model, Fig. 61b. It is well known that a circular cylinder produces the separation shock which, however, was thought to be reasonably weak and did not significantly affect the pressure-recovery process, particularly because of its upward orientation even at $M_1 = 6$ (cf. Dewey, Ref. 21). These observations were made at a relatively low Reynolds number. The present model, on one hand, eliminates the low subsonic field behind the detached bow shock which exists in front of a circular cylinder. The shadowgraphs shown in Fig. 61b, moreover, were taken at a higher Reynolds number, approximately 3×10^5, based upon the free-stream condition and the diameter of the fully rounded tail end (0.9 in.), compared with approximately 2×10^4 in Dewey's experiment. Under such circumstances, the lip shock can be seen to be tilted downward and to be strong enough to form the slip stream. Therefore, the effects of the lip shock must be present in the pressure-recovery process and in the near-wake velocity profile. Such complications are even more enhanced, as with any other models, when the wedge boundary layers are made turbulent by the tripping device (Fig. 61b, at bottom).

Perhaps, the most advanced theory concerning the base flow and base pressure is that developed by Reeves and Lees (Ref. 25). One task involved in the theory is to join the separated free-shear layer and the reattached near-wake flow with the oncoming boundary layer. When the boundary layer separates from a sharp edge, it is indeed quite difficult to theoretically cope with the many phenomena that take place nearly simultaneously in the separating flow. Therefore, the joining procedure leaves a considerable uncertainty. The fully rounded model was and still is being tested in order to provide experimental data which can be compared with a more elaborate version of the theory, for the theory might be able to deal with the separation and even the lip-shock formation in this case where the radius of curvature is much larger than the boundary-layer thickness. It is hoped that the theory can be made complete and will succeed in the case of low Reynolds numbers in which the shock quickly emerges out of the boundary layer and does not participate in the pressure-recovery process (e.g., cf. Fig. 61a, at bottom). It is certain, however, that the additional complications have to be taken into account in the turbulent case in which the lip shock is imbedded in the free-shear layer and interacts with the wake shock, which itself is formed within the reattached shear layer. This interaction results in the slip stream, which is also laid inside of the viscous near wake.

The previous observations deduced from the shadowgraphs were also substantiated by the surface-pressure distributions presented in Figs. 62–65. In all cases, the flow indeed overexpands to cause a minimum pressure and is then recompressed to the nearly constant base pressure, as can be most clearly seen on the largest two radii.

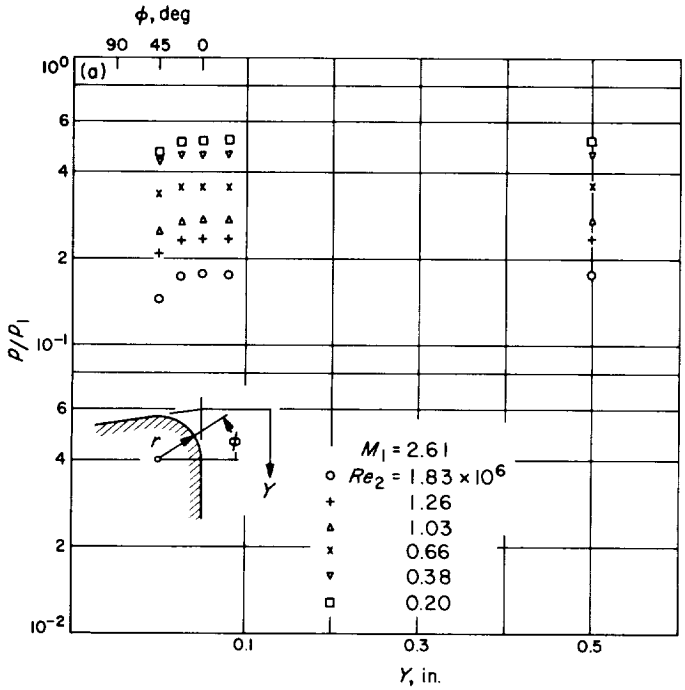

Fig. 62. Surface-pressure distribution (r = 0.05 in.)

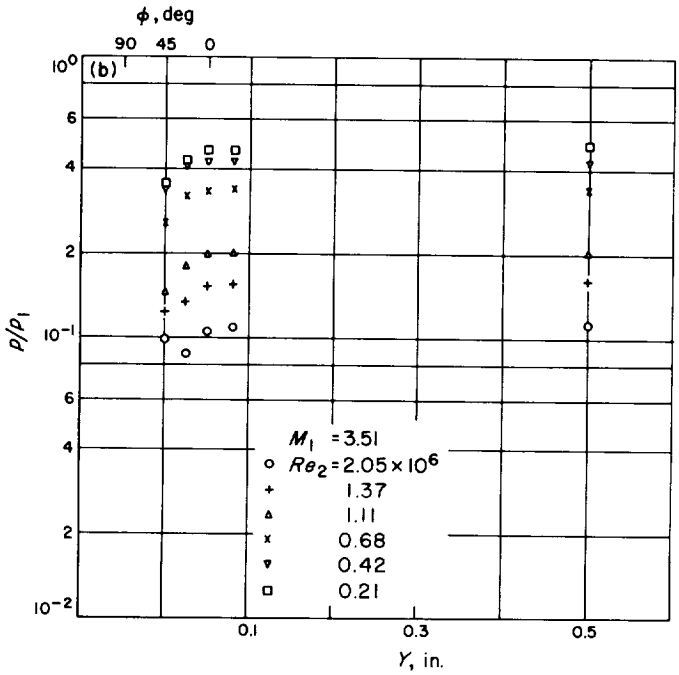

Fig. 62 (contd)

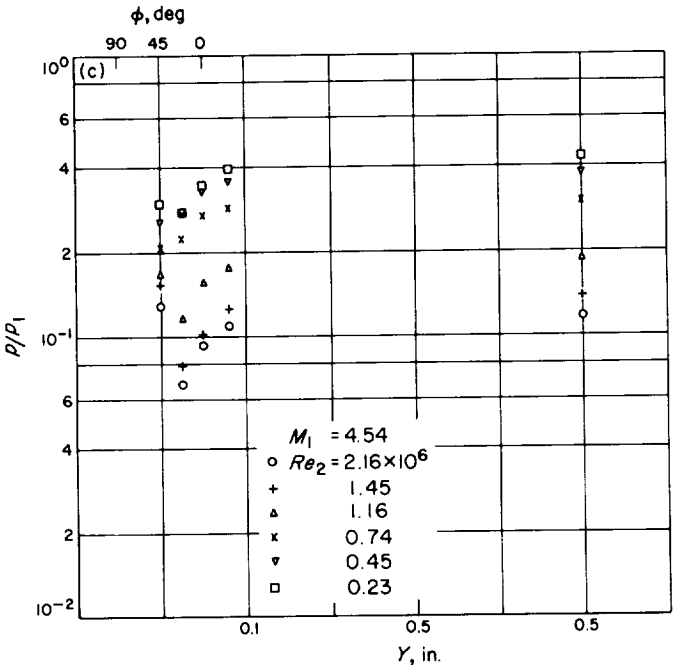

Fig. 62 (contd)

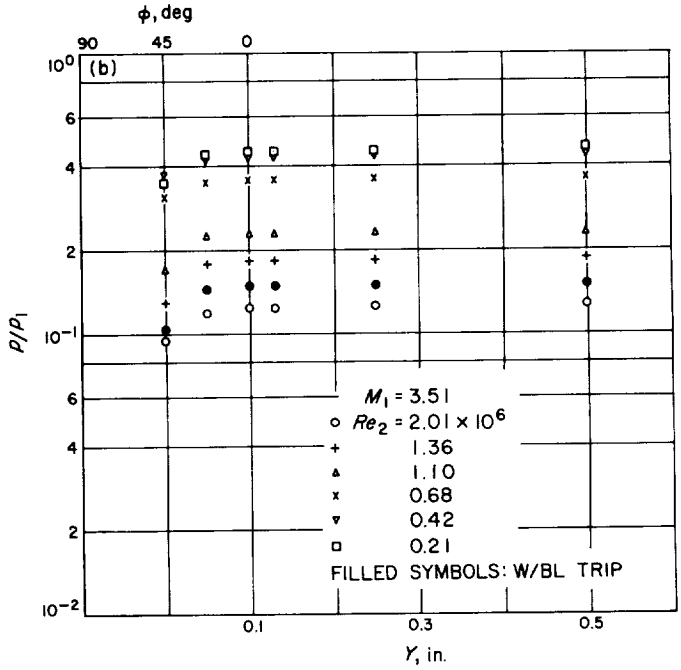

Fig. 63 (contd)

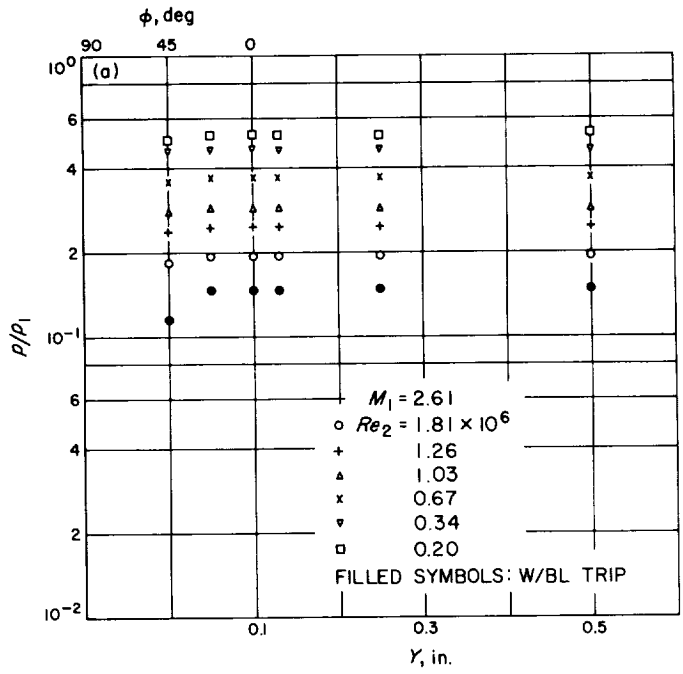

Fig. 63. Surface-pressure distribution (r = 0.10 in.)

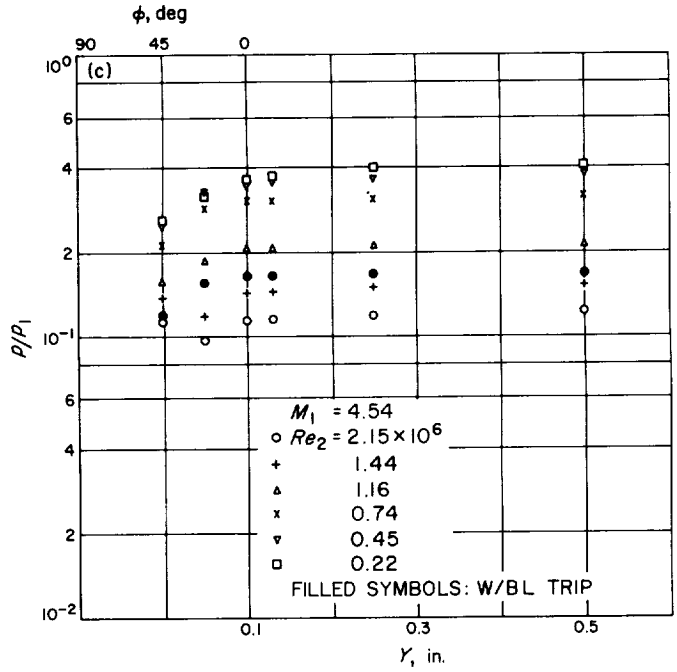

Fig. 63 (contd)

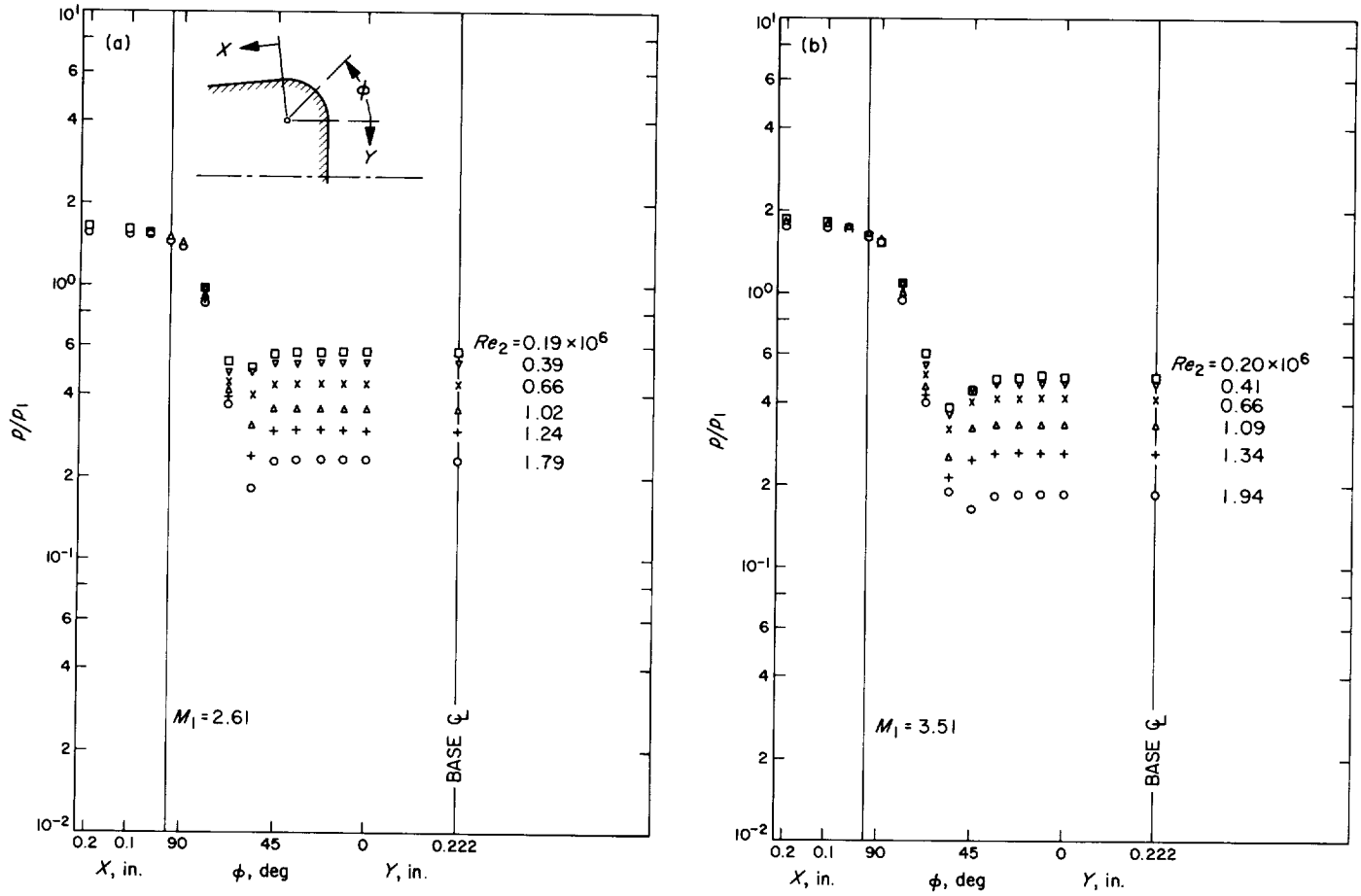

Fig. 64. Surface-pressure distribution ($r = 0.25$ in.)

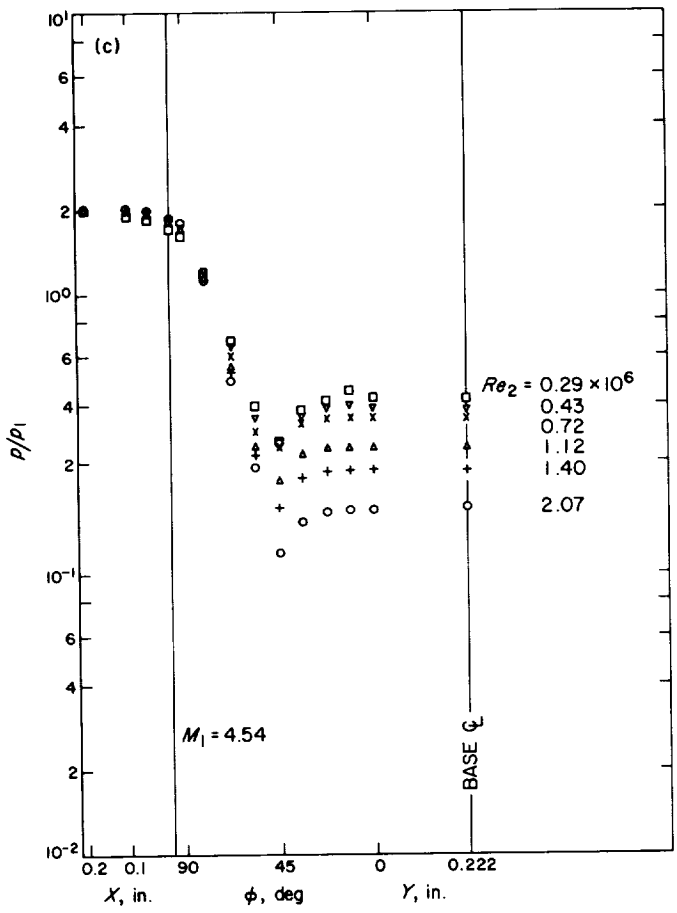

Fig. 64 (contd)

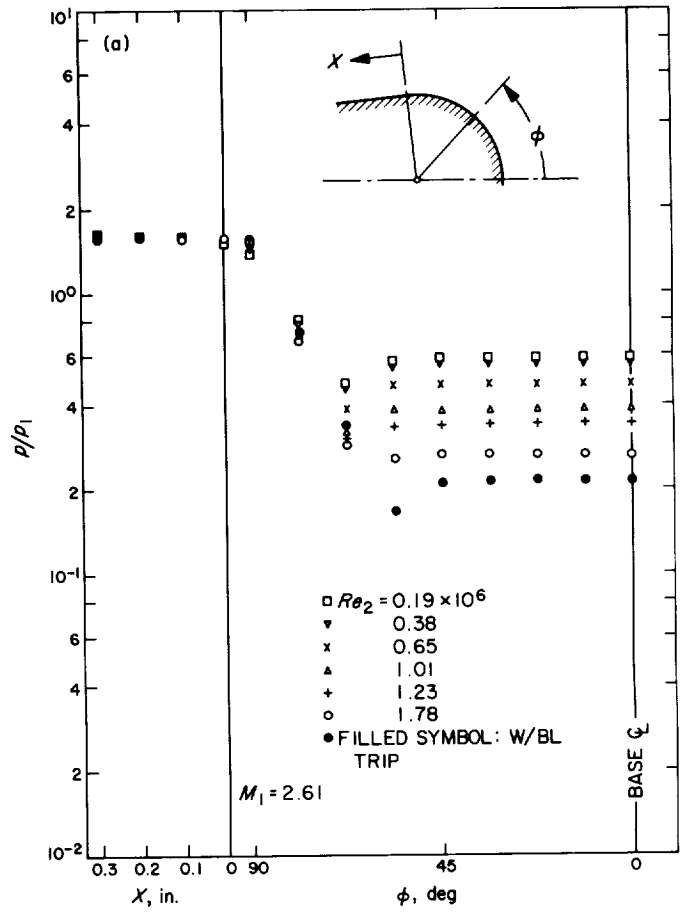

Fig. 65. Surface-pressure distribution (r = 0.45 in.)

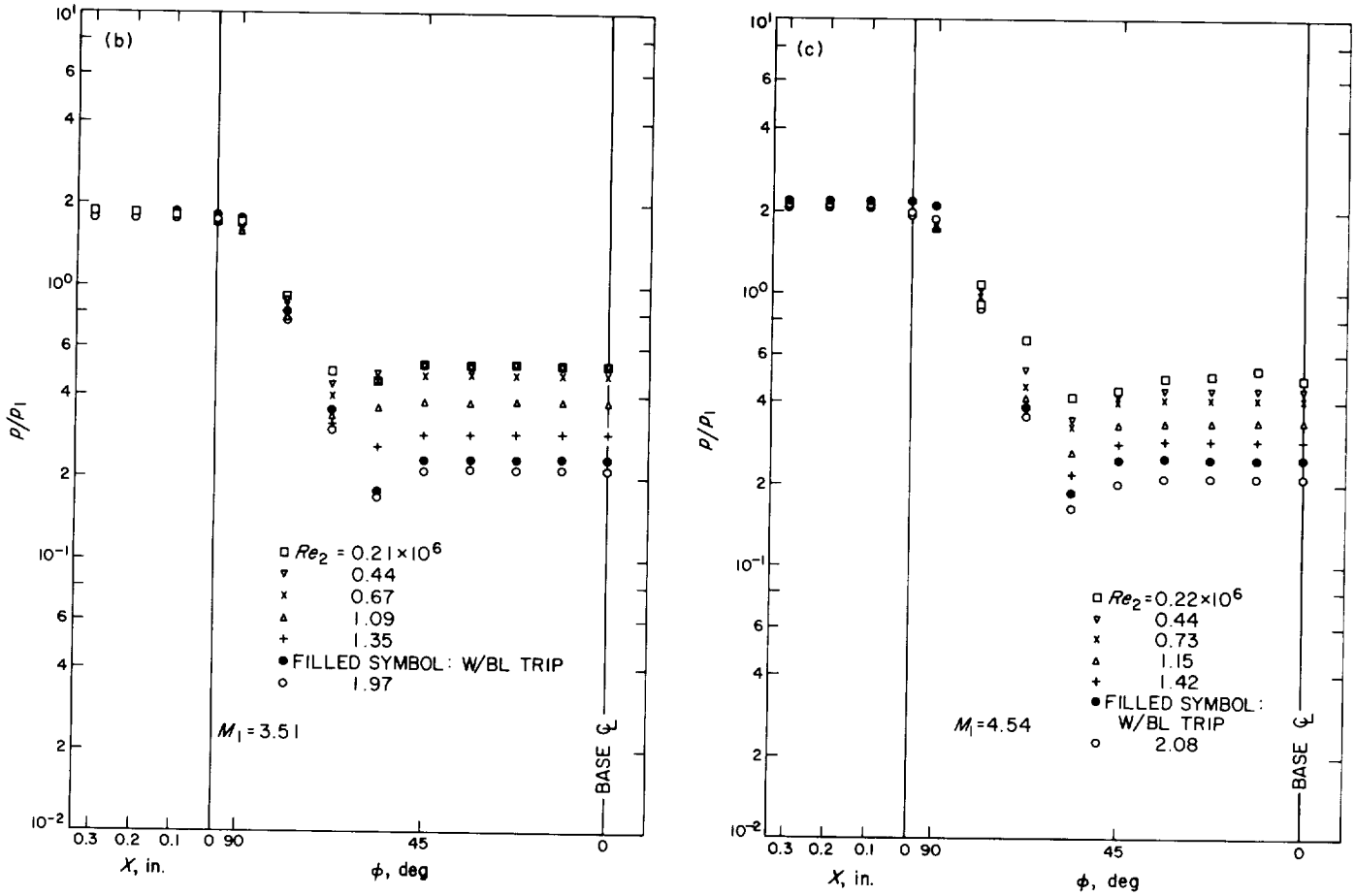
(b)
p/p_1
Re_2 = 0.21×10^6
0.44
0.67
1.09
1.35
FILLED SYMBOL: W/BL TRIP
1.97
M_1 = 3.51
BASE ℄
X, in.
ϕ, deg
(c)
Re_2 = 0.22×10^6
0.44
0.73
1.15
1.42
FILLED SYMBOL: W/BL TRIP
2.08
M_1 = 4.54

Fig. 65 (contd)

This behavior is similar to what has already been observed by Dewey on a circular cylinder. With this sort of pressure distribution, it is now understandable that the boundary layer can separate from the surface with a finite deflection angle in the region of adverse pressure gradient, as already depicted in Fig. 58(b).

In general, the higher the Mach number, the more the flow overexpands. The most interesting observation is the tendency that, for a given free-stream condition, the flow follows the surface longer and overexpands more as the radius of curvature is decreased. Compare, for example, the pressure distributions on the four rounded-edge models at $M_1 = 4.54$ and the highest Reynolds number. On the 0.05-in. model, the pressure minimum is about 0.066 at 22.5 deg; on the 0.10-in. model, it is 0.097 at around 22.5 deg (unfortunately, the models were not provided with a sufficient number of pressure taps to distinguish any difference in overexpansion angles); but the overexpansion is down only to 0.119 at 45 deg and 0.162 at 56.25 deg, respectively, on the 0.25-in. model and on the 0.45-in. model. The angles being measured from the base face, these angles mean 73.5-, 73.5-, 51-, and 39.75-deg expansions from the wedge surface, respectively. This tendency points out the possibility that the flow might turn around the sharp edge of the regular wedge. Yet, it is reasonable to expect that the true separation point must be extremely close to the edge.

One final remark on the dependence of the overexpansion on the Reynolds number is in order. The measured pressure distributions show that the flow overexpands more as the Reynolds number increases. This dependence, as well as the other observations stated above, is in accord with the variations of the lip-shock strength. On the contrary, Dewey's pressure distributions on a circular cylinder clearly demonstrate the opposite; the flow overexpands more and the separation point moves downstream with decreasing Reynolds number. Other than pointing out the difference in model geometry, no direct explanations of the contrasting results will be offered at this time. We are

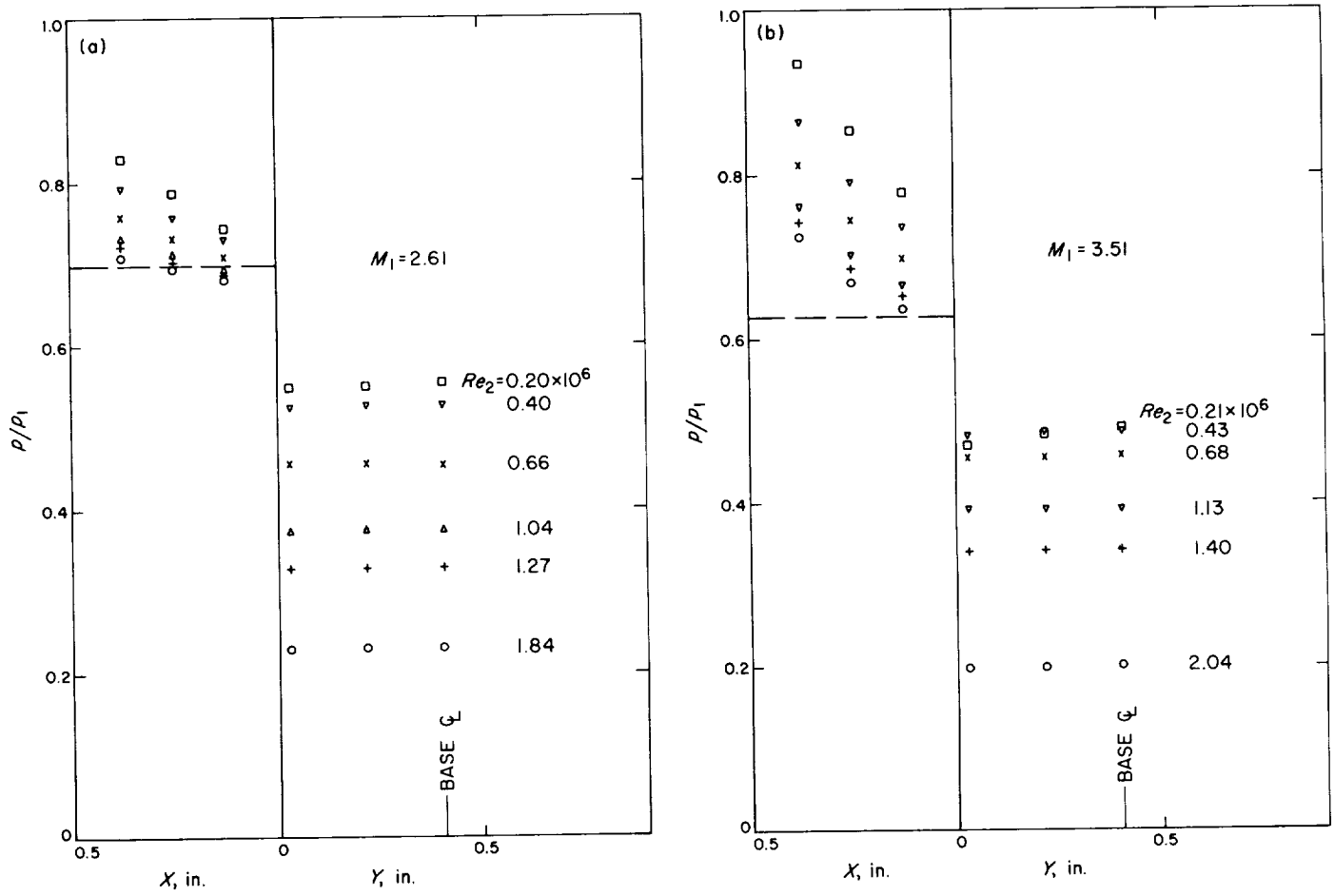

Fig. 66. Surface-pressure distribution (5-deg boattail)

reminded, however, that the base pressure increases with increasing Reynolds number in Dewey's test conditions, whereas our Reynolds-number range is such that the base pressure decreases. Undoubtedly, the overexpansion is strongly affected by the base pressure, which is chiefly controlled by the reattachment condition, and cannot be separately considered as the behavior of the separating shear flow.

Experience with the boattail models was instructive in many respects. The surface-pressure distributions are presented in Figs. 66 a, b, c; 67 a, b, c, and 68 a, b, c. A set of shadowgraphs taken at an identical free-stream condition $M_1 = 2.61$ and $Re_2 = 1.0 \times 10^6$ is shown in Fig. 69.

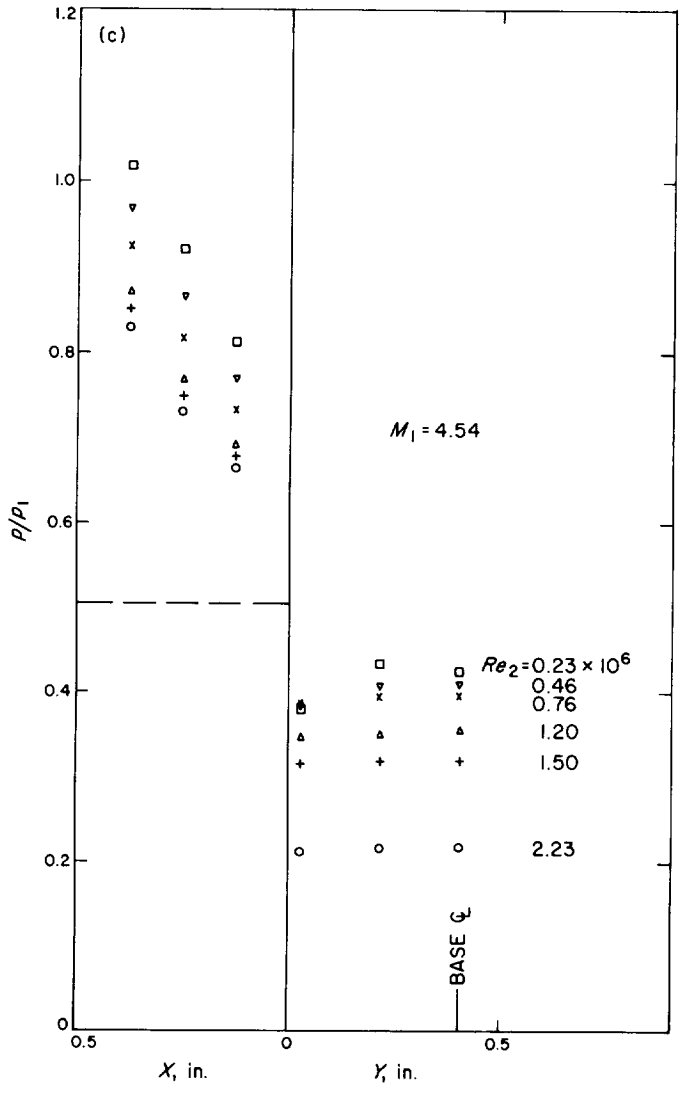

Fig. 66 (contd)

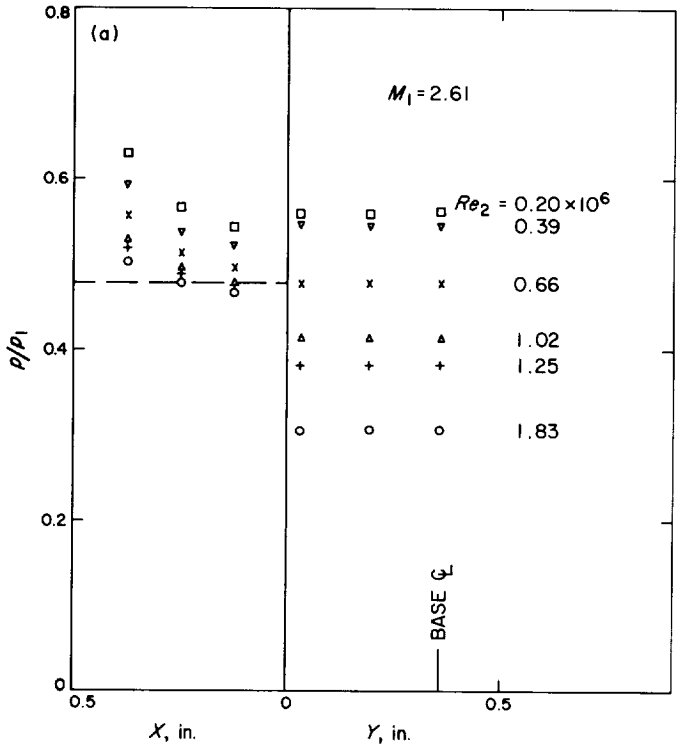

Fig. 67. Surface-pressure distribution (10-deg boattail)

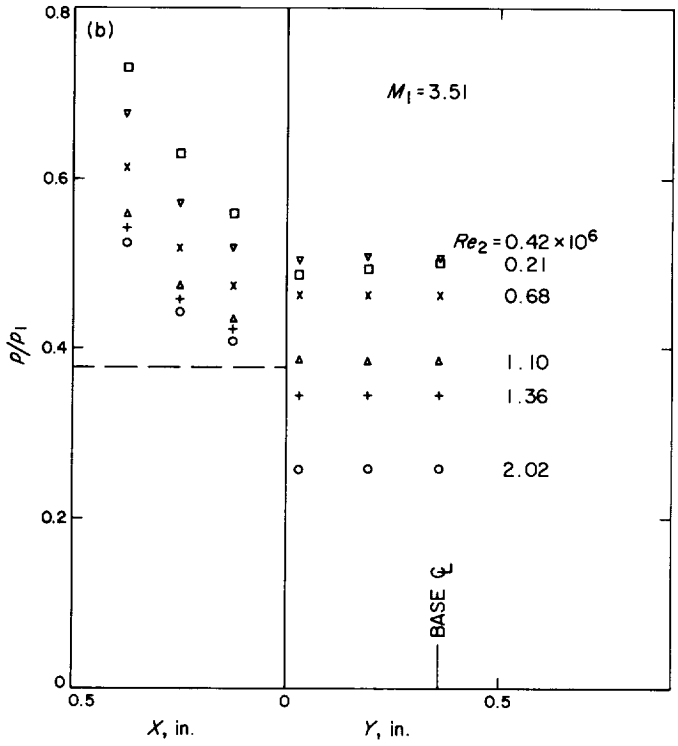

Fig. 67 (contd)

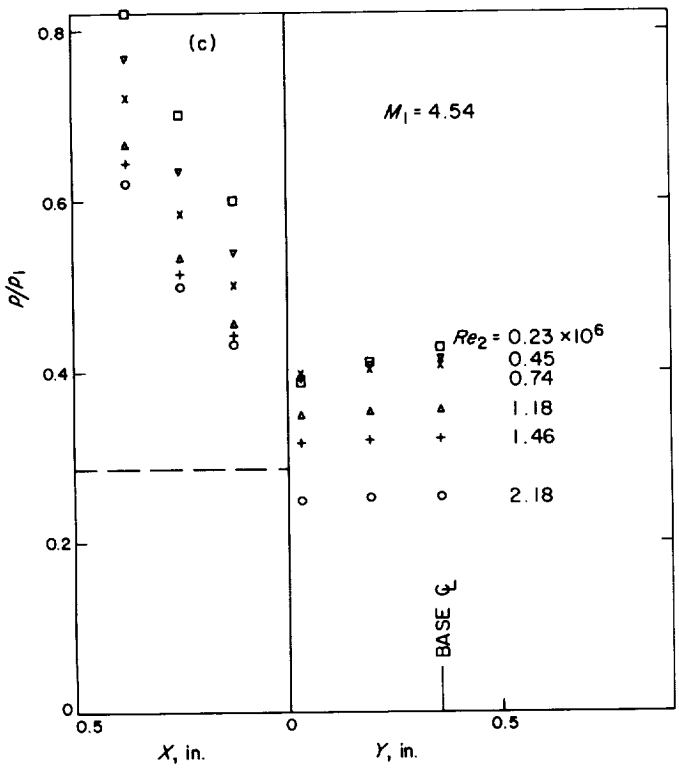

Fig. 67 (contd)

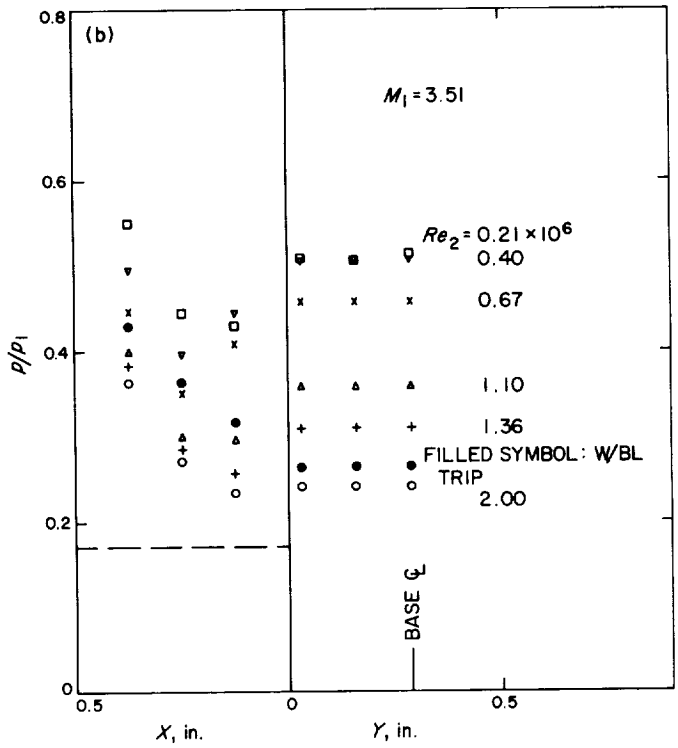

Fig. 68 (contd)

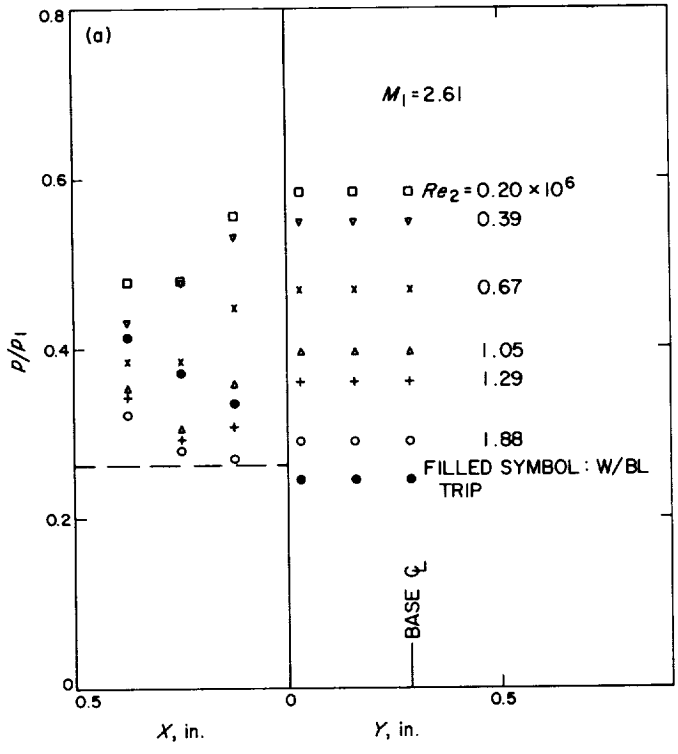

Fig. 68. Surface-pressure distribution (17-deg boattail)

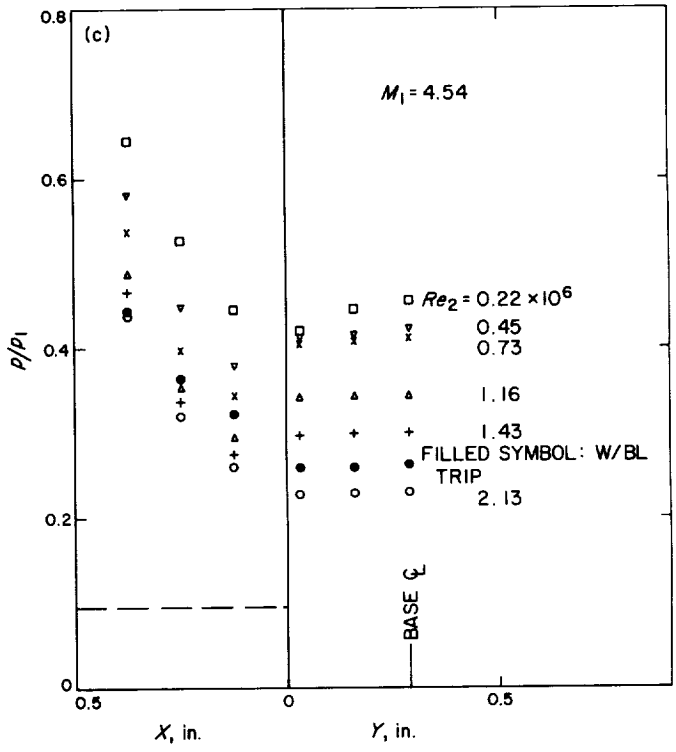

Fig. 68 (contd)

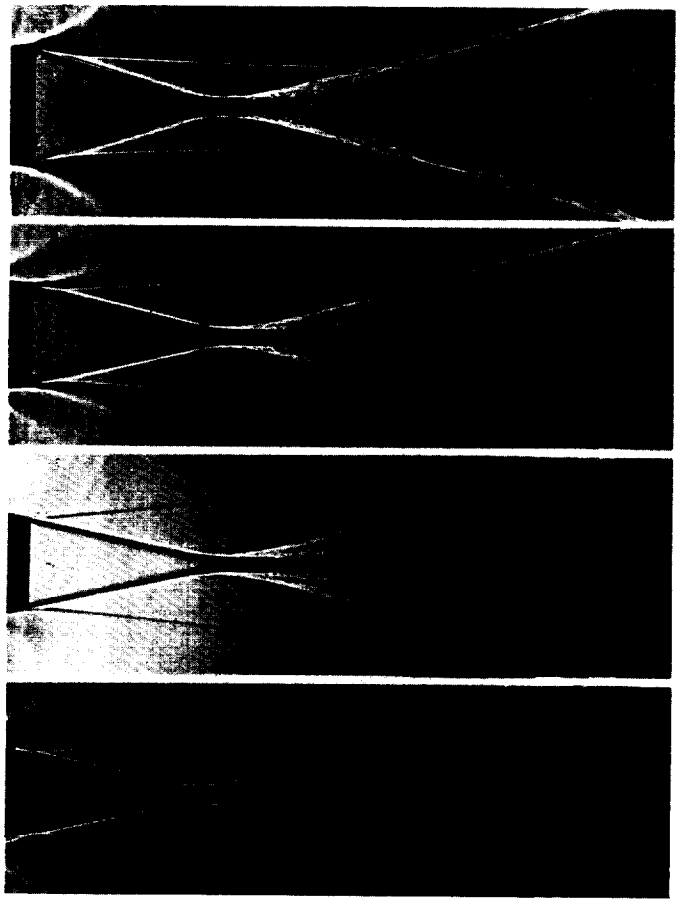

Fig. 69. Shadowgraphs at $M_1 = 2.61$ and $Re_2 = 1.0 \times 10^6$; from top: regular wedge, 5-, 10-, and 17-deg boattail wedges

It is first noticed that the interaction between the boundary layer and the expansion fan at the expansion corner preceding the boattail takes quite a long distance so that the surface pressure on the boattail portion seldom reaches the inviscid value which is indicated by a horizontal broken line in each figure.

In the case of the 5-deg boattail model, the flow always encounters an expansion at the rear separation edge under all the conditions tested. Therefore, the regular lip shock emerges from the separation edge. By boattailing, however, the surface pressure before separation is drastically reduced and consequently the amount of expansion is also much less than in the case of regular wedge. The reduction of expansion is in fact even more enhanced because of the larger base pressure behind the boattail models. Since the lip-shock strength could be correlated with the amount of expansion, the lip shock off the boattail models must be weaker under the same test condition as already shown in Fig. 38 in comparison with Fig. 37. The shadowgraph (the second from the top in Fig. 69) also clearly shows that the orientation of the lip shock is opened out in comparison with that off the regular wedge (the top shadowgraph) and that the slip stream can be seen only very faintly.

With the 10-deg boattail model, the flow still makes an expansion at the rear edge under most of the test conditions, except at $M_1 = 2.61$ and very low Reynolds numbers in which cases the pressure distribution and the flow behavior resemble those of the steeper boattail model. The pressure on the boattail surface is further reduced from that on the 5-deg boattail model. For example, for the third shadowgraph in Fig. 69 the expansion is only from about 0.47 to 0.412 compared with 1.5 to 0.265 for the regular wedge and 0.67 to 0.373 for the 5-deg model. The expansion having been further reduced, the lip shock is indeed seen to be feeble, and the estimated strength was 1.09. The slip stream was only vaguely visible in the schlieren picture but could not be detected in the shadowgraph.

In contrast, over the steepest 17-deg boattail model, the flow did not expand at the rear edge under the present test conditions. Instead, there was a pressure minimum on the boattail surface lower than the base pressure, and the boundary layer could separate in the region of adverse pressure gradient. For the shadowgraph at the bottom of Fig. 69, for example, the surface pressure reaches the minimum of 0.29 but the base pressure is 0.36. The boundary layer can be seen to have separated from the boattail surface, and a shock wave is formed from the separation. The shock wave is therefore the conventional separation shock, but it is emphasized that its appearance is indeed quite similar to the regular lip shock shown in the top three shadowgraphs. This is to reassert that the lip shock and the separation shock are not essentially different. The shock, furthermore, appears to be stronger than that of the 5-deg model as well as that of the 10-deg model; the shock is more distinct and the slip stream can be seen more clearly.

The 17-deg model was tested also with the boundary-layer trips. The pressure distributions are included in Figs. 68 a, b, c, and the shadowgraphs are presented in Fig. 70. Because of the thickened boundary layer, the interaction at the expansion corner preceding the boattail portion is even slower and the pressure on the boattail surface is larger than the untripped case at a comparable free-stream condition. Under the conditions tested, the turbulent boundary layer did not separate from the boattail surface, and there was always a small expansion at the rear edge. The

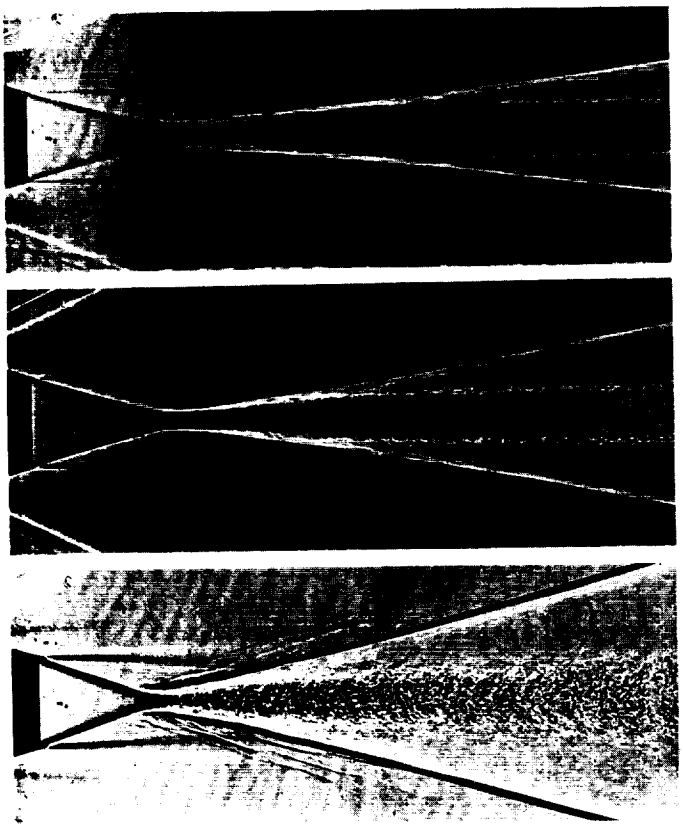

Fig. 70. Shadowgraphs behind 17-deg boattail wedge with boundary-layer trip; from top: $M_1 = 4.54$, 3.51, and 2.61

base pressure was either lower ($M_1 = 2.61$) or higher ($M_1 = 3.51$ and 4.54) than the estimated isentropic pressure corresponding to the boattail angle. Because of the smallness of the expansion, only weak waves emanated from the rear edge. Perhaps, these weak waves observable in the shadowgraphs were no more than a narrow expansion fan which was imbedded in the thick free-shear layer. The convex wave pattern, contrary to the generally concave lip shock, may be due to this situation. Since a substantial expansion existed at the expansion corner, it is conceivable that the near-surface portion of the tripped boundary layer might have been partially laminated (Refs. 26, 27). A well-defined line emanating from the rear edge, which resembles the laminar free-shear layer and must be the outer edge of the inner shear layer (cf. Fig. 47), suggests this possibility. By the boattailing, in any event, the lip-shock strength is drastically reduced in the laminar case, or the lip shock itself is almost entirely eliminated in the turbulent case. Hence the effect of the lip shock on the pressure-recovery distribution, for example, can be substantially alleviated, as demonstrated by Roshko.

The experimental evidence so far presented has led to the conclusion, beyond reasonable doubt, that the lip shock is not essentially different from the separation shock even in the case of a sharp regular wedge. Experimental results of the knife-edge model, however, turned out to be somewhat of a surprise to us. The test of this model was originally conceived based upon an expectation that,

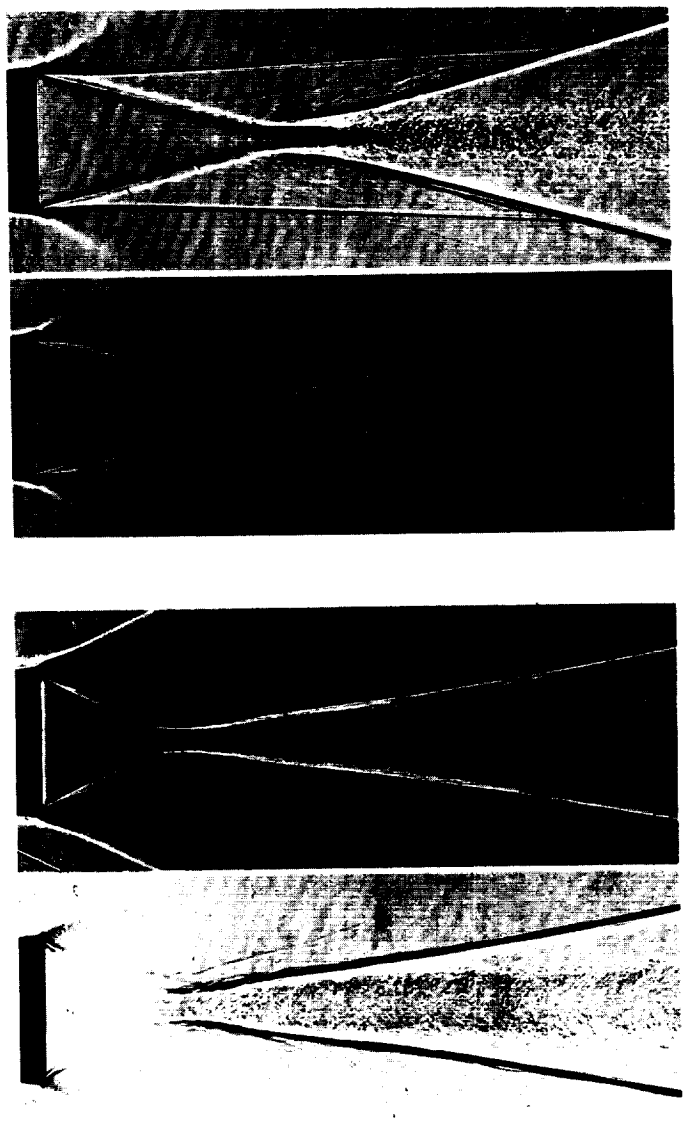

Fig. 71. Comparative shadowgraphs for regular wedge and knife-edge wedge; top set: $M_1 = 2.61$, $Re_2 = 0.65 \times 10^6$; bottom set: $M_1 = 3.51$ with boundary-layer trip; in each set, top: regular wedge, bottom: knife-edge model

if the blade tip is sufficiently sharp, the oncoming boundary layer would directly leave from the tip without going through the process of overexpansion and viscous-layer separation from the base face, and therefore the lip shock might not be formed.

Quite contrary to our naive expectation, not only the base pressure was virtually unchanged (Fig. 17), but also the lip shock was formed almost exactly in the same manner under either laminar or turbulent conditions (Fig. 71), and the lip-shock strength was correlated perfectly with the regular wedge results (Fig. 33). In other words, the knife-edge model resulted in nothing different from the regular wedge.

In order to reconcile the difference between the expectation and the experimental evidence, we may speculate that a more probable flow behavior around either the knife edge or the regular separation edge is as sketched in Fig. 58(c) rather than the possibly oversimplified Fig. 58(a). We are not at all certain of this view because it is difficult to experimentally verify the flow behavior in an extremely narrow region and because other possibilities are equally probable. For example, the separation could have taken place within such a short distance (0.001 in.) from the separation edge that there was no difference between the two. Or, the separation from the knife edge might be on the inner surface of the blade but at such a short distance from the tip that, again, the difference, if any, was unnoticeable. More rigorous theoretical studies on the separation phenomena are indeed desirable in order to resolve these questions.

VII. Summary

The present investigation was conducted in the 20-in. supersonic wind tunnel at the Jet Propulsion Laboratory in the Mach number range 2.0–4.5 and in the Reynolds number range 0.2×10^6–2.0×10^6 in order to obtain extensive data on the base pressure of a wedge, 6 deg half-angle and 1-in. base height. However, more emphasis was placed on the investigations of the so-called lip shock.

The base pressure was measured not only behind the wedge, but also with a wedge-plate configuration in which the plate surface was aligned with the centerline of the wedge, in an effort to find a difference in base pressures for the different reattachment conditions. The difference was found to be small, but the base pressure of the wedge alone was somewhat smaller than that of the wedge-plate configuration. The measurements were also made on wedges of basically the same dimension but with various separation-edge shapes, including razor-sharp knife edges, rounded edges of four different radii, and three boattails. These models were tested to determine the cause of the lip shock rather than to obtain engineering data.

Relative orientation of the wake shock and the lip shock varies appreciably depending on the Mach number as well as the Reynolds number. The static-pressure recovery distribution in the wake was also found to assume a variety of patterns, and the appearance of peak and hump in the pressure distribution was attributed to the interaction between the two shocks. The interaction caused a distortion in the near-wake velocity profile in some cases.

The lip-shock strength (the static-pressure ratio across the shock) was estimated from shadowgraphs. Contrary to the prevailing belief, the strength was found to be substantial (Ref. 28). The estimation was affirmed by cross-examinations of the procedure and also more directly by pitot-pressure surveys.

An inquiry was made into the cause of the lip shock by measuring surface-pressure distribution, particularly near the separation edge, as well as by observing shock patterns on the wedges of various separation-edge shapes. The essential mechanism to form the lip shock appears to be the viscous separation phenomena similar to the separation shock from a circular cylinder, rather than the inviscid rotational effect.

References

1. Roshko, A., and Thomke, G. J., "Observations of Turbulent Reattachment behind an Axisymmetric Downstream-Facing Step in Supersonic Flow," *AIAA Journal*, Vol. 4, June 1966, pp. 975–980.

2. Chapman, D. R., Kuehn, D. M., and Larson, H. K., *Investigation of Separated Flows in Supersonic and Subsonic Streams with Emphasis on the E×ect of Transition*, National Advisory Committee for Aeronautics, Washington, D. C., Technical Note 3869, March 1957 (superseded by Report 1356, 1958).

3. Korst, H. H., "A Theory for Base Pressures in Transonic and Supersonic Flow," *Journal of Applied Mechanics*, Vol. 23, 1956, pp. 593–600.

4. Nash, J. F., *An Analysis of Two-Dimensional Turbulent Base Flow, Including the Effect of the Approaching Boundary Layer*, Aeronautical Research Council, National Physical Laboratory, Teddington, Middlesex, England, Report and Memorandum 3344, July 1962.

5. Hama, F. R., "An Efficient Tripping Device," *The Journal of the Aeronautical Sciences*, Vol. 24, March 1957, p. 236.

6. Hama, F. R., "Boundary-Layer Tripping in Super- and Hyper-sonic Flows," Jet Propulsion Laboratory, Pasadena, Calif., *Space Programs Summary No. 37-29*, Vol. IV, Oct. 31, 1964, pp. 163–168.

7. Batt, R. G., private communication.

8. Ginoux, J. J., *On the Existence of Cross Flows in Separated Supersonic Streams*, Training Center for Experimental Aerodynamics, Royal Academy of Belgium, Technical Note 6, February 1962.

9. Lewis, J. E., private communication.

10. Roshko, A., and Lau, J. C., "Some Observations on Transition and Reattachment of a Free Shear Layer in Incompressible Flow," *Proceedings of the 1965 Heat Transfer and Fluid Mechanics Institute*, Stanford University Press, Stanford, Calif., 1965, pp. 157–167.

11. Holder, D. W., and Gadd, G. E., "The Interaction between Shock Waves and Boundary Layers and Its Relation to Base Pressure in Supersonic Flow," in *Boundary Layer Effects in Aerodynamics*, Philosophical Library, New York, 1955, pp. 8p. 1–65.

12. Roshko, A., "A Look at Our Present Understanding of Separated Flow," presented at AGARD Specialists' Meeting on Separated Flows, Brussels, Belgium, North Atlantic Treaty Organization Advisory Group for Aerospace Research and Development, May 1966.

13. Tani, I., "Experimental Investigation of Flow Separation over a Step," in *Boundary Layer Research, IUTAM Symposium Freiburg/Br. 1957*, H. Goertler (ed.), Springer–Verlag, 1958, pp. 377–386.

14. Kubota, T., private communication.

15. Oswatitsch, K., "Die Abloesungsbedingung von Grenzschichten," in *Boundary Layer Research, IUTAM Symposium Freiburg/Br. 1957*, H. Goertler (ed.), Springer–Verlag, 1958, pp. 357–367.

References (contd)

16. Hastings, R. C., *Turbulent Flow Past Two-Dimensional Bases in Supersonic Streams*, Royal Aircraft Establishment, Farnborough, Hampshire, England, Technical Note Aero. 2931, 1963.

17. Charwat, A. F., and Yakura, J. K., "An Investigation of Two-Dimensional Supersonic Base Pressures," *The Journal of the Aeronautical Sciences*, Vol. 25, 1958, pp. 122–128.

18. Larson, R. E., Scott, C. J., Elgin, D. R., and Seiver, R. E., *Turbulent Base Flow Investigations at Mach Number 3*, Rosemount Aeronautical Laboratory, University of Minnesota, Minneapolis, Minn., Research Report 183, 1962.

19. Weinbaum, S., *The Rapid Expansion of a Supersonic Shear Flow*, AVCO Everett Research Laboratory, Everett, Mass., Report 204, January 1965.

20. Weiss, R. F., and Weinbaum, S., *Hypersonic Boundary Layer Separation and the Base Flow Problem*, AVCO Everett Research Laboratory, Everett, Mass., Research Report 221, July 1965.

21. Dewey, C. F., Jr., "Near Wake of a Blunt Body at Hypersonic Speeds," *AIAA Journal*, Vol. 3, June 1965, pp. 1001–1010.

22. Kavanau, L. L., "Base Pressure Studies in Rarefied Supersonic Flows," *The Journal of the Aeronautical Sciences*, Vol. 23, March 1956, pp. 193–207.

23. Hama, F. R., "Experimental Investigations of the Base-Flow Problem, II. Wedge," Jet Propulsion Laboratory, Pasadena, Calif., *Space Programs Summary No. 37-35*, Vol. IV, Oct. 31, 1965, pp. 237–240.

24. Weinbaum, S., *Laminar Incompressible and Trailing Edge Flows and the Near Wake Rear Stagnation Point*, General Electric Company, Missile and Space Division, Philadelphia, Pa., Report R66SD25, May 1966.

25. Reeves, B. L., and Lees, L., "Theory of Laminar Near Wake of Blunt Bodies in Hypersonic Flow," *AIAA Journal*, Vol. 3, Nov. 1965, pp. 2061–2074.

26. Sternberg, J., *Transition from a Turbulent to Laminar Boundary Layer*, Ballistics Research Laboratory, U.S. Army Ordnance Corps, Aberdeen, Proving Ground, Md., Report 906, May 1954.

27. Launder, B. E., *Laminarization of the Turbulent Boundary Layer by Acceleration*, Gas Turbine Laboratory, Massachusetts Institute of Technology, Cambridge, Mass., Report 77, Nov. 1964.

28. Hama, F. R., "Estimation of the Strength of Lip Shock," *AIAA Journal*, Vol. 4, Jan. 1966, pp. 166–167 (also Technical Report 32-874, Jet Propulsion Laboratory, Pasadena, Calif., March 1966).